Manipulation of Molecular Structures
with Magnetic Fields

Cover

Front:
Domain structures in Side Chain Polymer Liquid Crystals observed in crossed polarized microscopy. For in-depth explanations see sect.2.3 or sect.3.3.

Back:
Sunrise over the Faculty of Science seen from the window of the apartment where I lived during the Ph.D. period.
Sunset over the university campus seen from the roof of the Faculty of Science.

Taken at the end of the first Ph.D. year, Dec. 1998 (the sunrise) and at the beginning of the last Ph.D. year, Jan. 2001 (the sunset) the pictures intend to illustrate the ups and downs of this work.

Manipulation of Molecular Structures with Magnetic Fields

een wetenschappelijke proeve op het gebied van
de Natuurwetenschappen, Wiskunde en Informatica

Proefschrift

ter verkrijging van de graad van doctor aan
de Katholieke Universiteit Nijmegen, op gezag
van de Rector Magnificus Prof. Dr. C.W.P.M Blom,
volgens besluit van het College van Decanen
in het openbaar te verdedigen
op woensdag 2 april 2003,
des namiddags om 1.30 uur precies

door

Marius Iosif Boamfă

geboren op 9 juni 1972
te Făgăraş, Roemenië

Pentru Iulia şi Anamaria

Preface

There were a lot of people that gave me an important support during this long quest and this preface is a tribute to them.

It all started in a sunny day of August 1997. I came to Nijmegen for a few day visit, to undertake an interview for a Ph.D. position at the High Field Magnet Laboratory. Apparently I did well and I was offered the job. The lab was impressive, the city was cozy and quiet and the weather was incredibly nice, so I gladly accepted the job. Today, after five years, I still keep my first opinion about Nijmegen – a lovely, peaceful city. The weather though… By now I got used with the Dutch weather and I have learned to live with the coincidence that the most sunny days I have spent here were my first three ones.

In January 1998, full of enthusiasm and highly motivated I returned back to Nijmegen to start my Ph.D. work. In my first day I was told that due to the long time it took to get my visa, the project I was initially appointed to, was given to somebody else. I was immediately assured that my position is still valid and all I have to do is to look around and find an appropriate subject for my future work. It was not really what I have hopped to hear, especially because Nijmegen it meant for me a sharp change from theoretical to experimental physics, I was not prepared to look around…

But time proved as always a universal solution. With the help of Jan Kees (Prof. Maan - my supervisor), I have slowly converged toward the field of Soft Condensed Matter. Thank you very much Jan Kees for your scientific assistance, commitment and diplomacy with which you have guided me to this thesis.

When it became obvious that my work has a lot to do with Optics I went to Jan Kees and asked for special help in this direction. Despite a busy program with lectures to give and a lot of other Ph.D. students to guide, Peter joined in and became my co-promoter. For all the help you gave me, thank you very much Peter. I did enjoy a lot our tutorials.

Before really turning toward Soft Condensed Matter, it seamed that I would pursue a work in the field of biophysics: "Magnetic field induced effects on living organisms". After a few months adventure, really convinced about the beauty of the field, I decided to postpone this project for a later time. I owe a special thanks to Mike, Liesbeth and Prof. Titi Mariani for a nice introduction to Plant Biology. As the time has passed, I have begun to see a lot of connections between Soft-Matter and Biology. Unfortunately when I started to see very clear these links I did not have the time to return to the puzzle of "Pollen growth in high magnetic fields". I hope that one day I will guide a Biology student through the Physics of this project.

It was a visit to the Organic Chemistry Department that clearly set me on the track of the present work. After a nice discussion with a group of very open and enthusiast chemists I got a little cuvette with one milligram of Crown Ether

Substituted Phthalocyanines. I have to say that when I reach back to my office I was already very worried about the things I could do with so little of a sample. But with the help of Hans, Alan and Prof. Nolte, it all went fine (they even gave me some more Phthalocyanine). Thank you very much for your continuing support ever since.

I still went astray from time to time, but since the Phthalocianines episode I knew to what sort of a thesis I was heading toward. Some oscillatory chemical reactions, magnetic levitation and the filming of it, water drops and their bubbles, plants or microorganisms growing in magnetic field, distracted my attention and segmented the present work. About all these, I think they enlarged a lot my scientific horizon.

About the end of my second year I was well set on my Ph.D. course, I had a functional set-up and even got some nice results. But I was still looking for an interesting related subject to test my set-up (and finish my thesis). In a perfect timing, Karin, Alf and Prof. Stelzer from Graz University contacted our lab about a possible experiment. I was assigned to be their local support and so I got in contact with the lovely field of Side Chain Liquid Crystals. I am very happy about this ongoing collaboration. The worse in this long series of experiments was the 160°C silicon oil violently spilling and its endless cleaning after. The best of it started just five minutes after the oil, when we saw that the sample was a total success; it is still lasting. A great thank you.

About a year later I had the great opportunity to host Prof. Robert Richardson for a week of experiments in the same field of Side Chain Polymer Liquid Crystals. The long measurement nights were the perfect occasion to ask all my questions about the field. Thanks a lot Robert for our intense scientific discussions.

I am greatly thankful to Mee Wee and Abbas for introducing me to the Liquid Crystals area.

All these years long Hung and Lijnis gave me a fantastic help. Hung took great care of the data acquisition part of the experiments. If by now I can make these programs on my own is due to him. Lijnis took me over my worries about too little space inside the magnet and kindly helped me to design the sample holders I have used. Their mechanical finishing was Lijnis hand as well.

As a senior researcher Prof. Andrey Geim kept his door always open to students and I used this opportunity many times. He took me along for a lot of "stunt" experiments, he showed me how science and fun have to go together and most important, from him I learn to dream big.

The lad that took my appointed project, Fabio, proved from the very first day a nice fellow. Throughout the four years our paths in the lab went side by side. We even lived next door for a couple of years. Among a lot of nice memories, I have particularly enjoyed our great chats about the Latin spirit, warm countries, nice food and Kalapushkin, on short about our common Dutch frustrations.

Andrea, Alex and Sjoerd were experienced Ph.D students when I reached the magnet lab. They have introduced me to "the magnetic way" and explained me the lab subtleties. We also shared a lot of amazing table tennis matches. Cecilia, Maaike,

Freddy and Igor were my room colleagues; we shared the little logistic resources of our office and many nice moments. Kostia, Cecile, Robert and Erich, were great colleagues. Marijn, Jos P., Jan and Stef W., senior researchers in the lab, were always open to help. The technical staff of the lab: Henk, Stef O., Hung, Lijnis, Jos R., Harry, Adri and Klass admirably kept running well the complex machinery that the magnet lab is. Martha, Ine and Sylvie, the secretaries of our group, took good care in all the organization details. To the whole maglab family many thanks for the years we were together.

I owe a lot of nice time to the Photoacoustic group of the Department of Molecular and Laser Physics, (where my wife is working). Frans, Cor, Simona, Sacco, Luc-Jan, Stefan and Tim adopted me completely in their group, for lunches, bowling, canoeing and a lot of other social events.

The Dutch administrative system is well organized but still very difficult when you do not know it. Mr. Claassen and Ms. van Hout from the personnel department helped me over many bureaucratic hurdles.

I would like to express my gratitude to the people from the mechanical and glass workshops of the university for their continuous and professional help. A special word of thanks to Ferry: with great pedagogic skills and original solutions he helped me thoroughly in my mechanical adventures at the self-service mechanical workshop.

In January 2002, I have finished my contract but the manuscript of the thesis was yet to be finished. When I needed the most Prof. Theo Rassing gave me the opportunity to continue as a postdoctoral researcher in the group of EVSF2, just one floor above my old office. This let me finish the manuscript and the lengthy procedure associated in a seamless effort. I am greatly thankful to Theo and to the people from EVSF2, here I found a new home and a warm group of new colleagues.

A big "Thank you!" to Markus, Albert and Luc-Jan for the Dutch translation of the Summary of this thesis, the Samenvatting section.

I have always thought to the Nijmegen period as a continuation of the year I have spent in Trieste as a diploma student. A strong theoretical understanding of Physics and an introduction to the international character of science (I was colleague with 30 young physicists from 28 countries) were the special gifts the International Centre for Theoretical Physics gave me. They helped me a lot during this thesis – thank you very much dear ICTP.

As a Ph.D. student I had the opportunity to attend a lot of scientific meetings. They inspired me for many of the ideas present in this thesis. A kind word of thanks to the fine people I have met at these conferences.

On Fridays, during the lunch break, I used to play football, together with a bunch of admirable fellows, colleagues from all over the science faculty. Thank you all, I have enjoyed a lot. A special thanks to the senior members of the club: Roeland, Paul and Peter. (More than counterintuitive, there were only four Fridays in five years that it rained during our football matches.)

The wonderful vacations spent together with Isabelle, Hervé and Pierre Marius offered me a lot of pleasant and relaxing moments. Merci beaucoup chers amis.

Anca, Tibi, Nico, Lulu, the "Romanian Community" and the Muzenplaats group were of great support and always open to big times. Mulţumesc, Grazie, Merci, Bedankt, Спасибо.

Hand in hand, always next to me for all these years was Iulia, my wife. With love, understanding and reciprocal help we managed our way without to feel the real toughness of this period. Long nights and weekends were the only allowed time to operate the magnet for experiments, but we used to joke about the advantages of experimental nights: "I could work till late in the morning and still be home early". As a family, these years have given us the most precious gift a parent can get. Our daughter, Anamaria, is now three years and seven months. She knows already how a physics lab looks like, she puts a lot of questions about all is to be seen there but still she is more impressed by the shinny wending machine from the end of the corridor. Dragele mele Iulia şi Anamaria, vă mulţumesc din suflet şi vă iubesc tare. Privesc cu incredere spre viitor - impreună vom reuşi oriunde paşii ne vor purta.

In timpul realizării acestei teze părinţii şi restul familiei mele au fost la 2000 de kilometri distanţă. In ciuda acestei mari depărtări i-am simţit alături de mine şi i-am purtat mereu in suflet. Mama şi tata m-au ajutat şi mi-au susţinut paşi catre o educatie ştiinţifică. Cu dragoste parintească, cu tact pedagogic sau cu alte "metode adecvate" au indrumat copilul rebel ce am fost către ziua de azi. Vă mulţumesc din inima dragi părinţi. Sora mea, Gabi, care mi-a inspirat pasiunea pentru fizică, buni Vica, bunu' Gigi, Roxi, Andrei şi Tibi mi-au oferit un suport important şi m-au incurajat continuu pe tot parcursul realizării acestei teze. Vă mulţumesc frumos dragii mei.

I came to Nijmegen fascinated by the idea of time reversal symmetry breaking by a magnetic field. After four years of interesting scientific pursuits I left the magnet lab more puzzled and ever wondering about the mythical Moses. In front of the Red Sea, did he have any thoughts about the "Moses Effect[i]"? I will always remember with nostalgia the times when I had the diamagnetic levitation at my "finger tips".

Marius Boamfă

Nijmegen, February 4, 2003.

---

[i] By making use of strong magnetic fields combined with strong magnetic field gradients the Red Sea splitting can be reproduced nowadays in laboratory, (although the available fields limit the experiment to the size of a dinner plate). The "Moses Effect" name was coined by a group of enthusiast Japanese researchers, but this happened only after they comment over the experiment uniqueness: "It does not look like anything we could think of!"

Table of Contents

Chapter 1

Introduction

Self-assembly and self-organization at molecular level is an intrinsic property of many materials, originating from the complex interplay of molecular interactions and thermal fluctuations. In the past decades the application of self-assembly has began to play a growing role in material engineering [1] and micro/nano-devices design [2-4]. Utilizing the self-organization of matter involves the collaborated efforts of disciplines such as molecular chemistry, physics, biology and engineering, with potential applications covering a wide range, from materials with novel mechanical properties [5], to digital data storage [6,7], non-linear optical devices [8,9], photographic and dye industry, flat display technologies [10] and molecular electronics [11]. With successes like the Kevlar[®] [12,13], the Liquid Crystal display [14], the Compact Disc on organic support [15] or the Carbon nano-tubes [16], to name just the most popular ones, the pay back of this interdisciplinary efforts are just beginning to take shape.

Liquid Crystals [17], Polymer Liquid Crystals [18,19] and Molecular Aggregates [20,21] are a few examples of systems that are currently being extensively studied in the acerb race for ever better material or faster devices.

Discovered at the end of the last century (1888 - Reinitzer), Liquid Crystals were considered an oddity with only pure academic value until about 30 years ago, when they were first considered for use in display technology. Nowadays they occupy a rapidly growing multi billion dollar a year market. This huge change was triggered

once the Liquid Crystallinity has been correctly understood as a form of orientational self-assembly and that the orientation of the molecules in a mesophase can be directed by the application of an external field.

The idea to combine the Liquid Crystals with Polymers dates as far back as 1922 (Staundinger and Vorlander), but it took another half of century until functionality was reached (1970 - Jackson at Eastman Kodak laboratories). At present Polymer Liquid Crystals is a well-established class of materials, which combines the useful and versatile properties of polymers with the self-organization of liquid crystals. Ironically, it was only after the Kevlar® success has made it around the world that the true nature of the spider web was uncovered [22].

Molecular aggregates are intermediate structures between single molecules and pure crystals and are formed by self-assembly of molecules in solution at high concentrations. They are best known for their two hundred-year-old tradition in the photographic industry, but as realized only recently they are also omnipresent in most photo-biological processes. Once again, the complex structure-function relationship found throughout nature is being slowly uncovered.

A large number of techniques are currently used to study and engineer the (Polymer) Liquid Crystals and Molecular Aggregates, such as surface fields [23,24], electric fields [25,26], mechanical fields [27], flow field [28,29] or polarized ultraviolet light [30]. Each of these methods has its own advantages and limitations, but better and novel methods are still very actively pursued.

One new approach is the use of magnetic fields, which can be favorably used to induce molecular ordering. They provide a unique combination of advantages, in particular a clean, contact-free method, which does not induce thermodynamic instabilities or create electrostatic charges, which works equally well for films and bulk samples. However, despite these significant advantages the technique has not been well studied or employed.

The present thesis deals with the use of *magnetic fields* as a handle to manipulate matter at a molecular level and as a tool to probe molecular properties or inter molecular interactions. The work consists of *in situ* optical studies of (polymer) liquid crystals and molecular aggregates in high magnetic fields up to *20T*, together with a description of the methods and set-ups developed and the theoretical interpretations of the obtained results.

Chapter 2 gives a general treatment of the magnetic field induced orientation mechanism and shows how this effect can be described in the frame of the Boltzman Statistics. More specifically, the Liquid Crystals, Polymer Liquid Crystals and Molecular Aggregates systems are studied in the presence of magnetic fields. The

chapter continues with a presentation of the set-ups developed and used for the purpose of this thesis and it ends with a section of data analysis methods.

Chapter 3 describes the magnetic field induced alignment of Side Chain Polymer Liquid Crystals and the particular role of the mesogen/backbone coupling in this phenomenon. Chapter 4 focuses on the Isotropic-Nematic phase transition of Side Chain Polymer Liquid Crystals in magnetic fields, an example of nonlinear physical phenomena: the magnetic field produces an energetic effect much larger that the direct energy it introduces into the system. Chapter 5 presents a study of thin Liquid Crystals cells in magnetic fields, discussing the effect of magnetic field on the surface anchoring and presents the first direct observation of a surface Isotropic-Nematic transition. Finally, Chapter 6 deals with Molecular Aggregates solutions in the presence of magnetic fields; a combined study of magnetic field induced orientation and system characterization.

References

[1] M. Ashby & D.R.H. Jones, *Engineering Materials 2: An Introduction to Microstructures, Processing and Design*, 2nd ed., Butterworth & Heinemann press, Oxford 1998.

[2] K.E. Drexler, *Nanosystems: molecular machinery, manufacturing, and computation*, John Wiley & Sons, 1992.

[3] B.C. Crandall, *Nanotechnology*, MIT Press,1996.

[4] D. Darling, *Beyond 2000: Micromachines and Nanotechnology : The Amazing New World of the Ultrasmall*, Scott Foresman, 1995.

[5] M. Ashby & D.R.H. Jones, *Engineering Materials 1: An Introduction to Their Properties and Applications*, 2nd ed., Butterworth & Heinemann, Oxford 1996.

[6] P.M. Lundquist, C. Poga, R.G. DeVoe, et al., *Optics Letters* **21**, 890,1996.

[7] M. Sawodny, *Makromolekulare Chemie* **46**, 217, 1991.

[8] G.J. Ashwell, *Organic Materials for Non-Linear Optics*, Springer Verlag, 1993.

[9] J.C. Dubois, et al., *Liquid Crystals* **14**, 197, 1993.

[10] L.E. Tannas Jr. et al., *Flat-Panel Display Technologies*, Noyes Publications, 1995.

[11] J. Jortner, M.A. Ratner, IUPAC, *Molecular Electronics*, Blackwell Science Inc., 1997.

[12]   G. Epstein, E. F. Bushman and F. D. Tabrisky, *Kevlar Composites*, TC Pub., 1980.

[13]   H. H. Yang, *Kevlar Aramid Fiber*, John Wiley & Sons, 1993.

[14]   E. Lueder & E. Lauder, *Liquid Crystal Displays: Addressing Schemes and Electro-Optical Effects*, John Wiley & Sons, 2001.

[15]   H. Nakajima, H. Ogawa, Compact Disc Technology, IOS Press,1993

[16]   M.S. Dresselhaus, G. Dresselhauss and P.Avouris, *Carbon Nanotubes: Synthesis, Structure, Properties and Applications*, Springer Verlag, 2001.

[17]   P. G. de Gennes and J. Prost, *The Physics of Liquid crystals,* 2nd ed.*,* Clarendon Press, Oxford, 1993.

[18]   A. Ciferri, W. R. Krigbaum and R. B. Meyer, in *Polymer Liquid crystals,* Academic Press, New York, 1982.

[19]   A. M. Donnald, and A. H. Windle, *Liquid Crystalline Polymers*, Cambridge University Press, Cambridge, 1992.

[20]   S. Elmau, *Organic Molecular Aggregates*, Springer Verlag, 1983.

[21]   T. Kobayashi, *J-Aggregates*, World Scientific, Singapore, 1996.

[22]   In 1964 at Textile lab of Dupont, Stephanie Kwolek made the first fibers of what appeared on the market in 1975 as Kevlar[®]. About a decade later the chemical structure of the web spider was found to be somehow similar, although much better structurally engineered by nature.

[23]   J.S. Patel & H. Yokohama, Nature **362**, 525, 1993.

[24]   V.N. Raja et al., *Liquid Crystals* **20,** 41, 1996.

[25]   H.S. Kitzerow, H. Molsen and G. Heppke, *Applied Physics Letters* **60**, 3093, 1992.

[26]   R.B. Findlay and A.H. Windle, *Molecular Crystals and Liquid Crystals* **206**, 55, 1991.

[27]   Y. Zhao, P. Roche and G.X. Yuan, *Macromolecules* **29**, 4619, 1996.

[28]   Z.R. Chen et al., *Science* **277**, 1248, 1997.

[29]   C. Pujolle-Robic and L. Noirez, *Nature* **409**, 167, 2001.

[30]   N. Kawatsuki, T. Yamamoto and H. Ono, *Applied Physics Letters* **74**, 935, 1999.

Chapter 2

Molecules in Magnetic Field: Fundamental Aspects and Experimental Methods

2.1 Magnetic field induced orientation

A magnetic field influences the orbital motion of electrons, which leads to an induced magnetic moment, $\vec{m}$, that at its turn interacts with the applied magnetic field [1]. Due to this mechanism, every molecule subjected to a magnetic field, B, acquires an extra energy [2]:

$$E_B = -\vec{m} \cdot \vec{B} = -\frac{\chi \cdot B^2}{N_A \cdot \mu_o} \tag{2.1}$$

where χ is the molar magnetic susceptibility tensor, μ_o the magnetic permeability of vacuum and N_A the Avogadro number. For $B = 1\,T$ the typical energy per molecule is in the range of $E_B \approx 10^{-27}\,J$. For almost all molecules χ exhibits anisotropy [2], (see table 2.1), $\Delta\chi = \chi_{||} - \chi_{\perp}$, where the indices $||$ and $\perp$ denote the magnetic susceptibilities parallel and perpendicular to the molecular axis. This anisotropy gives rise to an orientation dependent energy and forces molecules to align with respect to the magnetic field direction in such a way that the magnetic

energy is minimized. Because of the thermal fluctuations, the actual orientation of a molecule in magnetic field is described by an orientation distribution function, given by the Boltzman statistics:

$$f(\theta) = exp\left(-\frac{|\Delta\chi|\cdot B^2}{N_A \cdot \mu_o} \cdot \frac{1}{kT} \cdot sin^2\theta \right) \qquad (2.2)$$

for molecules with $\Delta\chi > 0$, that align their symmetry axis along the magnetic field direction, and:

$$f(\theta) = exp\left(-\frac{|\Delta\chi|\cdot B^2}{N_A \cdot \mu_o} \cdot \frac{1}{kT} \cdot cos^2\theta \right) \qquad (2.3)$$

for molecules with $\Delta\chi < 0$, that orient their main axis perpendicular to the magnetic field, where θ is the angle between the magnetic field and the symmetry axis of the molecule, fig.2.1. Please note that χ is a negative quantity for diamagnetic molecules.
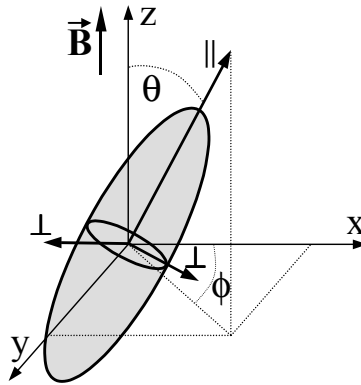

Figure 2.1 *Schematic representation of a molecule in magnetic field*

The typical values of $\Delta\chi$ given in table 2.1, show that the magnetic field induced alignment of individual molecules is a very small effect. However in the case of collective molecular behavior, such in molecular aggregates or liquid

crystalline phases, the magnetic field energy gain may become comparable with the thermal fluctuations, allowing important degree of orientation to be achieved.

Bond	$\Delta\chi = \chi_{\|} - \chi_{\perp}$		$\frac{\Delta\chi \cdot B^2}{N_A \cdot \mu_o} \cdot \frac{1}{k_B \cdot T}$,
	$[10^{-6} \cdot cm^3/mol]_{cgs}$	$[10^{-10} \cdot m^3/mol]_{SI}$	$[T = 300K, B = 20T]$
$C - C$	-1.3	-0.16	$2.08 \cdot 10^{-6}$
$C = C$	+8.2	+1.03	$1.36 \cdot 10^{-5}$
$C \equiv C$	+37	+4.6	$5.93 \cdot 10^{-5}$
$C = O$	+6.6	+0.82	$1.06 \cdot 10^{-5}$
Benzene ring	-59.7	-7.5	$0.96 \cdot 10^{-4}$

Table 2.1 *The anisotropy of the diamagnetic susceptibility, $\Delta\chi$, for some of the most common chemical bonds* [3-6].

In this case the orientation distribution function becomes:

$$f(\theta) = exp\left(- N_\xi \cdot Q \cdot \frac{|\Delta\chi| \cdot B^2}{N_A \cdot \mu_o} \cdot \frac{1}{kT} \cdot sin^2\theta \right) \quad \text{for} \quad \Delta\chi > 0 \qquad (2.4)$$

or:

$$f(\theta) = exp\left(- N_\xi \cdot Q \cdot \frac{|\Delta\chi| \cdot B^2}{N_A \cdot \mu_o} \cdot \frac{1}{kT} \cdot cos^2\theta \right) \quad \text{for} \quad \Delta\chi < 0 \qquad (2.5)$$

where N_ξ is the number of molecules acting collectively and Q describes the strength of the collective behavior, $0 \le Q \le 1$. In the case of (polymer) liquid crystal systems, Q is the local order parameter [7,8], which describes the mesophase[i], see sect.2.3. For the case of molecular aggregates Q , is a geometrical factor which describes the relative orientation of molecules within the aggregate structure [9], see sect.2.6.

---

[i] Mesophase – liquid crystalline phase.

2.2 From Orientation order to optical anisotropy

In the absence of macroscopic order the optical properties of a given media are isotropic, being described by the scalar refractive index $n = \eta + i \cdot \kappa$, with η and κ its real and respective imaginary part [10].

Light propagating through such a medium, fig.2.2 and [10], is described by:

$$I(\lambda) = I_o(\lambda) \cdot exp\left(-\frac{4 \cdot \pi \cdot \kappa}{\lambda} \cdot x - i \cdot \frac{4 \cdot \pi \cdot \eta}{\lambda} \cdot x \right) \qquad (2.6)$$

with I_o the initial light intensity, λ the light wavelength, x the sample thickness and I the final light intensity.
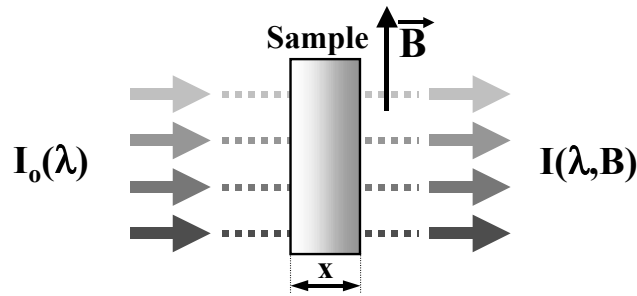
Figure 2.2 *Schematic propagation of light trough a sample subjected to a magnetic field.*

When order is present (or induced), the medium becomes anisotropic and the index of refraction is described by a tensor, if the dielectric properties of the component molecules are anisotropic. Schematically:

$$\Delta \chi \xrightarrow{\ B\ } ind.\ order \xrightarrow{molecular\ dielecric\ anistropy} macroscopic\ optical\ anisotropy$$

The light propagation equations for a medium in a magnetic field therefore become:

$$\begin{cases} I_{||}(\lambda, B) = I_o(\lambda) \cdot exp\left[-\dfrac{4 \cdot \pi \cdot \kappa_{||}(B)}{\lambda} \cdot x - i \cdot \dfrac{4 \cdot \pi \cdot \eta_{||}(B)}{\lambda} \cdot x \right] \\ I_{\perp}(\lambda, B) = I_o(\lambda) \cdot exp\left[-\dfrac{4 \cdot \pi \cdot \kappa_{\perp}(B)}{\lambda} \cdot x - i \cdot \dfrac{4 \cdot \pi \cdot \eta_{\perp}(B)}{\lambda} \cdot x \right] \end{cases} \qquad (2.7)$$

where the $||$ and $\perp$ indices denote the light polarization being parallel and perpendicular to the magnetic field. The optical properties of the medium are obtained from the averaging of the molecular contributions, using the Boltzman statistics [11-13]. The cases for liquid crystals and molecular aggregates solutions are described in detail in sect.2.3 and 2.6 respectively.

The change in the real part of the refractive index, is called the magnetic field induced birefringence and can be described:

$$b(B) = \frac{2 \cdot \pi \cdot \Delta\eta(B) \cdot x}{\lambda} \qquad (2.8)$$

i.e., the retardation between the ordinary and extraordinary waves. In the limit of low induced alignment, the magnitude of the retardation is proportional to B^2 and the effect is known as the Cotton-Mutton effect [14].

A change in the imaginary part of the refractive index is referred to as the magnetic field induced linear dichroism [10,15], and is usually characterized by the field induced dichroic ratio:

$$D(B) = \frac{\kappa_{||}(B)}{\kappa_{\perp}(B)} \qquad (2.9)$$

In media formed by chiral molecules or supramolecular chiral structures, the magnetic field can also induce circular birefringence or circular dichroism, corresponding to preferential retardation or absorption of circularly left and right polarized light.

2.3 Local order, domain orientation and optical anisotropy of Liquid Crystals in magnetic fields

The morphology of Polymer Liquid Crystals, (PLC), or Liquid Crystals, (LC), in thin cells consists of microscopic domains, which are strongly ordered locally, but have a randomly distributed orientation relative to each other, see fig.2.3 and fig.2.4.
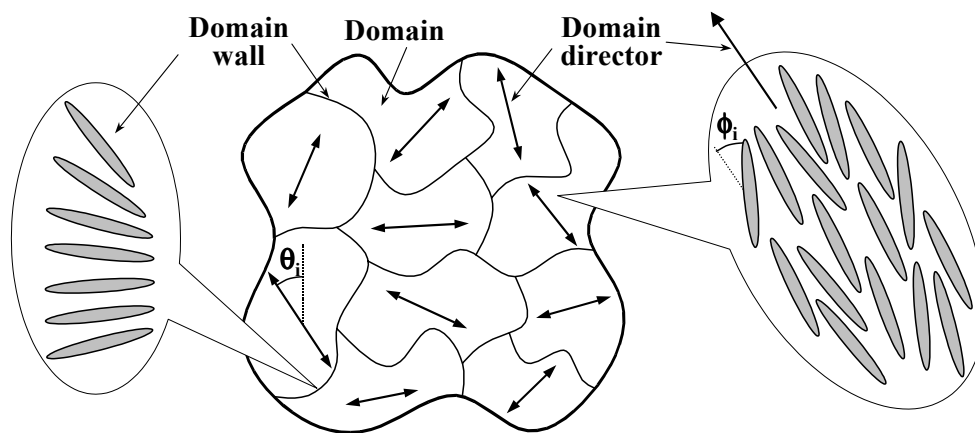

Figure 2.3 *Schematic representation of the morphology found in SCPLCs and thin LC cells. Pictorial representation of mesogen arrangement in a domain, side right, and in a domain wall, side left.*

The local order is due to the liquid crystalline behavior of the mesogens[ii], while the different domain morphology is due to the properties of the macroscopic mesophase [16]. When undergoing the isotropic-nematic transition, in a macroscopic sample, many nucleation centers are formed, as nematic islands, which are in equilibrium with the surrounding isotropic phase. In the absence of any perturbing external field, the orientation of the local direction in these nematic islands is unperturbed, as long as they are far apart. As the transition evolves, the islands grow in size, which brings them closer together. When the local director has a different orientation in neighboring islands this costs extra elastic energy at the boundary, therefore the islands tend to rotate their directors, in order to minimize the elastic

---

[ii] Mesogen – molecule capable of forming liquid crystalline phases.

energy. If this rotation does not cost energy, the process occurs throughout the sample and the final nematic phase is a monodomain. This situation is found in bulk samples of low molecular weight liquid crystals.
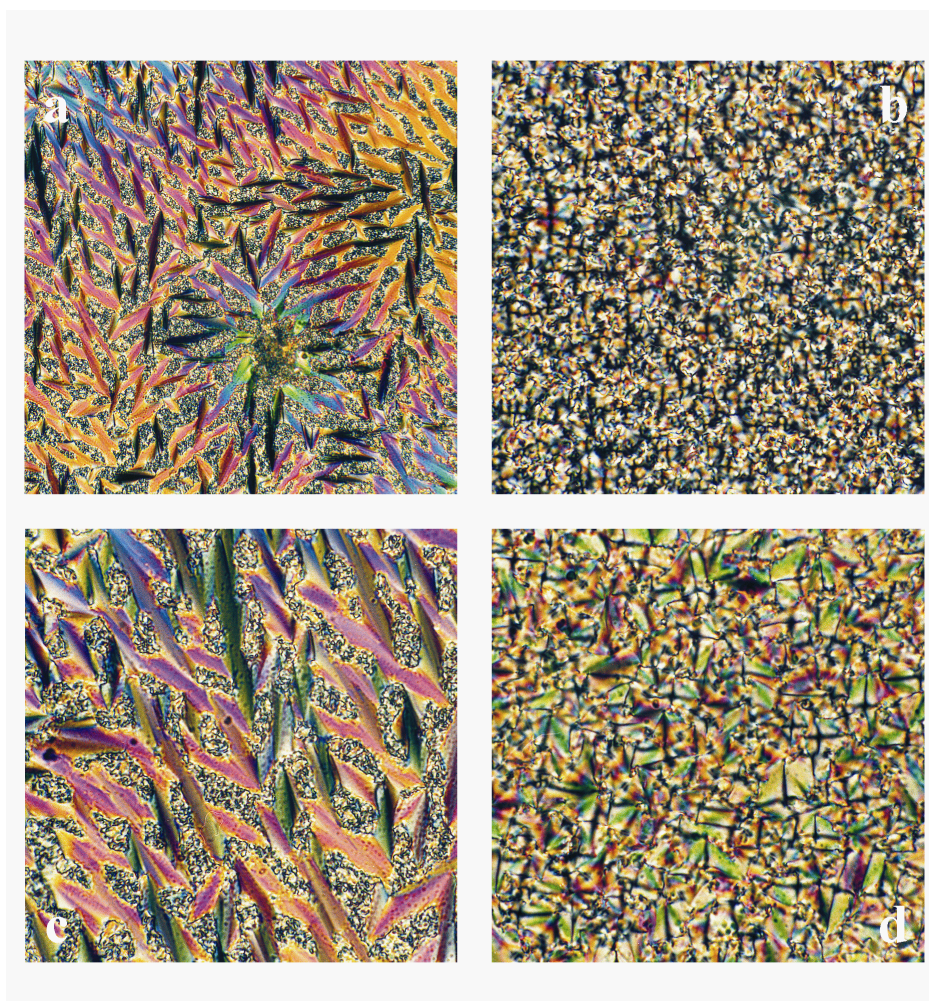
Figure 2.4 *Domain structures in SCPLCs, visualized by crossed polarizer microscopy. **(a)**. $200 \times 200 \mu m$ photo of a $10 \mu m$ thick C5 sample **(b)**. $200 \times 200 \mu m$ photo of a $10 \mu m$ thick B4 sample. **(c)**. $100 \times 100 \mu m$ photo of a $10 \mu m$ thick C5 sample **(d)**. $100 \times 100 \mu m$ photo of a $10 \mu m$ thick B4 sample. (For C5 and B4 chemical formulas and characteristics see Chapter 3)*

However when the rotation of the nematic islands is not energy free, their initial orientation is preserved and the director changes its orientation only over a finite length, the domain wall. This is a compromise solution, which is the result of a balance between the energy lost due to rotated volume and the lowering of the elastic energy. This behavior is found in thin LC cells, where the nematic islands rotation is hindered by surface anchoring and in Side Chain Polymer Liquid Crystals, (SCPLCs), where the mesogen-backbone coupling impends the free rotation of the nematic domains, see fig.2.3 and fig.2.4. The degree of order in a sample with different domains can be described by the total order parameter [17,18]:

$$Q = Q_D \cdot Q_N \qquad (2.10)$$

which is a combination of the local order parameter, Q_N [18,19], and the domain order parameter, Q_D. The local order parameter, nematic order in our case, describes the strength of the local correlation among the molecules within a given domain.

The presence of an applied magnetic field influences the total degree of order. The magnetic field effect is small at the level of individual molecules, (see sect.2.1), and thus does not affect the local order:

$$Q_N \neq Q_N(B) \qquad (2.11)$$

Q_N is therefore only temperature dependent. Using the angular notation from fig.2.3 the nematic order parameter is given by:

$$Q_N = \frac{3 \cdot \langle cos^2 \phi_i \rangle - 1}{2} \qquad (2.12)$$

where the angle ϕ_i describes the orientation of the symmetry axis of individual molecules relative to the domain director, fig.2.3.

The domain order parameter describes the orientation of individual domains as a whole, with respect to a given axis, in our case the magnetic field direction:

$$Q_D = \frac{3 \cdot \langle cos^2 \theta_i \rangle - 1}{2} \qquad (2.13)$$

where the angle θ_i describes the orientation of individual domain directors with respect to the magnetic field direction, fig.2.3. The average in eq.(2.13) involves the orientation distribution function, $f(\theta)$:

$$\langle cos^2\,\theta \rangle = \frac{\int f(\theta) \cdot cos^2\,\theta \cdot sin\theta \cdot d\theta}{\int f(\theta) \cdot sin\theta \cdot d\theta} \tag{2.14}$$

where $f(\theta)$ accounts for the statistical description of domain orientation in the magnetic field, given by eq.(2.4) for $\Delta\chi > 0$ and respectively eq.(2.5) for $\Delta\chi < 0$.

The case of $\Delta\chi < 0$ is specific for discotic-like molecules, where the symmetry axis is orthogonal to the molecular plane. The molecules prefer to orient their molecular planes parallel to each other and parallel to the magnetic field. Therefore it is preferable to describe the relative molecular orientation and the magnetic field induced alignment with help of the $(90° - \phi_i)$ and $(90° - \theta_i)$ angles, rather than ϕ_i and θ_i. This mathematical choice ensures that the two order parameters comply with the condition $0 \le Q \le 1$.

Within this convention [20] the local order parameter for discotic molecules is:

$$Q_N = \frac{3 \cdot \langle sin^2\,\phi_i \rangle - 1}{2} \tag{2.15}$$

and the director order parameter is given by:

$$Q_D = \frac{3 \cdot \langle sin^2\,\theta_i \rangle - 1}{2} \tag{2.16}$$

The dependency of the total order parameter as function of the magnetic field is:

$$Q(B) = Q_D(B, Q_N) \cdot Q_N \tag{2.17}$$

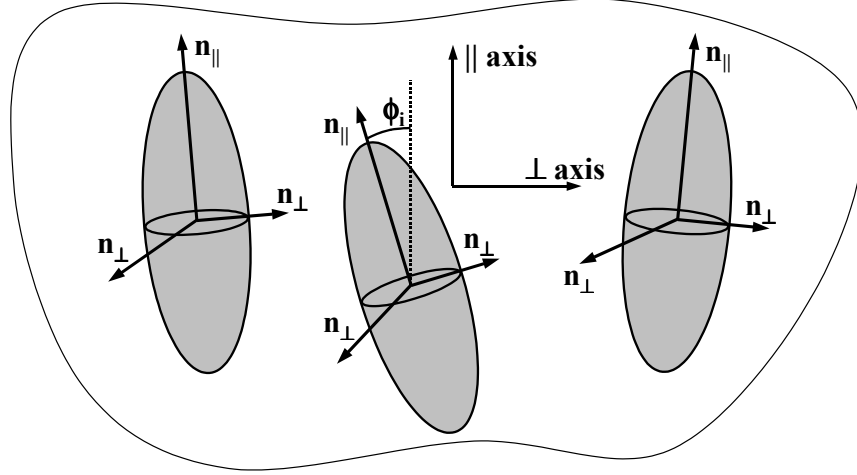Fig.2.5 shows how the optical properties of a domain can be determined considering all the molecular contributions.

Figure 2.5 *Molecular contributions to the optical properties of a domain, in its own reference frame, with the || axis along the domain director.*

Using the angular notation from fig.2.5 the quantities with which a molecule contributes to the domain refractive index can be written as:

$$|| \; axis \; contribution = n_{||} \cdot cos^2 \, \phi_i + n_\perp \cdot \left(1 - cos^2 \, \phi_i \right)$$
$$\perp \; axis \; contribution = n_{||} \cdot \left(1 - cos^2 \, \phi_i \right)/2 + n_\perp \cdot cos^2 \, \phi_i + n_\perp \cdot \left(1 - cos^2 \, \phi_i \right)/2$$

$$(2.18)$$

The $n_{||}$ and $n_\perp$ components are constant quantities, magnetic field independent, obtained from the dielectric tensor of individual molecules:

$$\begin{pmatrix} n_{||} & 0 & 0 \\ 0 & n_\perp & 0 \\ 0 & 0 & n_\perp \end{pmatrix} = \sqrt{\mu_r} \cdot \begin{pmatrix} \sqrt{\varepsilon_{r\,||}} & 0 & 0 \\ 0 & \sqrt{\varepsilon_{r\perp}} & 0 \\ 0 & 0 & \sqrt{\varepsilon_{r\perp}} \end{pmatrix} \qquad (2.19)$$

with μ_r the relative magnetic permeability and $\varepsilon_{||}$, $\varepsilon_\perp$ the dielectric tensor components in the molecule reference frame.

Considering the average contribution of all molecules present within a domain, by averaging of eq.(2.18), and using the local order parameter definition formula, eq.(2.12), the refractive index of a domain, n_N, in its own reference frame, with the $\parallel$ axis along the director, becomes:

$$n_N = \begin{pmatrix} n_{N\parallel} & 0 & 0 \\ 0 & n_{N\perp} & 0 \\ 0 & 0 & n_{N\perp} \end{pmatrix} =$$
$$= n_o \cdot (1 - Q_N) \cdot \begin{pmatrix} 1 & 0 & 0 \\ 0 & 1 & 0 \\ 0 & 0 & 1 \end{pmatrix} + \begin{pmatrix} n_{\parallel} & 0 & 0 \\ 0 & n_{\perp} & 0 \\ 0 & 0 & n_{\perp} \end{pmatrix} \cdot Q_N \qquad (2.20)$$

with:

$$n_o = \left(n_{\parallel} + 2 \cdot n_{\perp} \right) / 3 \qquad (2.21)$$

the isotropic refractive index.

Extending the treatment to include all the projection of individual domains, the total refractive index, n_{tot}, describing the optical properties of the whole sample, is given by eq.(2.22), in a reference frame with the $\parallel$ axis along the magnetic field and for the case of molecules with $\Delta\chi > 0$, that align parallel to the field direction.

$$n_{tot} = \begin{pmatrix} n_{tot\,\parallel} & 0 & 0 \\ 0 & n_{tot\perp} & 0 \\ 0 & 0 & n_{tot\perp} \end{pmatrix} =$$
$$= n_o \cdot (1 - Q_D \cdot Q_N) \cdot \begin{pmatrix} 1 & 0 & 0 \\ 0 & 1 & 0 \\ 0 & 0 & 1 \end{pmatrix} + \begin{pmatrix} n_{\parallel} & 0 & 0 \\ 0 & n_{\perp} & 0 \\ 0 & 0 & n_{\perp} \end{pmatrix} \cdot Q_D \cdot Q_N \qquad (2.22)$$

The optical anisotropy of the real part of the refractive index, measured experimentally as magnetic field induced birefringence, sect. 2.7 and 2.9, derived from eq.(2.22), is given by:

$$\Delta\eta_{tot}(B) = \eta_{tot\parallel}(B) - \eta_{tot\perp}(B) = \left(\eta_{\parallel} - \eta_{\perp} \right) \cdot Q_D(B) \cdot Q_N \qquad (2.23)$$

27

Molecules characterized by $\Delta\chi < 0$ align perpendicular to the magnetic field and therefore the total refractive index is expressed by:

$$
n_{tot} = \begin{pmatrix} n_{tot\parallel} & 0 & 0 \\ 0 & n_{tot\perp} & 0 \\ 0 & 0 & n_{tot\perp} \end{pmatrix} =
$$

$$
= n_o \cdot (1 - Q_D \cdot Q_N) \cdot \begin{pmatrix} 1 & 0 & 0 \\ 0 & 1 & 0 \\ 0 & 0 & 1 \end{pmatrix} + \begin{pmatrix} n_\perp & 0 & 0 \\ 0 & (n_\parallel + n_\perp)/2 & 0 \\ 0 & 0 & (n_\parallel + n_\perp)/2 \end{pmatrix} \cdot Q_D \cdot Q_N
$$

$$(2.24)$$

where the calculation is made in a reference frame with the $\parallel$ axis along the magnetic field.

In this case, the optical anisotropy of the real part of the refractive index, becomes:

$$
\Delta\eta_{tot}(B) = \eta_{tot\parallel}(B) - \eta_{tot\perp}(B) = \frac{\eta_\perp - \eta_\parallel}{2} \cdot Q_D(B) \cdot Q_N \qquad (2.25)
$$

2.4 Orientation order and light scattering

Due to the statistical nature of the magnetic field alignment process, the degree of induced order varies within the sample. The order fluctuations are directly related to refractive index fluctuations, which causes light scattering [7, 10, 21].

Light scattering is a process in which light interacts with matter. In the course of this process light scatters without appreciable change in wavelength, but with a random orientation [10]. The scattering affects the propagation of light through a medium by causing part of the initial intensity to be deflected from its initial direction. This process is polarization dependent and therefore anisotropic in the presence of magnetic field induced order.

In media where absorption is also present, the two contributions are difficult to be separated, which greatly hinders analysis of absorption spectra, except when light is absorbed resonantly, because the absorption is the only contribution to light losses.

2.5 Orientation ordering and light scattering in Side Chain Polymer Liquid Crystals

In the presence of magnetic fields the isotropic-nematic, (IN), transition of SCPLCs, offers a rich variety of orientation ordering and light scattering related phenomena.

In contrast with low molecular mass LC, where the IN transition takes place at a well defined temperature [7], the IN transition of SCPLCs is extended over a broad temperature range [22], where the isotropic and nematic component coexist at equilibrium, the so called biphasic region.

Fig.2.6 describes the succession of isotropic-biphasic-nematic phases of a SCPLC as the temperature changes. In the isotropic phase the SCPLCs behave as an ordinary liquids and its optical properties are described by an isotropic refractive index n_o. At the temperature corresponding to the beginning of the IN transition, nematic islands nucleates at equilibrium with the surrounding isotropic component, and grows in size as the temperature lowers.
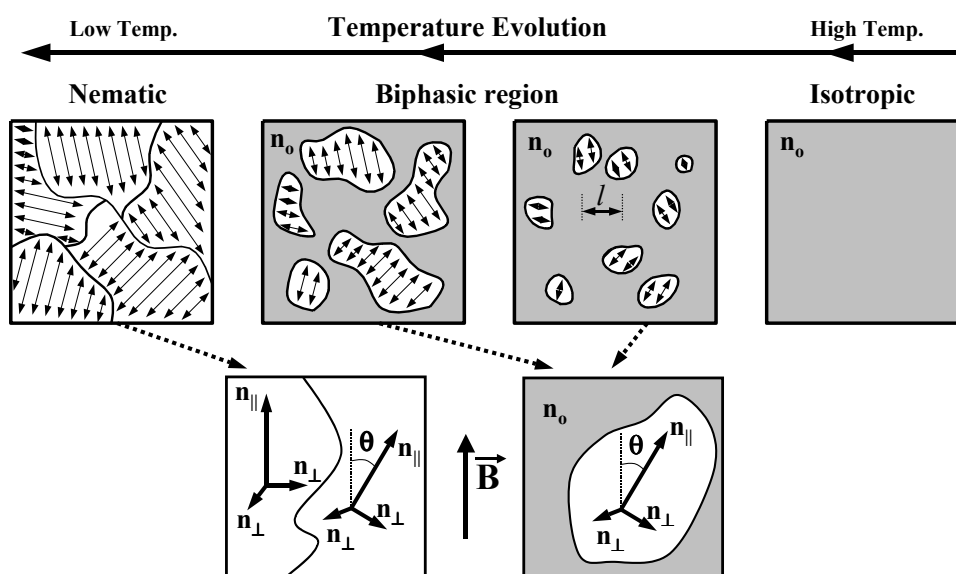

Figure 2.6 *The evolution of Polymer Liquid Crystals from the isotropic phase to the ordered nematic mesophase passes through a biphasic region, where the two phases coexist at equilibrium, upper part. Refractive index axes for a nematic island surrounded by an isotropic component and for two neighboring nematic domains, lower part.*

In the nematic phase the SCPLCs morphology consists in local domains, highly ordered but randomly oriented with respect to each other, unless an external field is applied. The nematic islands in the biphasic region and the nematic domains in the nematic phase are ordered entities and their optical properties are described by the tensor refractive index, n_N, see eq.(2.20).

Rayleigh found [23] the total scattered intensity due to a spherical particle, fig.2.7, of radius r and refractive index n_2, surrounded by a medium with n_1 refractive index, to be expressed by: $I_{scat} = I_o \cdot \alpha^2 \cdot (n_2 / n_1 - 1)^2$ where the notation $\alpha = 2 \cdot \pi \cdot r / \lambda$ and the approximation:

$$2 \cdot \left(\frac{n_2 - n_1}{n_1 + 2 \cdot n_2} \right)^2 \approx \left(\frac{n_2}{n_1} - 1 \right)^2 \tag{2.26}$$

(valid only for $n_2 / n_1 \leq 1.4$), are used.

Making use of this observation, any scattering medium can be described as a collection of individual scattering centers, with corrections for geometrical shapes different than spheres and polarization consideration accounted for.

Light, with initial intensity I_o, propagating through a media of refractive index n_1, suffers scattering losses $-dI_o = I_{scat}$ on each scattering center, of refractive index n_2.
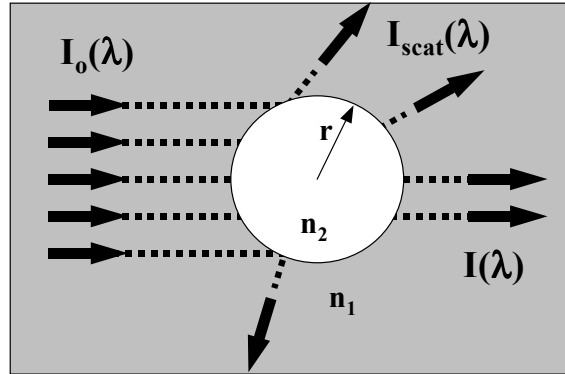

Figure 2.7 *Light scattering by a spherical particle as described by Rayleigh*

The total light, I, transmitted trough a media of optical path x, can be described by the solution of the differential equation (2.27):

$$-\frac{dI_o}{I_o} = \alpha^2 \cdot \left(\frac{n_2}{n_1} - 1\right)^2 \cdot \frac{dx}{l} \qquad (2.27)$$

with l the average distance between the scattering centers.
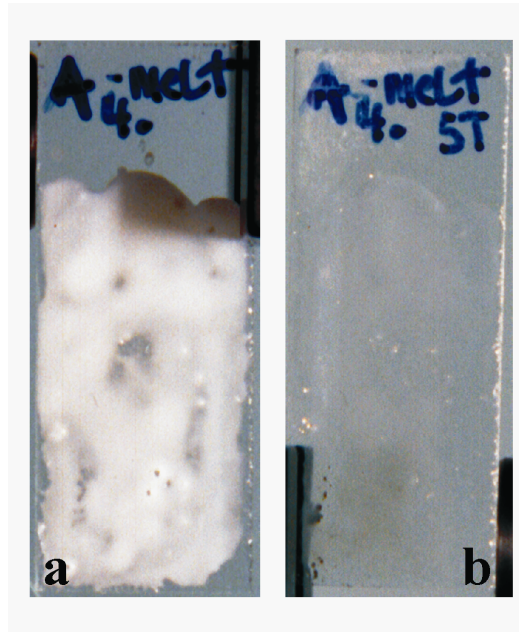
Figure 2.8 *Unaligned SCPLCs causes light scattering **(a)** while an ordered SCPLCs structure is transparent **(b)**. 100 µm thick film of a polyacrylate based SCPLCs sample before **(a)** and after **(b)** being oriented in a 5T magnetic field. See Chapter 3 for sample characterization and experimental details.*

In the above work frame, the light scattering of the biphasic region of a SCPLSc exposed to magnetic field, can be calculated by considering all possible orientation of the nematic islands with the probability given by the orientation distribution function, see eq.(2.4):

$$\left(\frac{\eta_{nematic}}{\eta_o} - 1\right)^2_{||} = \left[\frac{(\eta_{||} - \eta_o)\cdot Q_N}{\eta_o}\right]^2 \cdot <cos^2\theta> + \left[\frac{(\eta_\perp - \eta_o)\cdot Q_N}{\eta_o}\right]^2 \cdot \left(1 - <cos^2\theta>\right)$$

$$(2.28)$$

$$\left(\frac{\eta_{nematic}}{\eta_o}-1\right)^2_\perp = \left[\frac{(\eta_\| - \eta_o)\cdot Q_N}{\eta_o}\right]^2 \cdot \frac{1-<cos^2\theta>}{2} + \left[\frac{(\eta_\perp - \eta_o)\cdot Q_N}{\eta_o}\right]^2 \cdot \frac{1+<cos^2\theta>}{2}$$

$$(2.29)$$

By making use of $\eta_o = (\eta_\| + 2\cdot\eta_\perp)/3$ and $\Delta\eta = \eta_\| - \eta_\perp$ the total light propagating through a SCPLC sample of thickness x is given by:

$$I_\| \approx I_o \cdot exp\left[-\left(\frac{2\cdot\pi\cdot r}{\lambda}\right)^2 \cdot \left(\frac{\Delta\eta\cdot Q_N}{3\cdot\eta_o}\right)^2 \cdot (1+3\cdot<cos^2\theta>)\cdot\frac{x}{l}\right] \quad (2.30)$$

$$I_\perp \approx I_o \cdot exp\left[-\left(\frac{2\cdot\pi\cdot r}{\lambda}\right)^2 \cdot \left(\frac{\Delta\eta\cdot Q_N}{3\cdot\eta_o}\right)^2 \cdot \frac{5-3<cos^2\theta>}{2}\cdot\frac{x}{l}\right] \quad (2.31)$$

with the $\|$ or $\perp$ indices describing the polarization of the incoming light to the magnetic field direction, θ the angle describing the orientation of the local nematic director, (see fig.2.6), and $\Delta\eta\cdot Q_N$ the refractive index anisotropy for the nematic islands.

Only the real part of the refractive index has been considered, as almost all LCs do not absorb light in the visible spectrum and molecules are considered to align parallel to the magnetic field direction, $\Delta\chi > 0$.

However, toward the end of the biphasic region, when $l \approx \xi$ and $r \approx \xi$, there is a cross over to a different regime, where no isotropic component is present, this regime can be described by:

$$I_{\|,\perp} \approx I_o \cdot exp\left[-\left(\frac{\pi\cdot\xi}{\lambda}\right)^2 \cdot \psi_{\|,\perp} \cdot \frac{x}{\xi}\right] \quad (2.32)$$

with:

$$\psi_\| = A_D^2 \cdot \left[<cos^2\theta>^2 + (1-<cos^2\theta>)^2\right] +$$
$$+ <cos^2\theta> \cdot (1-<cos^2\theta>)\cdot\Delta\eta^2 \cdot \left(\frac{1}{\eta_\|^2} + \frac{1}{\eta_\perp^2}\right) \quad (2.33)$$

$$\psi_\perp = \frac{A_D^2}{4} \cdot \left[\left(1 + <cos^2\theta> \right)^2 + \left(1 - <cos^2\theta> \right)^2 \right] +$$

$$+ \frac{\left(1 + <cos^2\theta>\right)}{4} \cdot \left(1 - <cos^2\theta>\right) \cdot \Delta\eta^2 \cdot \left(\frac{1}{\eta_{||}^2} + \frac{1}{\eta_\perp^2} \right) \qquad (2.34)$$

Figure 2.9 *Light scattering by SCPLCs in the biphasic region (**a**) and in the nematic phase (**b**). Numerical implementation of the eq.(2.30-2.34) for a sample thickness corresponding to 100 scattering centers, with* $\eta_{||} = 1.5$ *,* $\eta_\perp = 1.3$ *, with the number of molecules in the average correlation volume,* N_ξ *, corresponding to* $N_\xi \cdot Q_N \cdot \Delta\chi \cdot B^2 / k \cdot T = 150$ *, for* $B = 20T$

where $A_D = \langle cos^2\theta - \langle cos^2\theta \rangle \rangle$ is the amplitude of the director order fluctuations and ξ is the average correlation length, which describes the ordered mesophase.

Even though the formulas tend to become very lengthy, simple conclusions can be readily reached. As shown in fig.2.9, the biphasic region scatters light even when magnetic field orients the director of the nematic islands, while the pure nematic phase becomes less scattering as the nematic domains are aligned along a common direction, with no scattering limit for the case of perfect monodomain alignment. The experimental observations, (see fig.2.8), fully support these predictions.

33

2.6 Orientation ordering, absorption and light scattering in

molecular aggregate solutions

Molecular aggregates, MA, are ordered structures formed by self-assembling of molecules in solution at high concentration [24], fig.2.10, and have intermediate properties between single molecules and pure crystals.

Within an aggregate, molecules are arranged in a defined structure [9], due to Van der Waals or $\pi-\pi$ interaction cohesion forces. As entities, MA have symmetries axes, defined by the internal molecular arrangement, but in the absence of an external applied field, they are randomly oriented in solution.
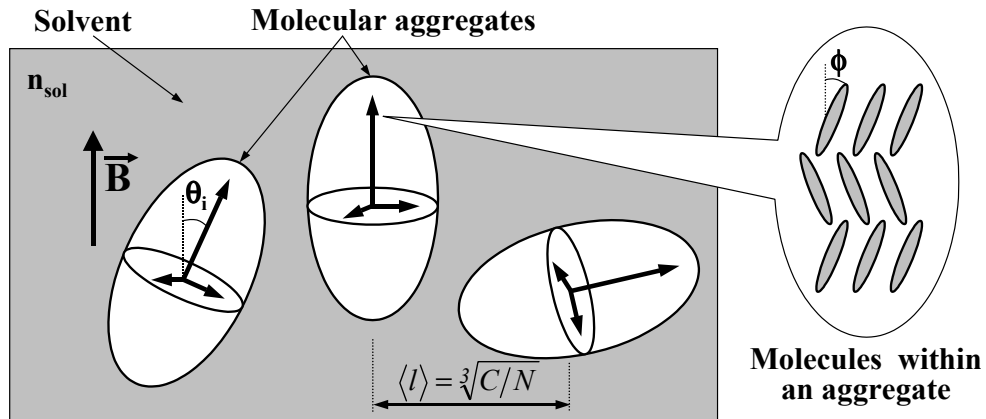
Figure 2.10 Molecular aggregate solution with a representation of molecular arrangement within an aggregate, right inset.

The presence of a magnetic field induces orientation ordering in the MA solution, (see sect.2.1). The statistical angular distribution of the aggregates with respect to the magnetic field direction is described by the orientation distribution function, $f(\theta)$, see eq. (2.4) and (2.5).

The local order parameter, Q_L, describing the molecular arrangement within a MA is given by:

$$Q_L = \frac{3 \cdot \cos^2 \phi - 1}{2} \tag{2.35}$$

Where ϕ is the angle between the symmetry axis of the molecule direction and the symmetry axis of the MA, note that no average is required because the molecular arrangement is well defined and is not statistical.

The molecular aggregate order parameter:

$$Q_{MA}(B) = \frac{3 \cdot \langle cos^2\,\theta \rangle - 1}{2} \tag{2.36}$$

describes the average degree of orientation of MA to the field direction.

The optical properties of MA solution are difficult to be described because an effective refractive index approach does not hold and light scattering is always present.

Via a calculus similar to the one presented in sect.2.3 for the derivation of eq.(2.22), the refractive index of the MA part, n_{MA}, can be expressed as:

$$
n_{MA}(B) = \begin{pmatrix} n_{MA||}(B) & 0 & 0 \\ 0 & n_{MA\perp}(B) & 0 \\ 0 & 0 & n_{MA\perp}(B) \end{pmatrix}
$$
$$
= n_o \cdot \left[1 - Q_{MA}(B) \cdot Q_L\right] \begin{pmatrix} 1 & 0 & 0 \\ 0 & 1 & 0 \\ 0 & 0 & 1 \end{pmatrix} + \begin{pmatrix} n_{||} & 0 & 0 \\ 0 & n_\perp & 0 \\ 0 & 0 & n_\perp \end{pmatrix} \cdot Q_{MA}(B) \cdot Q_L \tag{2.37}
$$

for molecules that align parallel to the field direction and respectively:

$$
n_{MA}(B) = \begin{pmatrix} n_{MA||}(B) & 0 & 0 \\ 0 & n_{MA\perp}(B) & 0 \\ 0 & 0 & n_{MA\perp}(B) \end{pmatrix} =
$$
$$
= n_o \cdot \left[1 - Q_{MA}(B) \cdot Q_L\right] \begin{pmatrix} 1 & 0 & 0 \\ 0 & 1 & 0 \\ 0 & 0 & 1 \end{pmatrix} + \begin{pmatrix} n_\perp & 0 & 0 \\ 0 & (n_{||} + n_\perp)/2 & 0 \\ 0 & 0 & (n_{||} + n_\perp)/2 \end{pmatrix} \cdot Q_{MA}(B) \cdot Q_L
$$

$$\tag{2.38}$$

for molecules that align perpendicular to the magnetic field, where the order parameters are given in the $(90°-\phi_i)$ and $(90°-\theta_i)$ convention, described in sect.2.3, (2.15) and (2.16).

The $n_{||}$ and $n_\perp$ are obtained from the dielectric tensor of molecules in a MA environment, and are different from the tensor that describes individual molecules [9] and we made use of the $n_o = (n_{||} + 2 \cdot n_\perp)/3$ notation.

The equation (2.39) describes the light intensity transmitted trough a MA solution of optical path x, from an initial intensity beam I_o:

$$I_{||,\perp} \approx I_o \cdot exp\left[-\left(\frac{2\cdot\pi\cdot r_{MA}(C)}{\lambda}\right)^2 \cdot \left(\frac{n_{MA\,||,\perp}}{n_{sol}} - 1\right)^2 \cdot \frac{x}{\sqrt[3]{C/N}} \right.$$
$$\left. -\frac{4\cdot\pi}{\lambda}\cdot\left[\kappa_{MA\,||,\perp}\cdot C + \kappa_{sol}\cdot(1-C)\right]\cdot x \right] \quad (2.39)$$

where C is the MA molar concentration, r_{MA} the average radius of the MA, concentration dependent, and $\sqrt[3]{C/N}$ represents the average distance between MA, (using the volume concentration). The $||$ and $\perp$ indices describe the light polarization and are relative to the field direction. The first part of the exponent describes the losses due to scattering, via a Rayleigh-Debye approach, and the second part describes absorption losses.

Experimentally, the limit where the scattering contribution becomes important is marked by the onset of deviation from an exponential behavior of the transmitted light versus the concentration curve, see fig.2.11.

At the particular wavelengths of resonant absorption lines, the scattering part of (2.39) is minimized, only reflection losses on the MA surfaces are still present [25]. This allows Polarized Absorption Spectroscopy techniques to be use for MA solution analysis, see sect. 2.8 and sect. 2.10.

An important case is when saturation alignment of the MA solution is achieved. In the saturation limit the MA order parameter is close to unity, $Q_{MA}(B > B_{sat}) \approx 1$, in which limit the imaginary part of the molecular components, the $\kappa_{||}$ and $\kappa_\perp$, are directly measurable, with B_{sat} the magnetic field value for which the saturation is reached. The concentration and sample thickness dependence, (2.39), can be avoided by expressing the experimental data as:

$$\frac{ln\,I_o - ln\,I_{||,\perp}(B)}{ln\,I_o - ln\,I_{||,\perp}(B=0)} = \frac{\kappa_{MA||,\perp}(B)}{\kappa_{MA||,\perp}(B=0)} \quad (2.40)$$
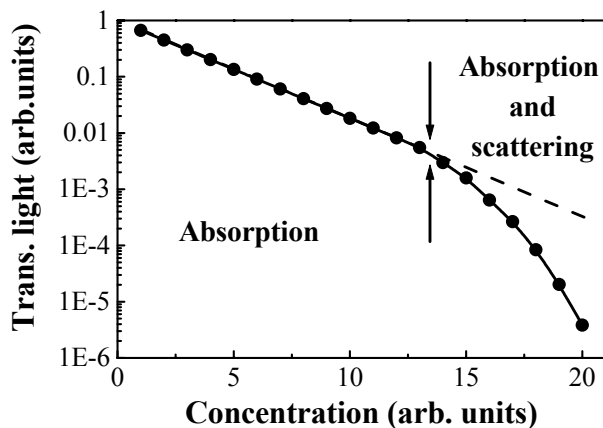
***Figure 2.11** Concentration dependence of the transmitted light intensity through a MA solution. The arrows mark the onset of deviation from the exponential behavior, clear indication that the scattering contribution becomes important. Numerical implementation of eq.(2.39).*

Using the imaginary part of (2.37), the formula (2.40) can be rewritten as:

$$\frac{ln\,I_o - ln\,I_{||,\perp}(B)}{ln\,I_o - ln\,I_{||,\perp}(B=0)} = 1 - Q_{MA}(B)\cdot Q_L + \frac{\kappa_{||,\perp}}{\kappa_o}\cdot Q_{MA}(B)\cdot Q_L \qquad (2.41)$$

The above is a very useful quantity because it allows direct determination of the order parameter from the measured quantities. Magnetic Field Induced Birefringence, measurements can be used as well to probe the degree of order in MA solutions, with the direct output of the $Q_{MA}(B)\cdot Q_L$ quantity. A method that is scattering and absorption independent is described in the next section.

Polarized Absorption Spectroscopy in high magnetic fields complemented by Magnetic Field Induced Birefringence form together a powerful tool in the study of MA solutions, allowing MA size determination, diamagnetic anisotropy measurements or precise absorption line identification, in the context that intrinsically the absorption lines are blurred by scattering.

2.7 Principles of magnetic field induced birefringence

measurements

As shown previously, magnetic field induced order is associated with changes in the optical properties. The change of the real part of the refractive index, called the magnetic field induced birefringence, (MFIB), is probably the most sensitive method or the detection of induced order [2].

Fig.2.12 presents a method of MFIB measurement based on phase modulation technique.

The electrical vector of light [10]: is described by:

$$E = \begin{pmatrix} E_{||} \\ E_{\perp} \end{pmatrix} \qquad (2.42)$$

where $E_{||}$ and $E_{\perp}$, are the two components, with axes as in fig.5. The unpolarized light emitted from the laser, with an initial electric vector E_o becomes:

$$E_i = \begin{pmatrix} E_{i_{||}} \\ E_{i_{\perp}} \end{pmatrix} = E_o \cdot \frac{1}{2} \cdot \begin{pmatrix} 1 \\ 1 \end{pmatrix} \qquad (2.43)$$

after passing the first polarizer. A Photo-Elastic Modulator, (PEM), with the axes aligned along the $||$ and the $\perp$ directions, induces a harmonic retardation, $\varphi = \varphi_o \cdot cos(\Omega \cdot t)$, between the $E_{||}$ and $E_{\perp}$ components, where Ω is the PEM operating frequency [26-28].
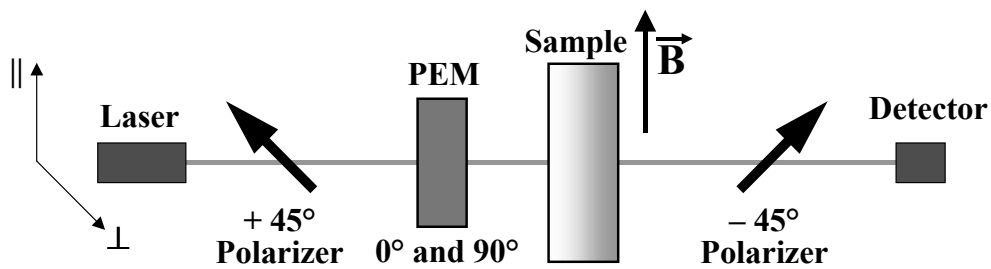

Figure 2.12 *The principle of Magnetic Field Induced Birefringence measurements, employing a Photo-Elastic Modulator.*

The electric vector of the light that reaches the detector is given by:

$$E_f = M_{-45° \, pol} \cdot M_{sample} \cdot M_{PEM} \cdot E_i =$$

$$= E_o \cdot \frac{1}{4} \cdot \begin{pmatrix} a_{||} \cdot e^{+i \cdot (b+\varphi)/2} - a_{\perp} \cdot e^{-i \cdot (b+\varphi)/2} \\ -a_{||} \cdot e^{+i \cdot (b+\varphi)/2} + a_{\perp} \cdot e^{-i \cdot (b+\varphi)/2} \end{pmatrix} = \begin{pmatrix} E_{f||} \\ E_{f\perp} \end{pmatrix} \qquad (2.44)$$

where:

$$M_{PEM} = \begin{pmatrix} e^{+i \cdot \varphi/2} & 0 \\ 0 & e^{-i \cdot \varphi/2} \end{pmatrix}, \quad M_{sample} = \begin{pmatrix} a_{||} \cdot e^{+i \cdot b/2} & 0 \\ 0 & a_{\perp} \cdot e^{-i \cdot b/2} \end{pmatrix},$$

$$M_{-45° \, pol} = \frac{1}{2} \cdot \begin{pmatrix} 1 & -1 \\ -1 & 1 \end{pmatrix}$$

are the optical transfer matrices that describe the PEM, the sample and second polarizer respectively. b is the magnetic field induced birefringence within the sample, $a_{||}$ and $a_{\perp}$ are the coefficients that describe the losses of $||$ and $\perp$ polarized light, due to absorption and scattering:

$$a_{||,\perp}^2 = exp\left(-\frac{4 \cdot \pi}{\lambda} \cdot \kappa_{||,\perp} \cdot x - \alpha_{scat_{||,\perp}} \cdot x \right) \qquad (2.45)$$

with α_{scat} the scattering losses per sample unit length.

The intensity of light as recorded by the detector is $I = E_f^* \cdot E_f$; with $I_o = E_o^2$ the laser intensity, I becomes:

$$I = \frac{I_o}{4} \cdot \frac{a_{||}^2 + a_{\perp}^2}{2} - \frac{I_o}{4} \cdot a_{||} \cdot a_{\perp} \cdot cos(b+\varphi) \qquad (2.46)$$

The harmonic part of I can be split into its odd and even symmetric parts:

$$cos(b+\varphi) = cos[\varphi_o \cdot cos(\Omega \cdot t)] \cdot cos(b) - sin[\varphi_o \cdot cos(\Omega \cdot t)] \cdot sin(b)$$

$$(2.47).$$

The *cos* and *sin* components can be Fourier expanded:

$$cos[\varphi_o \cdot cos(\Omega \cdot t)] \cdot cos(b) = A_o(\varphi_o) \cdot cos(b) + A_2(\varphi_o) \cdot cos(b) \cdot cos(2 \cdot \Omega \cdot t) + ...$$

$$sin[\varphi_o \cdot cos(\Omega \cdot t)] \cdot sin(b) = A_1(\varphi_o) \cdot sin(b) \cdot cos(\Omega \cdot t) + ... \qquad (2.48)$$

with $A_o(\varphi_o)$, $A_1(\varphi_o)$ and $A_2(\varphi_o)$ the Fourier coefficients of the expansion.

With the help of a signal conditioning unit the signal is separated into its DC and AC parts and independently detected:

$$I_{DC} = \frac{I_o}{4} \cdot \left[\frac{\left(a_{||}^2 + a_{\perp}^2\right)}{2} - A_o(\varphi_o) \cdot a_{||} \cdot a_{\perp} \cdot cos(b) \right] \qquad (2.49)$$

$$\begin{cases} I_{1st\ harm} = \dfrac{I_o}{4} \cdot A_1(\varphi_o) \cdot a_{||} \cdot a_{\perp} \cdot sin(b) \\[2mm] I_{2nd\ harm} = \dfrac{I_o}{4} \cdot A_2(\varphi_o) \cdot a_{||} \cdot a_{\perp} \cdot cos(b) \end{cases} \qquad (2.50)$$

With the suitable choice of the PEM amplitude $\varphi_o = 2.405\ rad$ the DC component becomes birefringence independent, because $A_o(2.405) = 0$, and carries only information about the losses (absorption and scattering) light suffers in the sample:

$$I_{DC} = \frac{I_o}{8} \cdot \left(a_{||}^2 + a_{\perp}^2\right) \qquad (2.51)$$

The birefringence is obtained using the first and second harmonic of the AC signal:

$$b = a\,tan\left[\frac{I_{1st\ harm} \cdot A_2(\varphi_o)}{I_{2nd\ harm} \cdot A_1(\varphi_o)} \right] \qquad (2.52)$$

with $A_1(2.405) = 0.5191$ and $A_2(2.405) = 0.4317$. The eq.(2.52) is used to analyze the experimental data.

The main advantage of this method is that the birefringence measurement is not influenced by absorption and scattering, or by the intensity fluctuations of the probing laser beam, I_o.

2.8 Principles of magnetic field induced dichroism measurements

Probing the refractive index anisotropy of the imaginary part of the refractive index is an alternative method to detect magnetic field induced alignment. Fig. 2.13 shows the principle of such a measurement, based on phase modulation technique.
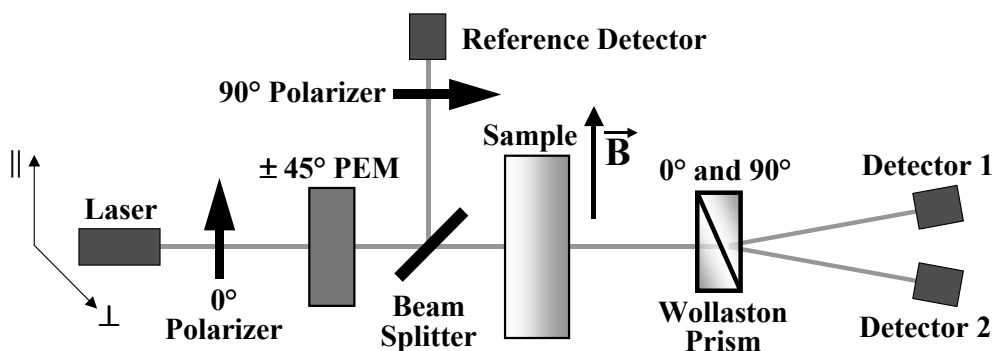
Figure 2.13 *The principle of Magnetic Field Induced Dichroism measurements, employing a Photo-Elastic Modulator.*

The electric field of the unpolarized probing beam after the first polarizer becomes:

$$E_i = E_o \cdot \frac{1}{\sqrt{2}} \cdot \begin{pmatrix} 1 \\ 0 \end{pmatrix} \tag{2.53}$$

The PEM, with the axes oriented at $\pm 45°$, induces a harmonic retardation $\varphi = \varphi_o \cdot cos(\Omega \cdot t)$ between the two orthogonal components of probing light, with its transfer matrix given by:

$$M_{PEM} = \frac{1}{2} \cdot \begin{pmatrix} e^{i \cdot \varphi/2} + e^{-i \cdot \varphi/2} & e^{i \cdot \varphi/2} - e^{-i \cdot \varphi/2} \\ -e^{i \cdot \varphi/2} + e^{-i \cdot \varphi/2} & -e^{i \cdot \varphi/2} - e^{-i \cdot \varphi/2} \end{pmatrix} \tag{2.54}$$

The optic transfer matrix of the polarizers are given by:

$$M_{0° \, pol} = \begin{pmatrix} 1 & 0 \\ 0 & 0 \end{pmatrix} \text{ and } M_{90° \, pol} = \begin{pmatrix} 0 & 0 \\ 0 & 1 \end{pmatrix} \qquad (2.55)$$

The beam splitter is chosen to be polarization independent and to separate the initial beam into two separate sub-beams of identical energy, so its transfer matrix is:

$$M_{b.spl.} = \frac{1}{\sqrt{2}} + \frac{1}{\sqrt{2}} \qquad (2.56)$$

The Wollaston Prism splits the input beam in two separate sub-beams of orthogonal polarization and therefore its transfer matrix can be written as:

$$M_{W.pr.} = M_{0° \, pol} + M_{90° \, pol} \qquad (2.57)$$

With the sample transfer matrix the same as in the previous section, the electric field of the light reaching the three detectors is given by:

$$E_{Dref} = M_{PEM} \cdot M_{b.spl.} \cdot M_{90° \, pol} \cdot E_i = E_o \cdot \frac{1}{4} \cdot \begin{pmatrix} 0 \\ -e^{i\varphi/2} + e^{-i\varphi/2} \end{pmatrix} \quad (2.58)$$

$$E_{D1} = M_{PEM} \cdot M_{b.spl.} \cdot M_{sample} \cdot M_{90° \, pol} \cdot E_i =$$
$$= E_o \cdot \frac{1}{4} \cdot \begin{pmatrix} 0 \\ a_\perp \cdot \left(-e^{i\varphi/2} + e^{-i\varphi/2} \right) \cdot e^{-ib/2} \end{pmatrix} \qquad (2.59)$$

$$E_{D2} = M_{PEM} \cdot M_{b.spl.} \cdot M_{sample} \cdot M_{0° \, pol} \cdot E_i =$$
$$= E_o \cdot \frac{1}{4} \cdot \begin{pmatrix} a_{||} \cdot \left(e^{i\varphi/2} + e^{-i\varphi/2} \right) \cdot e^{ib/2} \\ 0 \end{pmatrix} \qquad (2.60)$$

where we have chosen the Wollaston prism oriented such that *Detector 1* , (*D1*), is reached by the $\perp$ polarized beam , and *Detector 2* , (*D2*), is reached by the $||$ polarized beam, respectively, fig.2.13.

The light intensity detected by the detectors is independent of the real part refractive index of the sample:

$$I_{Dref} = \frac{I_o}{8} \cdot [1 - cos(\varphi)]; \quad I_{D1} = \frac{I_o}{8} \cdot a_\perp^2 \cdot [1 - cos(\varphi)]; \quad I_{D2} = \frac{I_o}{8} \cdot a_\parallel^2 \cdot [1 + cos(\varphi)]$$

(2.61)

Following the Fourier expansion as in (2.48), the second harmonics in Ω of the signals are:

$$\begin{cases} I_{Dref\ 2nd\ harm} = I_o \cdot A_2(\varphi_o)/8 \\ I_{D1\ 2nd\ harm} = I_o \cdot A_2(\varphi_o) \cdot a_\perp^2/8 \\ I_{D2\ 2nd\ harm} = I_o \cdot A_2(\varphi_o) \cdot a_\parallel^2/8 \end{cases}$$

(2.62)

In the absence of scattering, this set-up has the advantage that can measure independently the two imaginary part components of the refractive index:

$$\kappa_\parallel = \frac{\lambda}{4 \cdot \pi \cdot x} \cdot ln\left[\frac{I_{Dref\ 2nd\ harm}}{I_{D1\ 2nd\ harm}} \right] \quad \text{and} \quad \kappa_\perp = \frac{\lambda}{4 \cdot \pi \cdot x} \cdot ln\left[\frac{I_{Dref\ 2nd\ harm}}{I_{D2\ 2nd\ harm}} \right]$$

(2.63)

The field induced dichroic ratio is given by:

$$D(B) = \frac{\kappa_\parallel(B)}{\kappa_\perp(B)} = \frac{ln(I_{Dref\ 2nd\ harm}) - ln(I_{D1\ 2nd\ harm})}{ln(I_{Dref\ 2nd\ harm}) - ln(I_{D2\ 2nd\ harm})}$$

(2.64)

For the analysis of the experimental data the eq.(2.63) and eq.(2.64) are used.

2.10 Birefringence set-up

Fig.2.14 shows the implementation of the birefringence set-up. The sample is placed in a temperature-controlled chamber with electrical heating, in the core of a *20T* Bitter magnet. With the help of a double walled tube, flushed with water at constant temperature $(20 \pm 0.05)°C$ the caloric contribution of the magnet body to the sample holder is eliminated. The sample holder can accommodate liquid samples, film samples on transparent support or (polymer) liquid crystal cells. To allow optical

measurements, the sample chamber has two glass windows, with non-parallel wedged faces, to avoid temperature dependent interference.
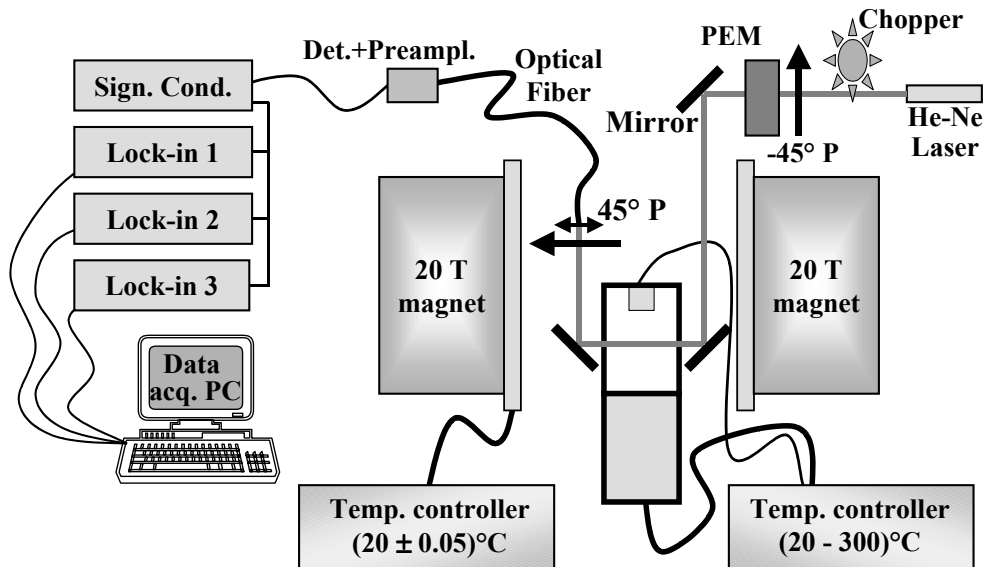
Figure 2.14 Magnetic Field Induced Birefringence set-up; Temperature range (20-300)°C, Temperature stability ±0.01°C; Birefringence detection limit $\Delta b = \pm 10^{-5}$ rad or $\Delta n = \pm 10^{-9}$ change in the refractive index for 1cm optical path sample; Optical transmission sensitivity 10^{-4}.

A stabilized He-Ne laser, $543.5\,nm$ or $632.8\,nm$, intensity modulated by a chopper at $(75-400)\,Hz$ and polarization modulated with a PEM, at $50\,kHz$, is employed to probe the sample. The laser is placed about $10\,m$ away from the magnet body and magnetically shielded to avoid stray field influences. The beam is guided by mirrors and passes the sample orthogonal with respect to the magnetic field direction, and hence no Faraday rotation [14] is measured. The light is collected in an optical fiber and guided to the detection diode. The signal from the diode is split into its Fourier components by a signal-conditioning unit and is detected phase sensitive.

As described in sect.2.8 the birefringence is obtained as eq.(2.52), with the major advantage that it is independent of the light source intensity fluctuations. Any misalignment of the second polarizer with the direction of the magnetic field causes

the $sin(b)$ and $cos(b)$ components to mix linearly in the two harmonics of the signal, thus limiting the absolute accuracy of the method.

We made use of the fact that the frequency cut-off for the DC filter of the signal-conditioning unit is about $1kHz$ and we superimposed a low frequency intensity modulation, by making use of the chopper, on top of the PEM polarization modulation. This decreases the noise in the "DC" part by one order of magnitude, making the detection less sensitive to the mechanic vibrations of the magnet.

If the wavelength of the probing laser is chosen such that the sample does not absorb it, the DC part of the signal, which is birefringence independent, is used as indication of the static scattering the beam suffers in the sample. In the particular cases of PLC and LC, the signal carries useful information about the sample domain morphology.

2.10 Polarized absorption spectroscopy set-up

Polarized absorption spectroscopy, PAS, offers an alternative method for the investigation of magnetic field induced alignment. This technique allows probing of the imaginary part of the refractive index. The PAS method can also follow simultaneously the orientation evolution of different molecules in a mixture or different bonds of a complex molecule, as long as each component absorbs at a different spectral wavelength.

The set-up, fig.2.15, is based on the same temperature controlled sample holder as presented in the previous section. As a light source we have used a broad spectral range lamp, $(200-1700)nm$, which is coupled directly to an optical fiber, via a de-polarizer, to avoid Faraday rotation on the section of the fiber which is exposed to the high fields. Light passes the sample perpendicular to the magnetic field direction and is guided out of the magnet tube. After it passes the analyzer the light is collected into a second optical fiber and guided to a Single Diode Array Spectrometer, which allows a full spectrum acquisition every $3\,ms$. This arrangement has the advantage that it avoids Faraday rotation in the analyzer and allows easy selection of the polarization. The collected spectra is corrected for background noise and then divided to the lamp spectral density. Because the sample is probed with unpolarized light no contribution from the real part of the refractive index is measured.
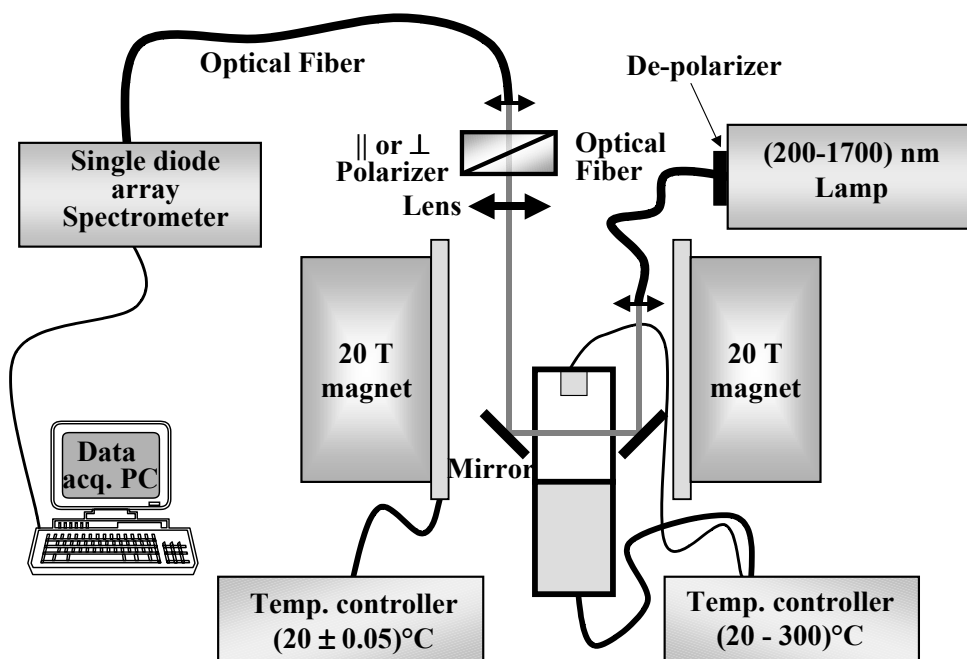
Figure 2.15 *Polarized absorption set-up; Spectral range* $(350-1100)nm$ *; Temperature range (20-300)°C, Temperature stability ±0.01°C; Relative change in the absorption coefficient sensitivity* $\Delta\alpha/\alpha = \pm 10^{-5}$ *for 1 cm optical path sample. Time resolving resolution 3 ms.*

Employing a dual channel spectrometer, the second channel can monitor the lamp stability and the ultimate set-up resolution can be significantly increased, by two orders of magnitude.

2.11 Data analysis

Unless the dielectric tensor of the studied molecule is known, the analysis as presented in the sect.2.3 is not immediately possible. For example the magnetic field induced anisotropy of the refractive index (the real part) is obtained using $\Delta\eta = b \cdot \lambda / 2 \cdot \pi \cdot x$, but the actual degree of order is not quantifiable. However if the anisotropy of an perfect aligned sample is known, $\Delta\eta_{max}$, or if the induced effect

saturates at a given field, i.e. when the sample is perfectly aligned, then the degree of order can be obtained as [2, 18]:

$$Q = \frac{\Delta\eta}{\Delta\eta_{max}} = \frac{b}{b_{max}} \qquad (2.65)$$

where b_{max} is the birefringence recorded at the saturation.

The raw birefringence data obtained experimentally are modulo $90°$, because of the trigonometric functions involved and due to the optical symmetry of the $0°-180°$ and $90°-270°$ axes, fig.2.16.a. If the experimental data are not noisy, than the data can be de-folded directly using an analytical formula, fig.2.16.b:

$$b_{de-folded} = \int abs\left[\frac{d\left(b_{|90°|}\right)}{dB} \right] \cdot dB \qquad (2.66)$$

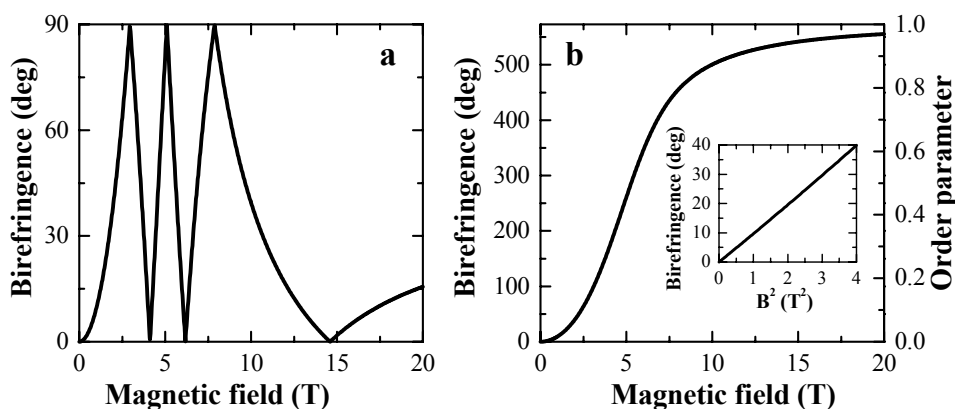In the case of noisy experimental data a numerical de-folding is preferred.

*Figure 2.16 **a**. Modulo 90° raw birefringence data; **b**. De-folded birefringence data; **Inset:** For low fields, the birefringence is linear in B^2. Numerical implementation according to eq.(2.4), eq.(2.13), eq.(2.14) and eq.(2.23).*

The absorption of light in a sample, fig2.2, is described by [10]:

$$I(\lambda, B) = I_o(\lambda) \cdot exp\left[-\frac{\kappa(\lambda, B) \cdot x}{4 \cdot \pi \cdot \lambda}\right] \qquad (2.67)$$

Even in the absence of saturation effect or incomplete knowledge about a perfectly aligned sample, the induced order can be obtained using the normalization to the isotropic value, fig.2.17:

$$\frac{\kappa(B)}{\kappa(B=0)} = \frac{ln\,I_o - ln\,I(B)}{ln\,I_o - ln\,I(B=0)} = f(Q) \qquad (2.68)$$
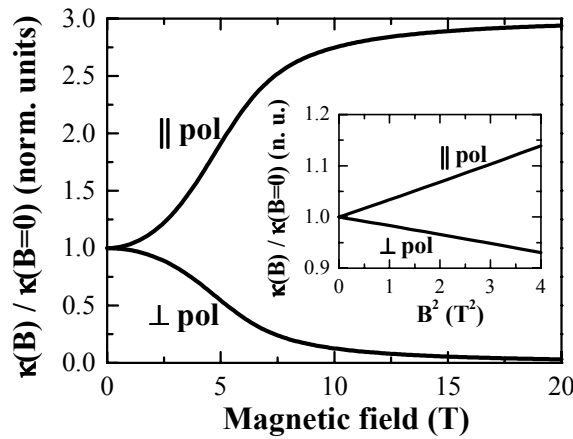
Figure 2.17 *Normalized absorption coefficients for molecules in magnetic field;* **Inset:** *The low field part of the curves is linear in* B^2. *Numerical implementation according to eq.(2.4), eq.(2.14), eq.(2.36) and eq.(2.37).*

The normalization $\kappa_{||}(B)/\kappa_{\perp}(B) = D(B) = f(Q)$ can be used equally well, where $D(B)$ is called the field induced dichroic ratio [eq.(2.9),15,29].

For molecular aggregates solutions with large size aggregates, this kind of analysis has to be performed only on the absorption lines, at any other wavelength the result is strongly affected by scattering, see sect.2.6.

2.11 Order characterization methods

The morphology of PLC samples or thin LC cells with polymer coated walls consist of microscopic domains, which are strongly ordered locally, but with their orientation randomly distributed with respect to each other, see fig.2.18.

The birefringence measured with the MFIB method is proportional to a convolution between the local order, Q_L, and the domain orientation, Q_D, and can not distinguish between the two: $b = f(Q) = f(Q_L \cdot Q_D)$, see sect. 2.3.

Rotating the sample between crossed polarizers, around the azimuthal, α, or polar angle, φ, and measuring the light passing trough, the set-up shown in fig.2.19, de-convolutes the local and director contribution terms. During an azimuthal rotation the total light intensity collected by the detector is the sum of all individual domain contributions, projected on a common axis:

$$I = I_o \cdot sin^2(b) \cdot \sum_i cos^2(2 \cdot \alpha_i) \tag{2.69}$$

The $sin^2(b)$ term represents the degree of local order, which is only temperature dependent, hence identical for all domains.
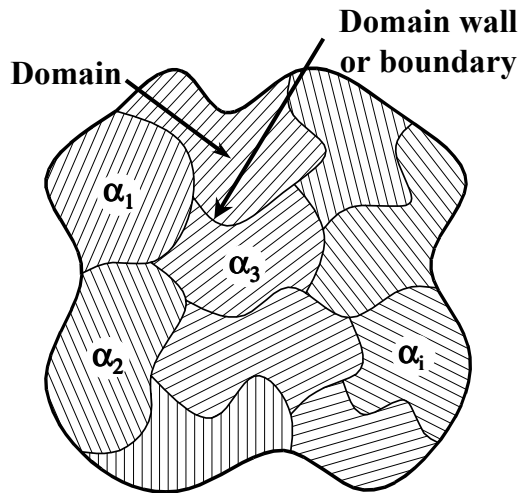
Figure 2.18 *Schematic domain structure in a polymer liquid crystal sample.*

Because of the four-fold symmetry of the axes, the total intensity, of a sample rotation in the plane orthogonal with the laser beam, can be expressed as:

$$I(\alpha) = I_o \cdot sin^2(b) \cdot \left[C_1 \cdot cos^2(2 \cdot \alpha) + C_2 \right] \qquad (2.70)$$

The fit parameters obey the constraint: $C_1 + C_2 = 1$. The domain order parameter is simply described by: $Q_D = C_1$.

The pinhole in front of the analyzer minimizes the scattering contribution, however for thick samples, secondary scattering can produce scattered photons with random polarization but with the same $\vec{k}$ vector as the incident photons [15], affecting the accuracy of the method.

Because the birefringence is obtained as an inverse of a trigonometric function, its value is known only as modulo $90°$ and cannot be used directly as a measure of the local order.

Figure 2.19 *Multi-domain sample characterization set-up and analytical implementation of eq.(2.70) for samples with different degree of induced order: Solid line $Q_D = 1$; Dotted line $Q_D = 0.66$; Dashed line $Q_D = 0.33$ and Dashed-dotted line $Q_D = 0$.*

Rotating the sample such that the polar angle φ with the laser beam is changed, the birefringence increases due to the optical path of light in the sample being changed: $db = 2 \cdot \pi \cdot \Delta\eta \cdot dx / \lambda$.

Because:

$$dx = x \cdot \left[1/cos\left(\varphi\right) - 1\right] \tag{2.71}$$
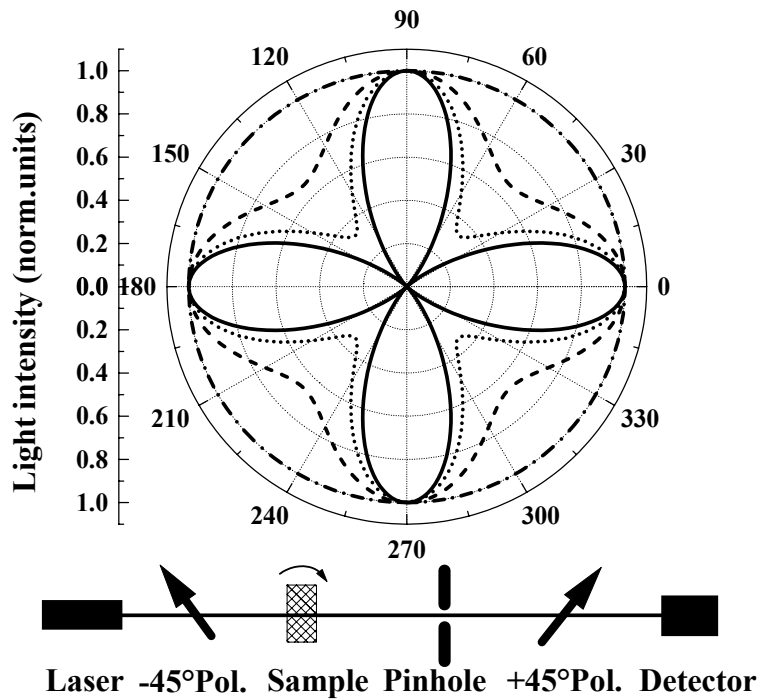
is known, the total birefringence or the absolute value of the refractive index anisotropy is obtained by integrating db/dx for the whole sample length x. Small rotations, $\varphi \leq 1°$, reduce the effect of the reflection on the accuracy of the method.

In the case of monodomain samples the method presented in sect 2.7 and fig.2.11, which makes use of polarization modulation technique using a PEM, is preferred. Simply rotating the sample around the azimuth angle α allows the determination of the birefringence, without of the modulo $90°$ constraint and does not require prior knowledge about sample thickness, fig.2.19. The direct measured quantity is $\left|b(\alpha)\right|_{meas.}$ and its representation in terms of the sample refractive indices is given by the analytical formula:

$$\left|b(\alpha)\right|_{meas.} = \frac{2 \cdot \pi}{\lambda} \cdot x \cdot \left| \frac{\eta_{\parallel} \cdot \eta_{\perp}}{\sqrt{\eta_{\perp}^2 \cdot cos^2\,\alpha + \eta_{\parallel}^2 \cdot sin^2\,\alpha}} - \frac{\eta_{\parallel} \cdot \eta_{\perp}}{\sqrt{\eta_{\perp}^2 \cdot sin^2\,\alpha + \eta_{\parallel}^2 \cdot cos^2\,\alpha}} \right| \tag{2.72}$$

The total birefringence $b = 2 \cdot \pi \cdot \Delta\eta \cdot x / \lambda$ is obtained by numerically integrating the measured quantity $\left|b(\alpha)\right|_{meas.}$:

$$b = \int_{0}^{\pi/2} \left|b(\alpha)\right|_{meas.} \cdot d\alpha \tag{2.73}$$

This method becomes particularly important when a rotation in the polar plane is performed, as is the case for the pretilt angle[iii] determination. As shown in sect. 2.7 the measurement is not affected by any light losses, such as scattering and reflection.

[iii] Pretilt angle – quantity related to LC cells, used to describe the angle made by the mesogen director with the plane of the cell.
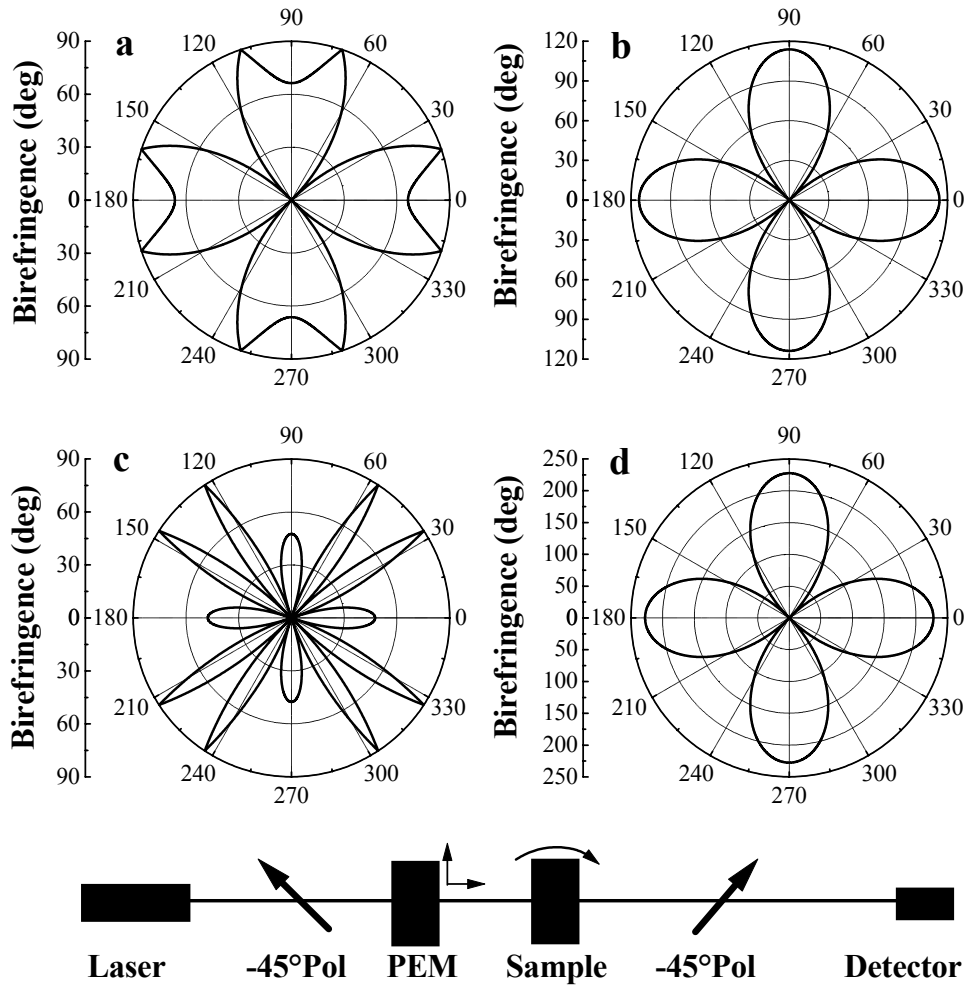
Figure 2.19 *Birefringence set-up and analytical modeling of different samples, following eq. (2.72). Raw data (as measured) of a 114° **(a)**, respectively 228° **(c)**, birefringence samples; **(b)** and **(d)** De-convoluted data from **(a)** and **(c)**, using eq. (2.73)*

References

[1]   D. Craik, Magnetism: Principles and Applications, Wiley, cop. 1995.

[2]   G. Maret, K. Dransfeld, *Topics in Applied Physics*, Vol **57**, 143-204, ed. F. Herlach, Springer, Berlin, 1985.

[3]   G.H. Meeten, *J. Chimie Physique* **7-8**, 1175, 1972.

[4]   S. Yamaguchi, S. Okuda, N. Nakagawa, *Chem. Pharm. Bull.* **11**, 1465, 1963.

[5]   W. Zeil, H. Burchert, *Z. Physik. Chem. Ser. 2*, **38**, 47, 1963.

[6]   P.T. Marasimham, M. T. Rogers, *J. Phys. Chem.* **63**, 1388, 1959.

[7]   S. Chandrasekhar, *Liquid Crystals*, Sec. Ed., Cambridge Univ. Press, 1993.

[8]   A.M. Donald, A.H. Windle, *Liquid Crystalline Polymers*, Cambridge Univ. Press 1992.

[9]   Kobayashi T, *J-Aggregates*, World Scientific, Singapore, 1996.

[10]   J.R. Meyer-Arendt, *Introduction to Classical and Modern Optics*, Prentice-Hall, New Jersey 1984.

[11]   M.P. Langevin, *C.R. Acad. Sci. Paris* **151,** 475, 1910.

[12]   A. Peterlin, H.A. Stuart*, Z. Physik* **112**, 129, 1939.

[13]   N. Everall, *Spectroscopy* **15**(9), 39, 2000.

[14]   A.K. Zvezdin and V.A. Kotov, *Modern Magnetooptics and Magnetooptical Materials*, IOP Publishing, Bristol and Philadelphia 1997.

[15]   I.M Ward, *Structure and Properties of Oriented Polymers,* chap.2 by G.L. Wilkes and R.S. Stein, Chapman & Hall, London, 1997.

[16]   Since all the compounds discussed in this thesis are nematic, only the nematic mesophase case is presented.

[17]   A.M. Donald, A.H. Windle, *Liquid Crystalline Polymers*, Cambridge Univ. Press 1992.

[18]   U.W. Gedde, G. Wilberg, *Mechanical and Thermophysical Properties of Polymer Liquid Crystals*, chap.10, Chapman & Hall, London, 1998.

[19]   S. Singh, *Phys. Rep*. **324**, 107-269, 2000.

[20]   Some books keep the classic notation in ϕ and θ which lead to more complicate expressions and to a counter intuitive limit for the order parameter, $Q = -1/2$, for perfect alignment.

[21]   M. Kerker, *The Scattering of Light and Other Electromagnetic Radiation*, Academic Press, New York and London, 1969.

[22]   D. Demus et al., *Handbook of Liquid Crystals*, vol3, Willey-VCH VerlagGhmb, Weinheim 1998.

[23]   M. Kerker, *The Scattering of Light and Other Electromagnetic Radiation*, Academic Press, New York and London, 1969.

[24]   G.M. Whitesides, J.P. Mathias, C.T. Seto, *Science* **254**, 1312-1319, 1991

[25]   M. Kerker, *The Scattering of Light and Other Electromagnetic Radiation*, Academic Press, New York and London, 1969.

[26]   K.W. Hipps and G. A. Crosby, *J. Phys. Chem* **83**, 555, 1979.

[27]   J. Badoz , M.P. Silverman, J.C. Canit , J Opt Soc Am. A **7** (4), 672, 1990.

[28]   For a detailed presentation of Hinds Photoelastic Modulator specifications and applications please consult *http://www.oceanoptics.com/*.

[29]   M. Grell, D.D.C. Bradley, *Advanced Materials* **11**, 895, 1999.

Chapter 3

Mesogen-polymer backbone coupling in Side Chain Polymer Liquid Crystals, studied by high magnetic field induced alignment

In this chapter we show that cooling Side Chain Polymer Liquid Crystals, (SCPLCs), in a magnetic field, from the isotropic to nematic phase and subsequently to the glass phase, results in a macroscopically ordered, transparent and strongly birefringent material. The aligned SCPLC retains its properties after the field is removed and can only be de-aligned by heating it to the isotropic phase. Our results show that the magnetic fields can be used to tailor the macroscopic properties of SCPLCs. We find that in order to induce complete alignment, a threshold field B_{th} is necessary, which strongly depends on the chemical structure of the polymer backbone, the polymerization degree and the length of the spacer with which the mesogen is attached to the main chain. We demonstrate that B_{th} reflects the strength of the mesogen-polymer backbone interaction and we show that this interaction is responsible for the stability of the induced alignment at zero fields.

3.1 Introduction

Side Chain Polymer Liquid Crystals [1], (SCPLCs) are composed of rigid mesogenic units attached to a polymeric backbone chain via a flexible spacer, fig.3.1, with enough freedom for the mesogens to form liquid crystalline mesophases. These molecules combine the self-organizing properties of liquid crystals with the structural advantages of polymers, being of technological interest for applications [2] such as optically nonlinear devices [3], displays [4,5] and optical data storage [6]. Their current limiting factor is the lack of a reliable method to control the SCPLCs molecular alignment at a macroscopic scale. The problem has been investigated using a large number of techniques, such as surface fields [7], electric fields [8], mechanical fields [9], flow fields [10] or polarised ultraviolet light [11], but to date only limited success has been obtained.
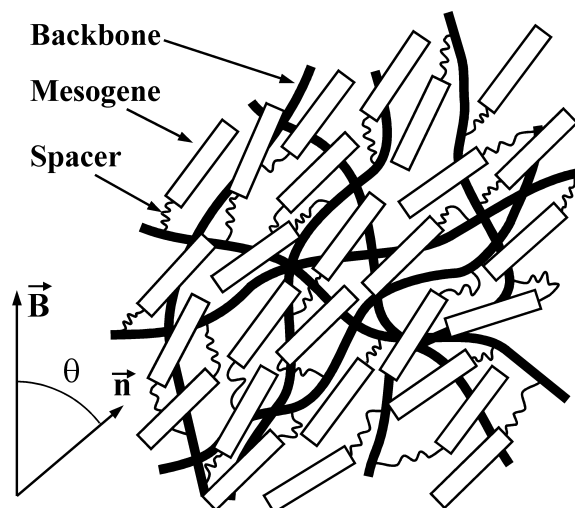
Figure 3.1 *Schematic representation of the SCPLC structure*

In this chapter we show that perfectly oriented SCPLC films can be obtained by cooling them in a magnetic field from the isotropic to nematic phase. Since we found the field alignment of the SCPLCs at a fixed temperature to be impossible, we conclude that the magnetic alignment occurs only in the biphasic region at the isotropic nematic phase boundary [12]. At this boundary, small liquid crystalline nuclei are formed, which undergo orientation in a small temperature window, where

the mesogen-backbone interaction is smaller than the magnetic field effect. Upon cooling, the system evolves into a monodomain orientation, strongly birefringent sample, which retains its properties after the field is switched off. This fully aligned material is technologically interesting because of its strong birefringence and forms an ideal target for further scientific studies such as X-ray or neutron scattering experiments. In comparison with other alignment techniques [7-11], magnetic alignment has several advantages, since the field exerts a well defined, contact free, torque force on all molecules, and can therefore be used for thin films as well as bulk samples.

Low molecular weight liquid crystals can be perfectly aligned in magnetic fields [13], but for liquid crystalline polymers the alignment process is often less effective and very time-consuming [14-19], because the rotational freedom of the mesogens is hindered by the polymer backbones. We have observed this hindrance and determined its strength, since the degree of alignment of different SCPLCs, each containing the same mesogenic units, is found to depend strongly on the chemical properties of both their backbone and the spacer. A proper understanding of the mesogen-backbone interaction is one of the key issues requested for the development of SCPLCs into materials that combine the best properties of polymers and liquid crystals. Experimentally the determination of this interaction is still an open question. Only recently, neutron scattering experiments [10,20-22] have demonstrated that the polymeric backbone configuration can indeed be correlated with the local mesogen director.

3.2 Experimental description

Two types of thermotropic nematic SCPLCs were used [23], one based on a polynorbornene and one on a polyacrylate-derivative backbone, each with cyanobiphenyl mesogenic groups. The molecular structures are shown in Table 3.1, together with their measured phase transition temperatures. The polynorbornene based SCPLC has a relatively stiff backbone due to the double bonds that connects the cyclo-pentylene units, and is synthesized by Ring Opening Metathesis Polymerization. The resulting polymer has a low polydispersity *PDI ~ 1.2* [24,25]. Two different spacers were used consisting of either *3* or *5* methylene units, configurations which we denote as *C3* and *C5* respectively. The polymerization degree of *C5* was varied from $n = 20$ to *40*.

The backbone of the polyacrylate-derivative (*B4*), which was synthesized by free radical polymerization (*PDI ~ 2*), is more flexible in comparison with the

polynorbornene. In this case a spacer length of *4* methylene units was used, and the polymerization degrees were $n = 20$ and 30.

Film samples (thickness $10 - 200\,\mu m$) were prepared on a glass substrate by spin coating from solution and subsequent solvent removal by thermal annealing.
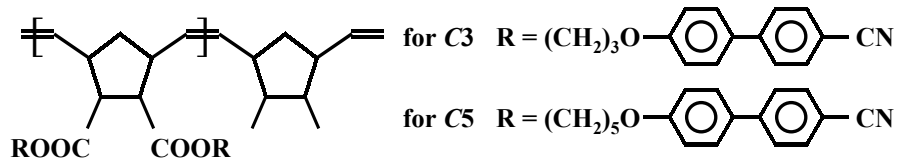
Poly[(±)–*exo,endo*-bis{3-[(4′-cyanobiphenyl-4-yl)oxy]propyl}norborn-5-ene-2,3-dicarboxylate], the *C3* compound and

Poly[(±)–*exo,endo*-bis{5-[(4′-cyanobiphenyl-4-yl)oxy]pentyl}norborn-5-ene-2,3-dicarboxylate], the *C5* compound.
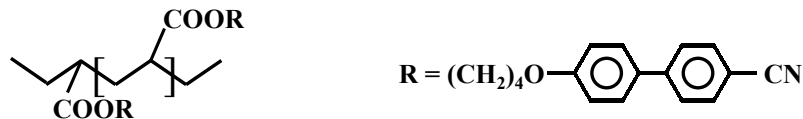
Poly-{4-[(4′-cyanobiphenyl-4-yl)oxy]butyl}acrylate, the *B4* compound.

Sample	$B_{th}(T)$	$K_{m/b}$ (10^{-26}N·m/mlc.)	Alignment preserved Upon cooling	β	Trans. temp (°C) g T_{NG} n T_{IN} i
C5, n=20	6	3.6	Yes	0.28	g 43 n 105.6 i
C5, n=30	10	10.0	Yes	0.28	g 43 n 109.2 i
C5, n=40	19	36.0	No	0.28	g 45 n 112.5 i
C3, n=20	>20	-	No induced effect	0.10	g 57 n 92.6 i
B4, n=20	2	0.4	Yes	0.40	g 43 n 94.0 i
B4, n=30	3.5	1.2	Yes	0.40	g 43 n 96.7 i

Table 3.1: *Molecular structures and material parameters of the samples.*

The samples were placed in a temperature-controlled chamber ($\pm 0.01°C$ stability) inside the bore of a *20T* resistive Bitter-magnet. All experiments were done at a cooling rate of $10°C/min$, which was sufficiently slow for the samples to be always in equilibrium. The linear birefringence was determined using a

polarization modulated *HeNe* - laser beam (wavelength $543.5\,nm$, and a precision of 10^{-4} radians phase retardation), at temperatures from *20* to *120°C*, see sect.2.9. The field-induced birefringence $b(B)$ divided by the birefringence of a perfectly oriented sample b_{max} measures the order parameter $Q(B)$ [15,16,26].
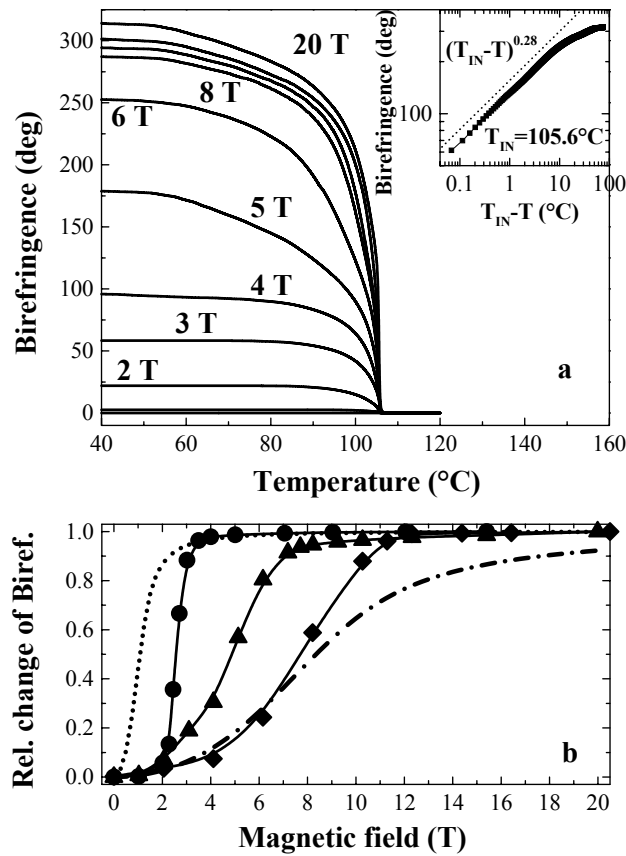
Figure 3.2 *Birefringence of SCPLCs induced in high magnetic fields.* **a**. *A 10 micron thick, n=20, C5 film is cooled down in different magnetic fields, from the isotropic phase, through the nematic phase into the glass phase.* **Inset**: *The birefringence of the same film, measured at 12 T, and plotted at a logarithmic scale, exhibiting a $(T_{IN}-T)^{\beta}$ power law.* **b**. *Comparison of the, field dependent, saturation values of the birefringence in the glass phase of different polynorbornene (▲ for C5, n=20 and ◆ for C5, n=30) and polyacrylate-based (●, B4, n=30) SCPLC films of 10 μm thickness. The dotted and dashed-dotted lines represent a calculation of the director order parameter neglecting the backbone/mesogen coupling, which describes either the low (dashed) or the high field (dotted) results.*

3.3 Results and discussions

Fig.3.2a shows the measured birefringence during cooling down of a $10\,\mu m$ thick $C5$, $n=20$ sample, from $120°C$, through the isotropic to nematic transition ($T_{IN}=105.6°C$), and subsequently entering the glass phase at $T_{NG}=43°C$, for different magnetic fields.
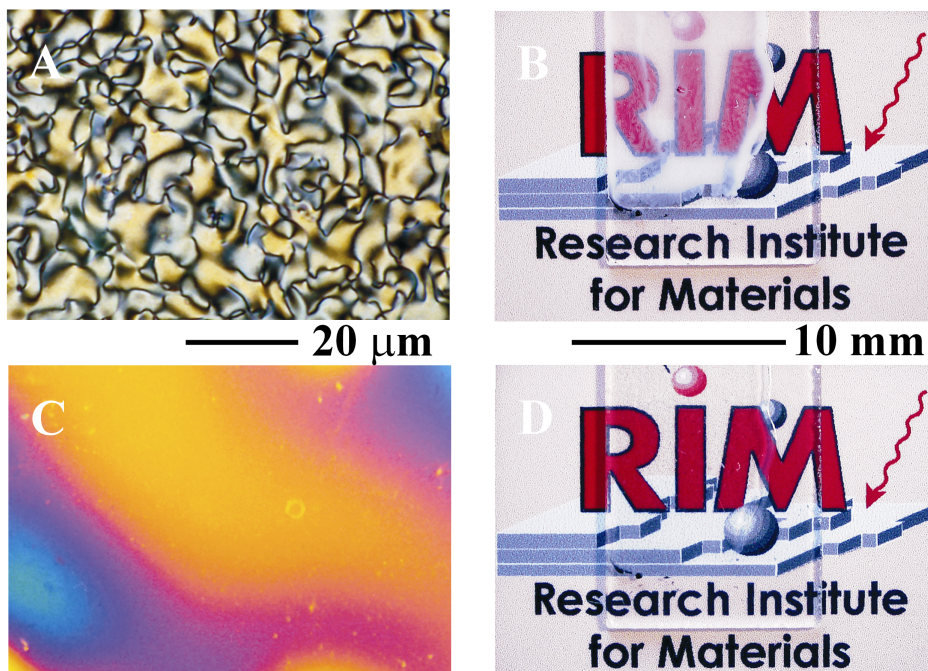
Figure 3.3: *Optical textures of (magnetically aligned) SCPLC films. **A**. Polarized microscope image, recorded with crossed polarizers, of an unprocessed 10 µm thick polyacrylate (B4, n=20) SCPLC film, showing micrometer sized domains. **B**. Photograph corresponding to image A: the unaligned film has an overall opaque appearance due to the domains that cause significant light scattering. **C**. Polarized microscope image of a 10 µm thick polyacrylate (B4, n=20) SCPLC film, aligned in a 5 T field. The film consists of a macroscopic monodomain; the color variations are due to small thickness variations. **D**. Photograph corresponding to image C: the aligned sample is fully transparent and strongly birefringent.*

No induced birefringence is observed (for all samples) either in the isotropic phase for all fields or in zero magnetic field in the nematic phase, although in the latter case local order exists inside micron sized domains (see the polarized microscope image in Fig.3.3.a). However, each domain has a differently oriented director, which destroys any macroscopic birefringence and which causes strong variations of the refractive index, leading to significant scattering and an overall opaque appearance (see Fig.3.3.b).
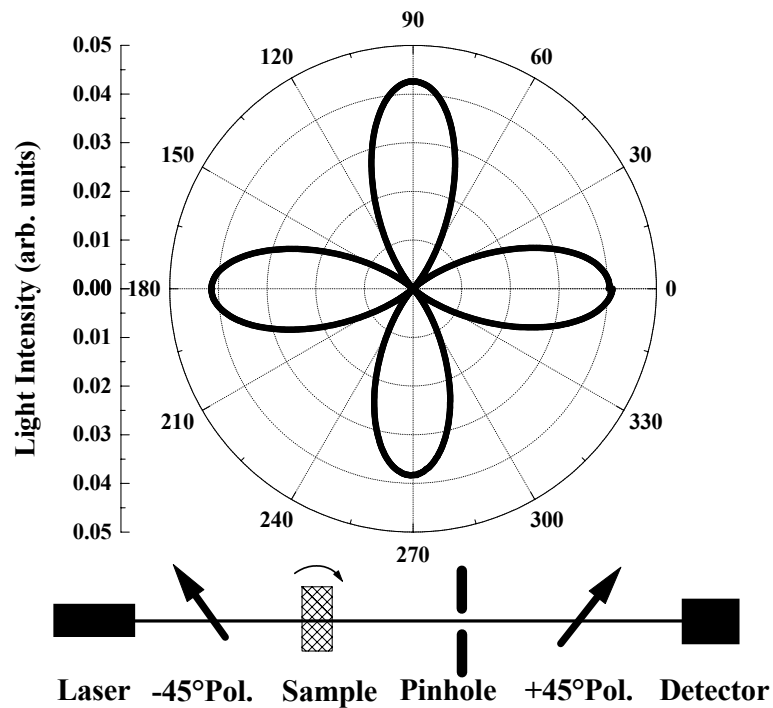
Figure 3.4 *Out of field director order parameter characterization of a 20 µm, n=20, C5 sample, after alignment in 17 T. By using the method described in Chapter 2, sect. 2.9, a director order parameter* $Q_D = 0.999 \pm 0.001$ *was measured.*

In finite fields birefringence appears around T_{IN}, which increases upon further cooling and finally saturates at T_{NG} (Fig.3.2a). With increasing fields the saturation value increases but the onset of the birefringence always occurs around T_{IN}. The inset of Fig.3.2a shows that around T_{IN} the induced birefringence follows a

$(T_{IN} - T)^{\beta}$ power law [13]. The critical exponent β has different values for the different SCPLCs (see table 3.1), but does not depend on the degree of polymerization or the magnetic field strength.
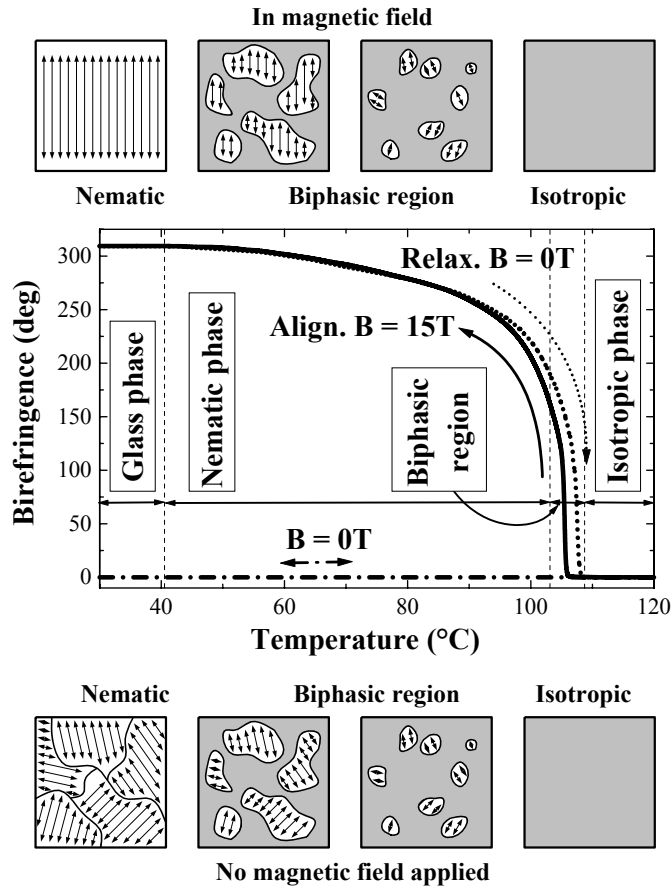
Figure 3.5 *Schematic representation of the magnetic alignment process of SCPLCs, occurring in the biphasic region close to the isotropic-nematic phase transition. The solid curve is the birefringence of a polynorbornene SCPLC film (C5, n=20) of 10 μm thickness cooled down in a 15 T field. Subsequently the field is switched off and the sample is heated (Dashed curve). The two curves are very similar; the alignment only disappears above T_{IN}. At zero field no birefringence is measured (dash-dotted curve) since the directors of the different domains are pointed in random directions (bottom panel). In a magnetic field the directors of the liquid crystalline islands align in the same direction, resulting in the development of a macroscopic monodomain (top panel).*

All samples, except the $C5$, $n = 40$, [27], remain aligned after removal of the field and show no further change, even after several months.

The oriented material exhibits extraordinary properties, such as macroscopic (cm) uniaxial monodomain alignment (Fig.3.3.c), full transparency (Fig.3.3.d), and large birefringence ($\Delta n = 0.1$), which corresponds to a director order parameter $Q_D = 0.999 \pm 0.001$ [15,16], see fig.3.4.

All experimental evidence shows that alignment occurs only in a narrow temperature window around T_{IN}. For instance, as shown in fig.3.5, heating of a pre-aligned sample at zero field leads to a very similar birefringence curve as the original one measured during cooling in an applied field. Reversing such a temperature sweep of a pre-aligned sample before reaching T_{IN} fully restores the initial aligned state. Finally, attempts to magnetically align a SCPLC film at a fixed temperature below the T_{IN} always failed. Although all data reported here are on films we have also observed the same results with bulk material in a $20 \times 10 \times 2\,mm$ cuvette.

3.4 Interpretation

In order to explain these unique observations the alignment mechanism should be considered in more detail. Due to the anisotropy of its diamagnetic susceptibility $\Delta\chi$, a molecule tends to orient relative to an applied magnetic field (B), such that its energy is minimized. For single molecules, the reduction in magnetic energy is small compared to the thermal energy ($\Delta\chi \cdot B^2 << kT$). Therefore, SCPLCs within the uncorrelated isotropic phase, exhibit no birefringence in a magnetic field. However, for collective molecular behavior, as in liquid crystalline mesophases, the difference in magnetic energy, added up for all molecules within a correlation volume (N_ξ), can become large enough ($N_\xi \cdot \Delta\chi \cdot B^2 > kT$) to induce magnetic alignment [13,26]. Quantitatively, for a biphenyl group 10^4 molecules are sufficient to achieve alignment at room temperature at a field strength of $10\,T$; $\Delta\chi = 120 \cdot 10^{-6}\,cm^3/mol\,(cgs)$, [26].

During cooling down, nuclei of ordered liquid crystals are formed around T_{IN}, which rapidly grow in size with decreasing temperature (biphasic region, see top and bottom panels in Fig.3.5). When these nuclei are sufficiently large ($N_\xi > 10^4$) the field aligns them provided they are not hindered by the interaction with the backbones. Consequently, the actual alignment occurs around T_{IN}, and is characterized by the sharp onset of the birefringence at T_{IN} in Fig.3.2a. The subsequent increase of the birefringence, characterized by the critical parameter β,

is caused by the usual (purely temperature driven) alignment of the mesogens with respect to the pre-aligned director [13] and is field independent. The local order parameter Q_N, describing the order within a correlation volume, is unaffected by the magnetic field. The field merely affects the director order parameter Q_D, leading to a high total order parameter Q, [15,16], as measured in the birefringence, which is given by $Q(B,T) = Q_N(T) \cdot Q_D(B)$.

Fig.3.6 shows a *B4* sample being cooled down from the isotropic phase in the presence of a magnetic field but few degrees below the IN transition the temperature is stabilized for 15 minutes. No further alignment or relaxation was observed to take place until the cooling process was restarted. Upon restoring the cooling process, the orientation process restarts and goes on until the NG transition is reached. This experiment further confirms that the director alignment is already complete few degrees below T_{IN}.
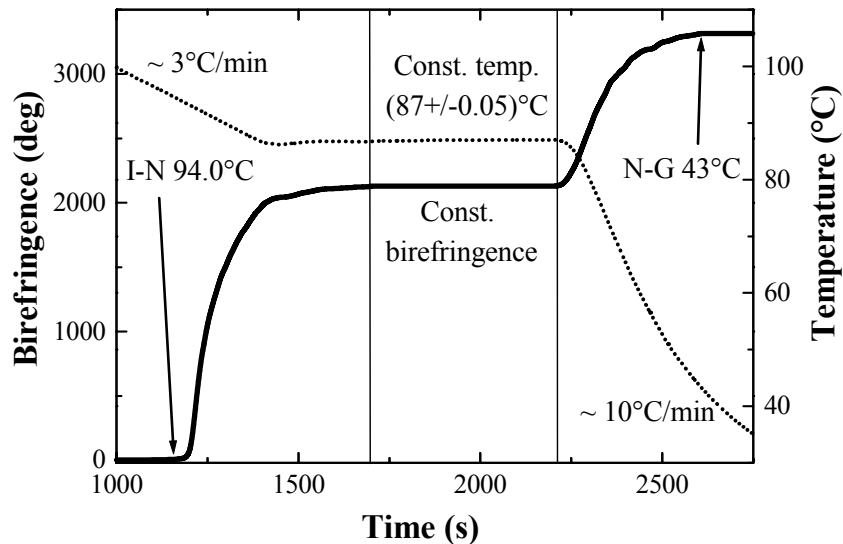
Figure 3.6 *Birefringence versus time for a 50 μm, n=20, B4 sample cooled in a 15 T magnetic field. At 87°C, few degrees below T_{IN} (94°C) the temperature is kept constant for 15 min. The birefringence is constant in this interval and increases only after the cooling process is restarted. The solid line represents the birefringence evolution and is associated with the left ordinate axis, while the dotted line represents the temperature evolution, linked with the right ordinate axis.*

The saturation value of the induced birefringence, trapped in the glass phase, as a function of the applied magnetic field for three different samples is plotted in Fig.3.2b. All samples show a gradual rise in the birefringence at low fields, followed by a rapid increase and saturation at high field.

Calculations of the magnetic alignment of bare cyanobiphenyl units, neglecting the coupling to the polymer backbone, cannot explain the experimental observations. The dotted and dashed-dotted curves in Fig.3.2.b correspond to such calculations of the director order parameter in which the magnetic field dependence is only governed by the $N_\xi \cdot Q_N \cdot \Delta\chi \cdot B^2 / kT$ ratio. Q_D describes a Langevin type of function, showing no alignment ($Q_D = 0$) at low fields and saturation ($Q_D = 1$) at high fields [13]. The dotted (dashed-dotted) curve reasonably describes the low (high) field results, but it is impossible to describe both low and high field behaviors simultaneously with a single fit parameter $N_\xi \cdot Q_N \cdot \Delta\chi / kT$. In particular, the measured magnetic alignment saturates rather abruptly at high fields even if at low fields no effect is seen, pointing to a certain threshold field B_{th}, which must be overcome in order to induce alignment.

Since the mesogenic units of all our SCPLCs are identical and since they only differ in their backbone and spacer, the different behavior of the samples can only be caused by the interaction of the mesogenic units with the backbones (either their own or backbones of other molecules). The backbone does not contribute actively to the mesophase and is not directly influenced by the magnetic field, but its presence hinders the mesogen degrees of freedom. Because the free volume per molecule in the nematic phase does not allow a free molecular rotation, any change of orientation of a mesogen needs to be accompanied by a local rearrangement of the surrounding polymer chains. The thermal hysteresis of the IN transition for SCPLCs, see fig.3.5, indicates the existence of entanglements and conformational barriers that impend the mesogen mobility [26]. The existence of sharp domain walls in intrinsic SCPLCs samples, see fig.3.3.a, strongly support the idea that mesogen rotation is energy dissipative. Simple energetic arguments of elastic energy minimization predict the mesogen director to change smoothly over a large distance scale, as it happens in low molecular weight Liquid Crystals. In reality the director changes sharply over a short distance indicating a compromise between the created elastic energy and the dissipated energy due to the rotation of the mesogen volume incorporated in the wall. We interpret this behavior as being consistent with the existence of a threshold field B_{th} and indicative for some type of mesogen backbone interaction. This mesogen/backbone coupling interaction accounts for all the backbone obstruction to the mesogen mobility and can be described as an "effective torque friction" acting at a molecular level [28], $K_{m/b}$. The quantity $K_{m/b} \cdot \Delta\theta$

represents the work dissipated to overcome the coupling during a $\Delta\theta$ rotation of a mesogen.

$$N_\xi \cdot \Delta\chi \cdot Q_N \cdot B^2 \cdot sin(2 \cdot \theta) - N_\xi \cdot K_{m/b} + \zeta_{kT} - K_{vis} \cdot \dot{\theta} = 0 \qquad (3.1)$$

The equation (3.1) describes the torque balance of all contributions acting on a correlated volume of N_ξ molecules, where $N_\xi \cdot \Delta\chi \cdot Q_N \cdot B^2 \cdot sin(2 \cdot \theta)$ is the magnetic torque, $N_\xi \cdot K_{m/b}$ is the mesogen/backbone coupling torque, (always opposing the motion), ζ_{kT} represents the temperature fluctuation random torque and $K_{vis} \cdot \dot{\theta}$ the viscosity torque, with θ the angle between the magnetic field and the local director, see fig.3.1.

The effective torque $K_{m/b}$ opposes the magnetic torque and acts as a barrier, leading to a threshold field B_{th}, above which magnetic field alignment can occur. The viscosity contributes only to the time scale of the alignment process while the temperature term is insignificant, (see next page estimation). B_{th} will therefore reflect the balance between the torque friction and the magnetic torque in a similar fashion as the balance between magnetic and surface anchoring forces leads to the Fredericksz transition [13,29]:

$$B_{th} = \sqrt{\frac{3 \cdot K_{m/b}}{2 \cdot \Delta\chi \cdot Q_N}} \qquad (3.2)$$

By defining B_{th} as the field needed to produce *50%* of the saturated birefringence, we calculate $K_{m/b}$ at T_{IN} for all samples measured. The resulting values, given in Table 3.1, show that for the same spacer length (see the *C5* compounds) the coupling increases with increasing polymerization degree ($n = 20$, *30* to *40*) as may be expected from the increasing entanglement. For the same $n = 20$ but changing the spacer length (compare *C5* to *C3*), an increasing spacer rigidity (*C3*) prohibiting an alignment of the mesogens parallel to the main chain leads to an enhanced coupling that prohibits magnetic alignment. Finally, the polyacrylates (*B4*) exhibit a lower coupling than the polynorbornenes (*C5*), which is to be expected because their main chain is more flexible, while they also show the same trend of increased friction with increasing polymerization degree.

The backbone conformation is weakly influenced by the mesogen director orientation in the vicinity of the IN transition, the rotation of the mesogenic units do not cause a direct rotation of the polymer chains. However, the thermal contraction of the backbone chains is influenced by the anisotropy of the mesophase, therefore

anisotropic polymeric conformations are more favored. Neutron scattering data confirms that the backbone anisotropy develops linearly in temperature throughout the mesophase. Only for SCPLCs with very short spacers, where a (partial) direct coupling exist, the polymer ordering follows closely the mesogen director ordering in the vicinity of the IN transition and it crosses over to a linear regime at lower temperatures [30].

The rather high value of the mesogen-backbone coupling, (valid around T_{IN}) $K_{m/b} \sim 10^{-25} \, N \cdot m/molecule$, is responsible for the alignment stability when the field is removed. The energy needed to rotate a typical correlated volume of SCPLCs mesogens in the nematic phase, which contains about 10^9 molecules, is about 10^4 times larger than the available kT energy.

3.5 Conclusions

In summary, we have shown that high optical quality, strongly birefringent SCPLC films can be produced, by cooling them from the isotropic to glass phase in an applied magnetic field. This dramatic result opens the way to many possible applications for these highly birefringent materials. We have proven that the effect arises from the field-induced orientation of liquid crystalline nuclei at the isotropic-liquid crystal phase boundary. The degree of alignment strongly depends on the chemical nature of the SCPLC compound. SCPLCs with long polymer chains are more difficult to orient compared to those containing shorter backbones. Shorter mesogen-polymer spacers prevent alignment and SCPLCs with flexible chains are easier to orient than more rigid ones. For the best results a well-defined degree of polymerization is necessary which has to be optimized for every polymer system. These results are interpreted in terms of a static torque friction between the mesogenic units and the surrounding polymer, leading to a quantitative determination of the mesogen-polymer interaction strength.

References

[1]   H. Finkelmann, H. Ringsdorf, J. H. Wendorff, *Macromol. Chem.*, **179**, 273, 1978.

[2]   C.S. Hsu, C.S., *Prog. In Pol. Sci.* **22**, 829, 1997.

[3]   J.C. Dubois, et al., *Liq. Cryst*. **14**, 197, 1993.

[4]   M. Murakami and H. Fujii, *Mol. Cryst. and Liq. Cryst.* **225**, 259, 1993.

[5]   P van de Witte et al., *Jap. J. of appl. Phys. Part 1* **38**, 748, 1999.

[6]   M. Sawodny, *Makromol. Chem.* **46**, 217, 1991.

[7]   V.N. Raja et al., *Liq. Cryst*. **20,** 41, 1996.

[8]   R.B. Findlay and A.H. Windle, *Mol. Cryst. and Liq. Cryst*. **206**, 55, 1991.

[9]   Y. Zhao, P. Roche and G.X. Yuan, *Macromol.* **29**, 4619, 1996.

[10]   C. Pujolle-Robic and L. Noirez, *Nature* **409**, 167, 2001.

[11]   N. Kawatsuki, T. Yamamoto and H. Ono, *Appl. Phys. Lett.* **74**, 935, 1999.

[12]   The Isotropic-Nematic transition of SCPLCs is a weak first order transition, it takes place over a wide temperature region, where the nematic mesophase coexist with the isotropic melt.

[13]   P. G. de Gennes and J. Prost, *The Physics of Liquid crystals,* 2nd ed.*,* Clarendon Press, Oxford, 1993.

[14]   W. R. Krigbaum in *Polymer Liquid Crystals,* chapt.10, A. Ciferri, W. R. Krigbaum, R. B. Meyer, Academic Press, New York, 1982.

[15]   A. M. Donnald, and A. H. Windle, *Liquid Crystalline Polymers*, Cambridge University Press, Cambridge, 1992.

[16]   U. W. Gedde and G. Wilberg, in *Mechanical and Thermophysical Properties of Polymer Liquid Crystals*, chap.10, W. Brostow , Chapman & Hall, London, 1998.

[17]   Y. Zhao and H. Lei, *Macromolecules* **25**, 4043, 1992.

[18]   P. Roche and Y. Zhao, *Macromolecules* **2**8, 2819, 1995.

[19]   K. Akagi and H. Shirakawa, *Current trends polym.* **2***,* 107, 1997.

[20]   L. Noirez, P. Keller and J. P. Cotton, *Liq. Cryst.* **18**, 129, 1995.

[21]   R. G. Kirste and H. G. Ohm, *Macromol. Chem. Rapid Comm.* **6**, 179, 1985.

[22]   L. Noirez, M. Ungerank, F. Stelzer, *Macromolecules*, **34**, 7885 2001.

[23]   All the SCPLCs materials used in this chapter were synthesized in the group of Prof. F. Stelzer, at the Institute for Chemistry & Technology of Organic Materials, Graz University of Technology, Austria.

[24]   M. Ungerank, B. Winkler, E. Eder and F. Stelzer, *Macromol. Chem. Phys.* **196,** 3623 1995.

[25]   M. Ungerank, B. Winkler, E. Eder and F. Stelzer, *Macromol. Chem. Phys.* **198,** 1391 1997.

[26]   G. Maret & K. Dransfeld, *Strong and Ultrastrong Magnetic Fields and Their Applications*, chapter 4, Springer–Verlag, Berlin, 1985.

[27]   The $C5$, $n = 40$ sample can be aligned above $19T$, but loses its alignment during cooling down, possibly due to the built-up of thermal stress close to T_{NG}, which is primarily important for polymers with relatively long chains.

[28]   For very low spacer length the mesogen/backbone interaction is mainly dominated by a direct coupling effect, which leads to the (partial) loss of the ordered mesophase.

[29]   In our case $\langle sin(2 \cdot \theta) \rangle_{3D} = 2/3$ because it is performed in tree dimensions, whereas the Fredericksz transition is a surface effect, $\langle sin(2 \cdot \theta) \rangle_{2D} = 2/\pi$.

[30]   Interpretation based on neutron scattering data from unpublished work of L. Noirez, F. Stelzer et al.

Chapter 4

Magnetic field induced changes of the Isotropic-Nematic phase transition in Side Chain Polymer Liquid Crystals.

The Isotropic-Nematic (IN) phase transition of Side Chain Polymer Liquid Crystals is intrinsically a weak first order transition with a biphasic region spread over a wide temperature interval. In the presence of high magnetic fields we find the IN transition to become first order in character. The IN biphasic region shrinks its temperature window as stronger magnetic fields are applied, until it completely disappears, giving rise to a sharp first order transition. We interpret this behavior as a nonlinear coupling of the magnetic field to the free energy of the system, via the suppression of the order fluctuations in the nematic mesophase at the IN transition crossing.

4.1 Introduction and Overview

Side Chain Polymer Liquid Crystals, (SCPLCs), are made of rigid mesogenic units attached laterally to a polymeric chain via a flexible spacer, which gives the mesogens enough freedom to form Liquid Crystalline mesophases [1-3]. The SCPLCs phase space is characterized by a glass phase at low temperatures followed by (an) intermediate ordered mesophase(s) and an isotropic phase at high temperatures. The SCPLCs phase transitions are very broad, taking place over a wide temperature range, where a mesophase co-exists with either the isotropic melt or another mesophase, behavior generally attributed to a certain degree of polydispersity [4].

Combining the properties of polymers with the self-organization of Liquid Crystals, SCPLCs are of both fundamental interest [2-4] and of importance for many applications [5] such as optically nonlinear devices [6], displays [7,8] and optical data storage [9]. The IN transition is a key point in understanding the properties of these hybrids and is a central feature in any method that deals with the SCPLCs processing [10-13].

In the present chapter we report a study on the IN phase transition of SCPLCs in high magnetic fields, via field-induced birefringence and optical transmission measurements. We show that the dynamics of the transition is modified in the presence of an applied magnetic field, changing from a weak first order transition in zero field to a sharp first order in high fields. We find that the IN biphasic region narrows as the applied magnetic field increases and eventually disappears for high fields. At this high fields the transition takes place abruptly at a defined temperature. Employing SCPLCs with different polymeric backbones, polymerization degree, n, polydispersity indices, PDI, and spacer lengths we find the effect to be of general nature, only the field values where the effect is observed depend on the SCPLCs chemistry details.

In the framework of the Landau-De Gennes (LDG) theory of the IN transition [14-16], we show the need to include the order parameter fluctuations contribution for a correct description of the SCPLCs. In agreement with the experimental results we find the magnetic field to reduce the elastic energy associated with order fluctuations, and hence influencing the IN transition path.

4.2 Experimental details

A polynorbornene and a polyacrylate-derivative SCPLC, with cyanobiphenyl groups as mesogens and methylene units as spacers were investigated [17].

We studied the polynorbornene SCPLC in two distinct conformations, with a spacer length of 5 methylene units and respective 3 methylene units: Poly[(±)–*exo,endo*-bis{5-[(4′-cyanobiphenyl-4-yl)oxy]pentyl}norborn-5-ene-2,3-dicarboxylate] [18], referred as *C5* and respectively: Poly[(±)–*exo,endo*-bis{3-[(4′-cyanobiphenyl-4-yl)oxy]propyl}norborn-5-ene-2,3-dicarboxylate], referred as *C3*, see table 3.1. The *C3* and *C5* polymers are both thermotropic SCPLCs with a glass-nematic-isotropic phase space. Their backbone is relatively stiff due to the double bonds that connect the cyclo-pentyl units. Synthesized by Ring Opening Methahesis Polymerization, with a living character, the *C3* and *C5* feature a relative low degree of polydispersity *PDI ~ 1.2* .

The polyacrylate-derivative is also a thermotropic nematic SCPLC, but its backbone chain is more flexible in comparison with the polynorbornene one. The spacer is 4 methylene units long and the mesogenic unit is the same cyanobiphenyl group: Poly-{4-[(4′-cyanobiphenyl-4-yl)oxy]butyl}acrylate, referred as *B4*, see table 3.1. Synthesized by free radical polymerization B4 polydispersity is relatively high, *PDI ~ 2* .

The samples were prepared as films on optical glass support by spin coating from solution and subsequent solvent removal by annealing. For experimental investigation, the sample is placed in a temperature-controlled chamber, (temperature range $20 - 300°C$, $±0.01°C$ stability), within the bore of a *20T* resistive "Bitter" magnet, see sect. 2.10. The sample is passed by a polarization-intensity double modulated laser beam, with the optical path perpendicular to the magnetic field, which allows simultaneous measurement of the magnetic field induced birefringence and of the optical transmission (10^{-6} radians, respectively 10^{-5} detection limits). The field induced birefringence signal is proportional to the macroscopic order parameter of the sample, $Q(B)=Q(B)/b_{max}$ [19], with b the magnetic field induced birefringence, b_{max} the birefringence of a perfectly oriented sample and B the magnetic field, see sect. 2.11. In the nematic phase the SCPLCs features a microscopic texture of locally ordered domains, randomly oriented to each other, which gives rise to incoherent light scattering. At the laser wavelength used for the experiments, $He - Ne \ 543.5 \ nm$, the samples do not absorb and the optical transmission is proportional only to the amount of scattered light. This allows direct monitoring of the sample domain morphology. All experiments were done at $10°C/min$ cooling-warming rate, which was sufficiently slow.

4.3 Experimental results

Fig.4.1.a presents the optical transmission recorded for a *B4*, *n = 30*, sample, cooled in different magnetic fields. In zero magnetic field, from high transmission in the isotropic phase the sample starts to scatter light as it undergoes the IN transition, the transmission constantly decreases during the biphasic region and in the nematic phase the sample ends up completely opaque. For low applied magnetic fields, the induced changes are small and the sample follows almost the same path as that observed for a sample cooled in a zero magnetic field.
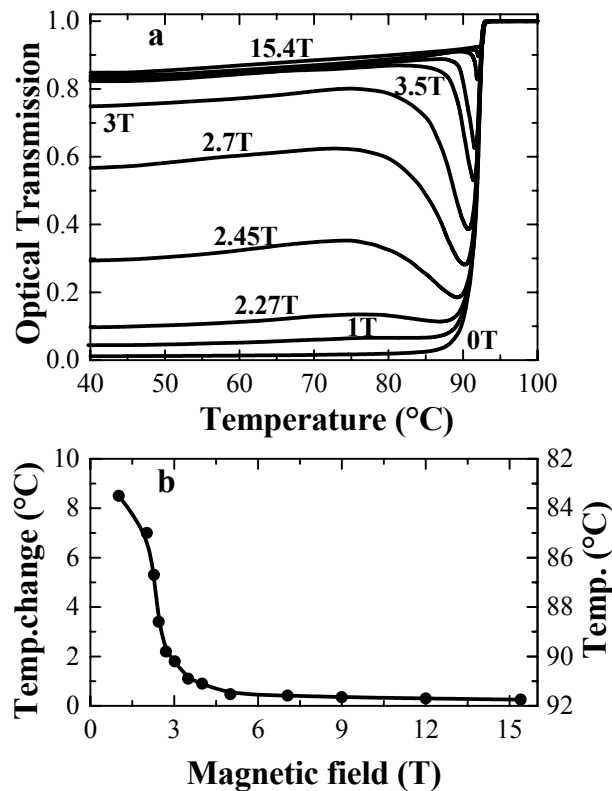
Figure 4.1 a. Optical transmission evolution recorded for a B4 sample, n = 30, PDI ~ 2, 20μm film, upon cooling in different magnetic fields, upper panel. b. Change in the optical transmission turning point versus the applied magnetic field, extracted from the upper panel curves, lower panel.

   In strong magnetic fields, at some point in the biphasic region, the transmission completely changes its trend, showing a sharp increase, followed by saturation at some intermediate value in the nematic phase. Higher applied magnetic fields move the transmission turning point toward the beginning of the IN transition, whilst the transmission saturates at higher values. For fields above *7T* the biphasic region completely disappears, the transition itself taking place in a very narrow interval of *0.5°C* . The transmission turning point evolution, presented in fig.4.1.b, shows a strong onset around *2.5T* , followed by saturation for fields above *7T* .
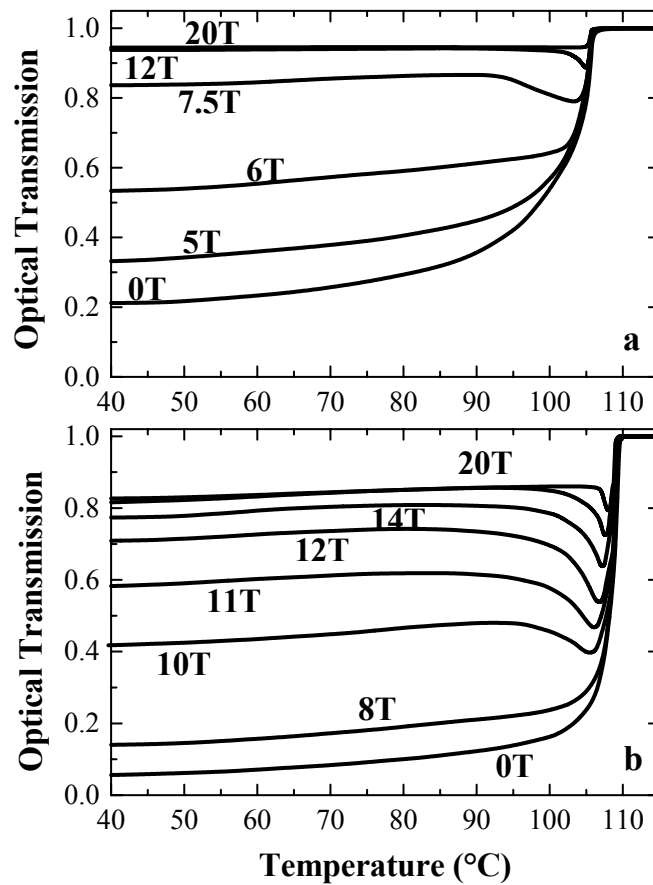

Figure 4.2 *Optical transmission evolution recorded for a C5 sample, n = 20 , PDI ~ 1.2 , 10 μm film, upon cooling in different magnetic fields, (**a**), respectively for a C5 sample, n = 30 , PDI ~ 1.2 , 20 μm film, (**b**).*

For a *B4* sample with a lower polymerization degree $n = 20$, a similar effect is observed, in this case the biphasic region disappears around *5.5T*. For a *C5* sample with $n = 20$, the results are analogous. The only difference is that significant effects start being observable at higher magnetic fields. Magnetic fields of about *5T* and *17T* are needed to completely close the biphasic region, fig.4.2.a. For a polymer *C5* with $n = 30$, the behavior shows a comparable trend, a significant effect appears around *8T* but for the maximum available field *20T* only partly close the biphasic region, fig.4.2.b. For a C5 sample with an even higher polymerization degree, $n = 40$, an effect is visible around *18T*, while until *20T* we observe only a modest narrowing of the biphasic region.

The *C3* samples did not show an effect in the maximum applied field of *20T* for any of the investigated polymerization degrees: $n = 20$, $n = 30$ and $n = 40$.
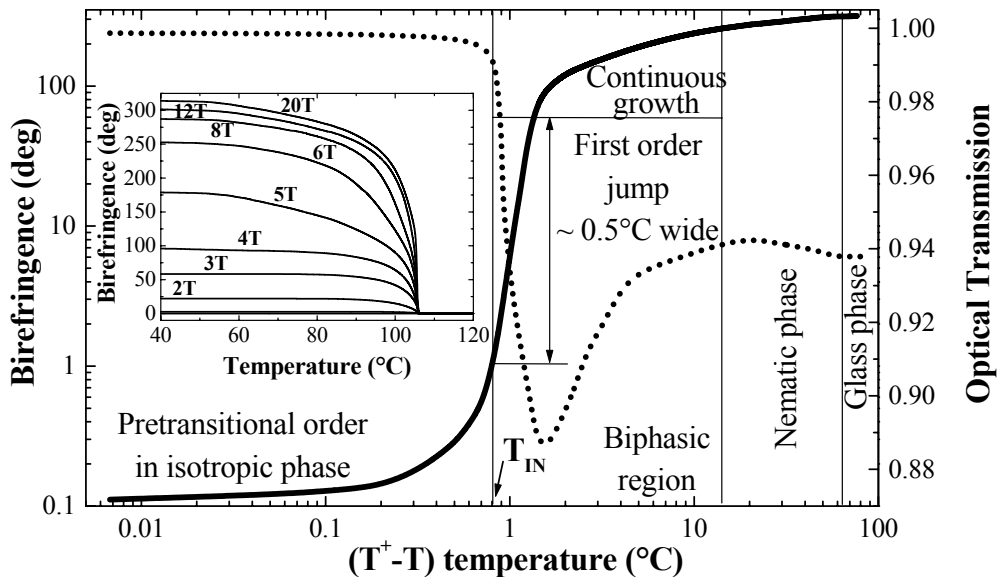
Figure 4.3 *Birefringence (full line) and optical transmission (dotted line), of a C5 sample, $n \sim 20$, PDI ~ 1.2, $10\,\mu m$ film, simultaneously recorded during cooling in 12 T at $10°C/min$ versus ($T^+ - T$) temperature scale, with $T^+ \approx T_{IN} + 1°C$.*
Inset: *Magnetic field induced birefringence of the same C5 sample, recorded upon cooling in different fields at $10°C/min$.*

Fig.4.3 shows the birefringence signal and the optical transmission of a *C5* polymer sample recorded upon cooling in a *12T* magnetic field. The birefringence

clearly shows the pre-transitional ordering followed by a sharp jump, in a narrow temperature interval, of about $0.5\,°C$. The curve continues with a smooth increase throughout the biphasic region, followed by saturation as it approaches the glass phase. Corresponding to the pre-transitional region the transmission features a small decrease followed by an abrupt decrease starting at T_{IN} and extended for the next approximately $0.5\,°C$. From this point on, the transmission changes its trend and continuously increases until the end of the biphasic region. In the nematic phase the transmission signal remains constant, indicating that the ordering, as revealed by the birefringence, affects uniformly the sample without to create more scattering. The inset presents the birefringence of the same sample as cooled in different fields. The onset of the birefringence always starts at T_{IN} and saturates toward the NG transition. Interestingly the saturation values are higher for larger applied fields.

4.4 The dynamic of the Isotropic-Nematic phase transition in SCPLCs

Intrinsically, the IN transition of SCPLCs is a two step process. A volume fraction of the sample undergoes a sharp first order jump at a fixed temperature, T_{IN}, via nucleation of nematic islands which are at equilibrium with the surrounding isotropic phase. The rest volume fraction of the sample changes continuously from isotropic to nematic over a large temperature range, via a growth mechanism on the already existing nematic nuclei, fig.4.4. This particular behavior originates in the fact that the rotational orientation of the mesogens is hindered by the polymer backbones [3, sect.3.4]. The mesogen-backbone coupling fixes the orientation of the nematic islands against thermal fluctuations and therefore introduces an extra elastic contribution to the nematic free energy due to the order fluctuations, see fig.4.4 and eq.4.1. To overcome this energetic barrier, a fraction of the sample has to undergo super-cooling in the isotropic state, impending the transition to be consumed at a fixed temperature. At the end of the biphasic region the sample volume becomes predominantly covered by nematic islands with different orientation relative to each other, which further evolve into nematic domains separated by sharp domain walls.

The presence of a magnetic field directs the IN transition to follow a modified path. Due to a finite correlation length, induced order of the mesogen moieties develops already in the pre-transitional region. As T_{IN} is reached nematic islands nucleate and in the same time undergo orientation along the magnetic field lines. This results in a strong suppression of the extra energetic barrier and a larger volume

77

fraction of the sample turns nematic at T_{IN}, fig.4.4, with the biphasic region shrinking accordingly.

No magnetic field applied

Nematic **Biphasic region** **Isotropic**

Nematic $B = 0$ **Isotropic**
Costs *extra* elastic energy

Nematic $B \neq 0$ **Isotropic**
Costs *no* elastic energy

Nematic **Biphasic region** **Isotropic**
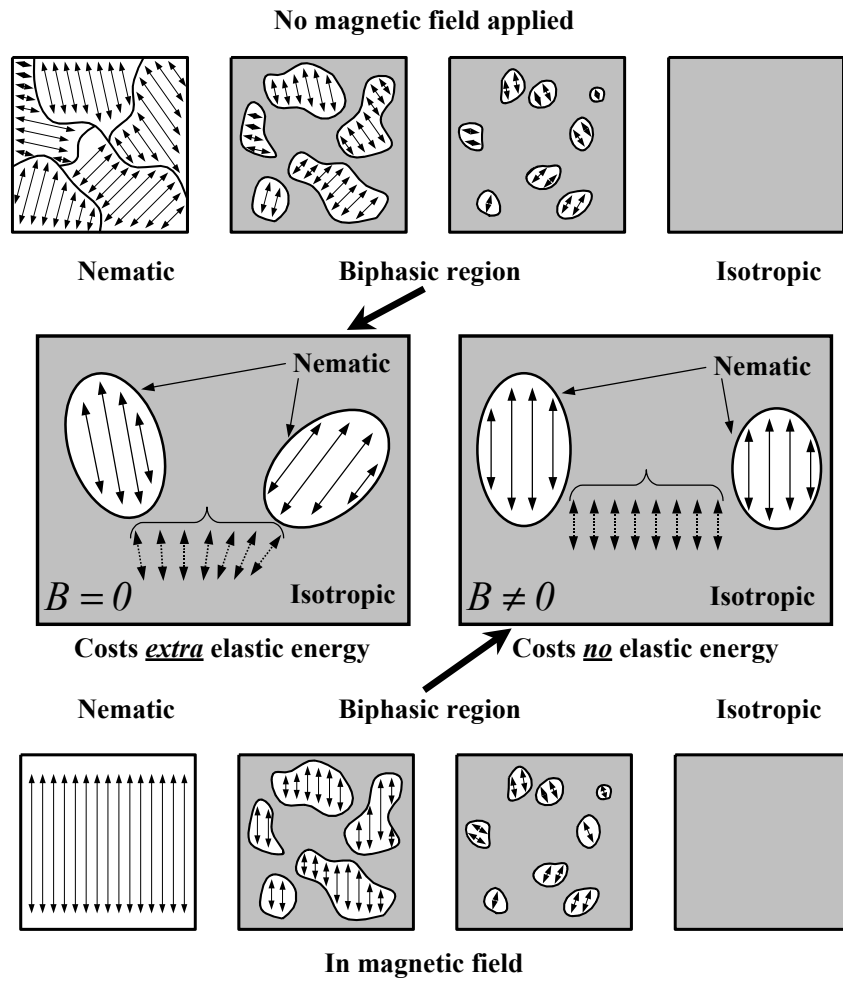
In magnetic field

Figure 4.4 *Schematic representation of the biphasic region where nematic nuclei co-exist at equilibrium with the surrounding isotropic component, in the absence and presence of an applied magnetic field. The central panels illustrate the possible configuration of isotropic component to become nematic and its energetic costs.*

The magnetic field leaves the local order unchanged, $Q_N \neq Q_N(B)$, because the magnetic energy per molecule is too small when compared to the thermal fluctuations, but does change the orientation of the nematic islands as a whole, affecting only the director order parameter, $Q_D = Q_D(B)$, see sect. 2.3. Toward the end of the biphasic region, when the nematic islands collide, the individual directors are aligned along the magnetic field, which cause the system to evolve into a monodomain morphology.

Following a Rayleight-Debye approach [20] we have studied the light scattering of the SCPLCs in the absence and presence of a magnetic field. We found two distinct scattering regimes, the beginning of the transition, in which the isotropic and nematic components have different refractive indices, and the end of the transition, in which nematic domains with the same refractive index exist, but different projections, see sect. 2.5.

In the absence of induced order, the IN transmission appears as a monotonic decrease of the optical transmission, with no discontinuities due to the crossover from one regime to the other. This is consistent with the experimental observations, see the $0T$ curve in fig.4.1 and fig.4.2.

In the presence of an applied magnetic field we find that the isotropic/nematic islands regime is dominated by the existence of two different refractive indices, whereas the field induced orientation of the nematic islands hardly influences the overall scattering. However, in the all-nematic regime, the scattering strongly depends of the magnetic field induced orientation, with the limit of no scattering in the case of total alignment. It is only at the crossover between the two regimes that a turn in transmission can occur.

Consequently, it is correct to associate the experimentally observed transmission turning point, fig.4.3 and fig.4.4, with a point within the biphasic region, with its value scaling relative to the temperature window of the biphasic region.

4.5 Interpretation

To analyze these observations we apply the LDG free energy expansion theory [14-16] to the specific case of SCPLCs in magnetic field:

$$F = a \cdot \left(T - T^*\right) \cdot Q^2 - B_{ct} \cdot Q^3 + C \cdot Q^4 + \Delta\chi \cdot B^2 \cdot Q + L \cdot \left(\frac{dQ}{dr}\right)^2 + K_{m/b} \cdot Q$$

$$(4.1)$$

Where Q, T and T^* are the uniaxial nematic order parameter, the temperature and the minimum super-cooling temperature. The expansion coefficients a, B_{ct}, C, are constants related to the SCPLCs properties. L is related to the elastic constants [16], $K_{m/b}$ is the mesogen/backbone coupling energy, $\Delta\chi$ is the anisotropy of the mesogen diamagnetic susceptibility and B the magnetic field induction.

The LDG framework [14,16] leads to the prediction that as the value of the applied magnetic field increases, the transition temperature moves to higher values while the order of the transition becomes more second order in nature. Pre-transitional magnetic field ordering weakens the order parameter jump at the transition and the theory even predicts a critical point where the transition becomes second order and for higher fields the transition completely disappears. However, typical numbers show that the possibility of such experimental observation is quite remote since it requires magnetic field of the order $10^3 - 10^4\,T$.

Since the typical fields used for our experiments are $B \leq 20\,T$, we neglect the direct diamagnetic contribution term $\Delta\chi \cdot B^2 \cdot Q$. The mesogen-backbone coupling term, $K_{m/b} \cdot Q$ is comparable with the magnetic one, see sect.3.4, and we neglect this parameter as well. However, both terms are indirectly present in the order fluctuation term $L \cdot (dQ/dr)^2$ one responsible for the its non-vanishing character (the magnetic contribution) and one for its value (the coupling contribution). Making use of the factorization:

$$L \cdot (dQ/dr)^2 = L \cdot Q^2 \cdot (A_D/\xi)^2 \tag{4.2}$$

and using [16]:

$$\xi = \left[L/a \cdot (T - T^*) \right]^{1/2} \tag{4.3}$$

the free energy can be described as:

$$F = a \cdot (T - T^*) \cdot Q^2 \cdot (1 + A_D^2) - B_{ct} \cdot Q^3 + C \cdot Q^4 \tag{4.4}$$

Where A_D is the amplitude of the domain order parameter fluctuations of the already nematic component and ξ the fluctuation correlation length.

Approaching the IN transition from higher temperatures, the A_D term induces the transition to have a weak first order character with a biphasic isotropic-nematic region extended from T_{IN} to T^*, where T_{IN} is the LDG result in the absence of

fluctuations, eq.(4.2). It can be clearly seen that via induced alignment the magnetic field reduces the contribution of the fluctuation term from $A_D^2(B) \sim 0.1$, [21], in the absence of any induced order to $A_D^2(B) \sim 0$ in the case of complete order. This results in the narrowing of the temperature range of the biphasic region. In the case of high induced ordering the fluctuation contribution tends to zero. The classic LDG result is restored and the transition is fully first order. For intermediate ordering the situation is a crossover, with the biphasic region shrinking as the magnetic induced alignment becomes larger.
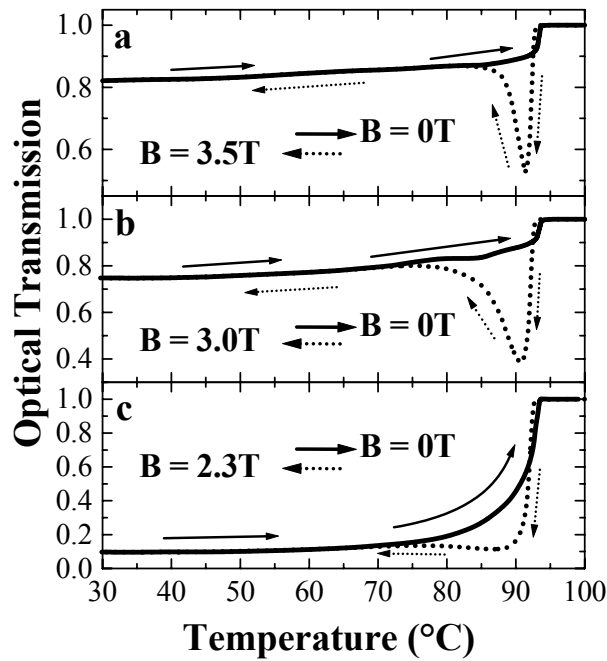

Figure 4.5 *Optical transmission for a B4 polymer sample with n ~ 30, 20μm film recorded during heating up (solid line) in zero field after cooling (dotted line) in a magnetic field of 2.3T **(a)**, 3.0T **(b)** and 3.5T **(c)**,*

When the IN transition is approached from below, the fluctuation term does not act anymore as an energetic barrier, with the important consequence that the transition is sharp and there is no biphasic region. Fig.4.5 presents the optical transmission recorded as the *B4* polymer sample approaches the IN transition from lower temperature. In complete agreement with our proposed model the curves clearly show no biphasic region. The presence of the mesogen/backbone coupling term $K_{m/b} \cdot Q$ has the important consequence that once order has been induced in the SCPLCs system, the sample alignment is stable until warmed to the isotropic phase, see sect.3.4.

The different magnetic field strengths needed to obtain an effect for various SCPLCs compounds can be understood via the fact that structures with stiffer backbones, shorter spacers or larger degrees of polymerization need higher magnetic fields to be aligned at the IN crossing, see sect.3.4.

4.6 Conclusions

We have shown experimentally that magnetic fields alter the IN transition of SCPLCs from a weak first order to a sharp first order via the suppression of the order fluctuations. We proposed a qualitative interpretation of this phenomenon within the framework of the LDG theory via the correct inclusion of the order parameter fluctuation. The present results suggest that the mesogen-backbone coupling is co-responsible for the existence of the isotropic-nematic biphasic region, complementary information to the current understanding of the field, namely that only a certain degree of polydispersity account for the presence of a biphasic region [4].

References

[1]   H. Finkelmann, H. Ringsdorf, J.H. Wendorff, *Macromol. Chem.*, **179**, 273, 1978.

[2]   C.B. McArdle, *Side chain Liquid Crystal Polymer*s, Chapman & Hall, New York, 1989.

[3]   C. Pujolle-Robic, L. Noirez, *Nature* **409**, 167, 2001.

[4]   D. Demus et al., *Handbook of Liquid Crystals*, vol.3, p.170, Wiley-VCH Velrag GmbH, Weinheim, 1998.

[5]   C.S. Hsu, Prog. In Pol. Sci. **22**, 829, 1997.

[6]   J.C. Dubois, P. Lebarny, P. Robin, V. Lemoine, H. Rajbenbach, Liq. Cryst. **14**, 197,1993.

[7]   M. Murakami, H. Fujii, Mol. Cryst. and Liq. Cryst. **225**, 259, 1993.

[8]   P. van de Witte et al., Jap. J. of appl. Phys. Part 1 **38**, 748, 1999.

[9]   M. Sawodny, Makromol. Chem. **46**, 217, 1991.

[10]   V.N. Raja et al., Liq. Cryst. **20**, 41, 1996.

[11]   R.B. Findlay, A.H. Windle, Mol. Cryst. and Liq. Cryst. **206**, 55, 1991.

[12]   Y. Zhao, P. Roche, G.X. Yuan, Macromol. **29**, 4619, 1996.

[13]   N. Kawatsuki, T. Yamamoto, H. Ono, Appl. Phys. Lett. **74**, 935, 1999.

[14]   E.F. Gramsbergen, L. Longa, W.H. de Jeu, *Phys. Rep*. **135**, 19, 1986.

[15]   A.J. Bray, *Adv. in Phys*. **43**, 357, 1994.

[16]   S. Singh, *Phys. Rep*. **324**, 107, 2000.

[17]   All the SCPLCs materials used in this chapter were synthesized in the group of Prof. F. Stelzer, at the Institute for Chemistry & Technology of Organic Materials, Graz University of Technology, Austria.

[18]   M. Ungerank, B. Winkler, E. Eder and F. Stelzer, *Macromol. Chem. Phys.* **196,** 3623 1995.

[19]   G.Maret, K. Dransfeld, *Strong and Ultrastrong Magnetic Fields and Their Applications*, chap.4, Springer –Verlag, Berlin, 1985.

[20]   M. Kerker, *The Scattering of Light and Other Electromagnetic Radiation*, Academic Press, New York and London, 1969.

[21]   Numerically calculated value for director fluctuation, based on Boltzman Statistics.

Chapter 5

Observation of surface and bulk phase transitions in nematic liquid crystals

We report the first observation of a pure Isotropic-Nematic (IN) surface phase transition of a nematic Liquid Crystal on a substrate, clearly separated from the bulk IN transition. Using a nematic LC mixture, we isolate the surface transition from the bulk transition, owing to the varied mixture ratio near the surface. This allowed us to study the two transitions independently, on various substrates and in magnetic fields up to $20T$. We find that the surface IN transition is of first order on surfaces with a weak anchoring energy and continuous on surfaces with a strong anchoring. We also show that the presence of high magnetic fields does not change the surface IN transition temperature, whereas the bulk IN transition temperature increases with field. We attribute this to the bulk/surface interaction energy, which is tuned by the magnetic field induced order of the surface-wetting layer.

5.1 Introduction and Overview

The critical behaviour of Liquid Crystals (LC) near a wall is of fundamental interest, since it is related to surface phase transition phenomena and wetting [1-14]. It is also of relevance for technological applications such as liquid crystals displays [15,16], where a good surface induced ordering is essential.

In a confined geometry the LC molecules interacting with the surface of the confining walls give rise to different LC behaviour at the surface and in the bulk. Upon undergoing the IN transition the delicate balance of intermolecular interactions tends to favour the LC-surface interaction in the nematic phase, whereas the LC-LC interaction is preferred in the isotropic phase. Due to this the new nematic phase occurs first at the surface, a phenomenon known as "wetting". The IN transition is relatively weak thermodynamically, therefore large pre-transitional effects take place prior to the transition. The interaction of these pre-ordered LC molecules with the surface is known as "pre-wetting". In a magnetic field the diamagnetic LC molecules feel a torque that forces them to orient relative to the field direction. Though at the level of individual molecules the magnetic field effect is negligibly small in the isotropic phase, the collective behaviour of the mesophase makes the molecular contribution to add up constructively resulting in a macroscopic orientation effect.

A wide variety of theoretical studies have addressed this wetting problem either at a general level of surface related phenomena [1,2] or for the particular case of liquid crystals [3,4]. Cahn [1] introduced a theory describing a first order Wetting Transition (WT), leading to an ordering film of finite thickness in any two-phase mixture of fluids contacting a third phase at a critical temperature. Later, Nakanishi [2] showed that pre-wetting (PW) of a highly ordered film with finite thickness on a surface continues to wetting via a first order or continuous WT. This PW, where a strongly anchored LC layer forms a uniform nematic phase adjacent to the substrate and near the isotropic bulk, has been often discussed for the case of strong surface fields [3,4]. Sluckin at al. [4] calculated a general phase diagram of nematic LC in the presence of both bulk LC and a magnetic field. It shows a WT changing from first order to continuous by increasing either the surface interaction or the applied magnetic field.

In contrast to all this theoretical work, the experimental data available to date are very limited. Polarised optical microscopy observations [5,6] gave evidence of different kinds of behaviour near the phase transition depending on the surface, and ellipsometry [7-10] and NMR [11] studies demonstrated surface pre-wetting in the isotropic phase. Despite these experimental efforts, there still does not exist a single

valuable observation to confirm the existence of a first order, combined first order/continuous or continuous surface transition. This lack of data is indicative of the experimental difficulties related to this type of investigation. Partly, this is due to the very close proximity of the surface transition to the bulk one in all the cases reported so far.

Here we report on what we believe to be the first observation of a pure surface phase transition of a nematic LC on a substrate, clearly separated from the bulk IN transition. To achieve the separation, we use a nematic LC mixture, in this way isolating the surface transition from the bulk one, owing to the varied mixture ratio near the surface. The surface and the bulk transitions are investigated by varying both surface and magnetic field strengths. We find the surface IN transition to be of first order on surfaces with a weak anchoring energy and continuous on surfaces with a strong anchoring. The bulk/surface interaction energy, tuned by the magnetic field induced order of the surface-wetting layer, causes the bulk transition to shift towards higher temperatures. The classic limit with the bulk and the surface transitions merging together is found only in very large magnetic fields.

5.2 Sample preparation and experimental description

Thermoplastic polymer films, polyvinyl cinnamate (PVCN) and polyvinyl formal PVFM, were prepared on a glass substrate from *2%* polymer solution via spin coating and subsequent thermal annealing for solvent removal. Planar cells prepared with the polymer coated (or clean) glass substrates adjusted to *5.6 μm* thickness, using polyethyleneterephthalate (PET) spacers, were filled with *E63* (Merck; $T_{IN} = 87.5°C$ composed [17] out of six LC mesogens, all diamagnetic) in the isotropic phase. The cells were placed in a temperature-controlled chamber inside a *20 T* Bitter magnet, with the glass plates parallel to the magnetic field. The field-induced birefringence and the optical transmission of the samples were measured simultaneously with the help of a polarization-intensity double modulated laser beam, *He − Ne 543.5 nm*, which passed through the sample at normal incidence relative to the magnetic field direction. We probed *in situ* the LC order, via birefringence [18], and the LC morphology, via light scattering [19], using the set-up presented in sect.2.9. Scattering is the only contribution to the optical transmission because the *E63* does not absorb light at the used wavelength.

5.3 Experimental results

Fig.5.1 shows the surface and the bulk IN phase transition on different substrates as the cells were cooled in a magnetic field of *2 T*. The surface IN transition appears as a small step in the birefringence base line (Δb_{IN}^s), taking place over a finite temperature range (ΔT_{IN}^s), a few Kelvin above the bulk transition. The non-zero birefringence base line slope represents the pre-transitional LC ordering. The surface transition is directly related to the molecular interaction between the LC and the substrate. On a clean glass substrate, characterized by a very weak surface anchoring, $G \approx 10^{-10} \, J/m^2$, we find the surface transition to have a sharp first order character and to appear at the lowest temperature among all studied cells, fig.5.1.a. For the PVFM substrate, with a medium anchoring energy, $G \approx 10^{-7} \, J/m^2$, originating mainly from Van der Waals interaction between polar groups, the surface transition occurs at a higher temperature and shows a combined first order/continuous appearance, fig.5.1.b. The PVCN substrate has a strong anchoring, $G \approx 10^{-5} \, J/m^2$, because the interaction also includes the π−π coupling with the cinnamoly groups, therefore the transition occurs at the highest temperature and has a clear continuous character, fig.5.1.c.

From Δb_{IN}^s (using the full cell birefringence at room temperature as reference) we estimate the thickness of the ordering LC film to be about one molecular layer, confirming the initial prediction of Cahn [1] and the NMR observations of Crawford [11]. One should realize that this corresponds to a wetting transition on a pre-wetted surface and does not contradict other wetting layer thickness estimations [13,14].

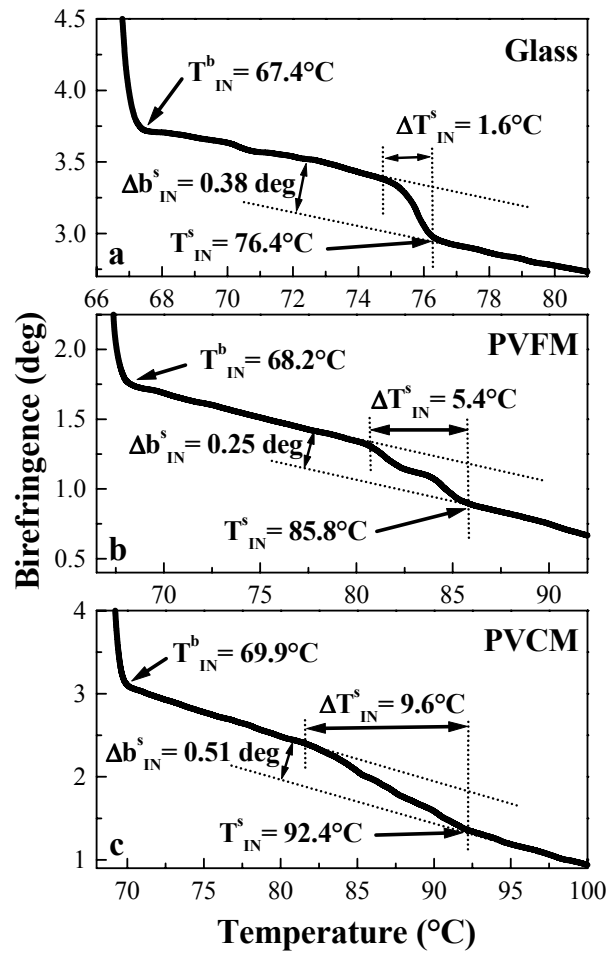**Figure 5.1** *Surface and bulk Isotropic-Nematic phase transitions on different substrates. Magnetic field induced birefringence of E63 on clean glass (a), PVFM (b) and PVCN (c) coated cells, in 2 T. Detail around the surface T_{IN}^s and bulk T_{IN}^b transition temperatures. ΔT_{IN}^s and Δb_{IN}^s are the temperature interval and respectively the field induced birefringence associated with the surface transition.*

Fig.5.2 shows that with increasing magnetic field, the bulk IN transition temperature (T_{IN}^b) shifts to higher values, but the surface IN transition temperature (T_{IN}^s) as well as its temperature window (ΔT_{IN}^s) remains unchanged. The slope of the birefringence versus temperature dependence, however, which is related to the pre-transitional order, gets steeper and the jump in the birefringence corresponding to the surface transition becomes larger for higher applied magnetic fields. For sufficiently large magnetic fields, T_{IN}^b approaches T_{IN}^s to such an extent that the two transitions are no longer seen as distinct, fig.5.2d.
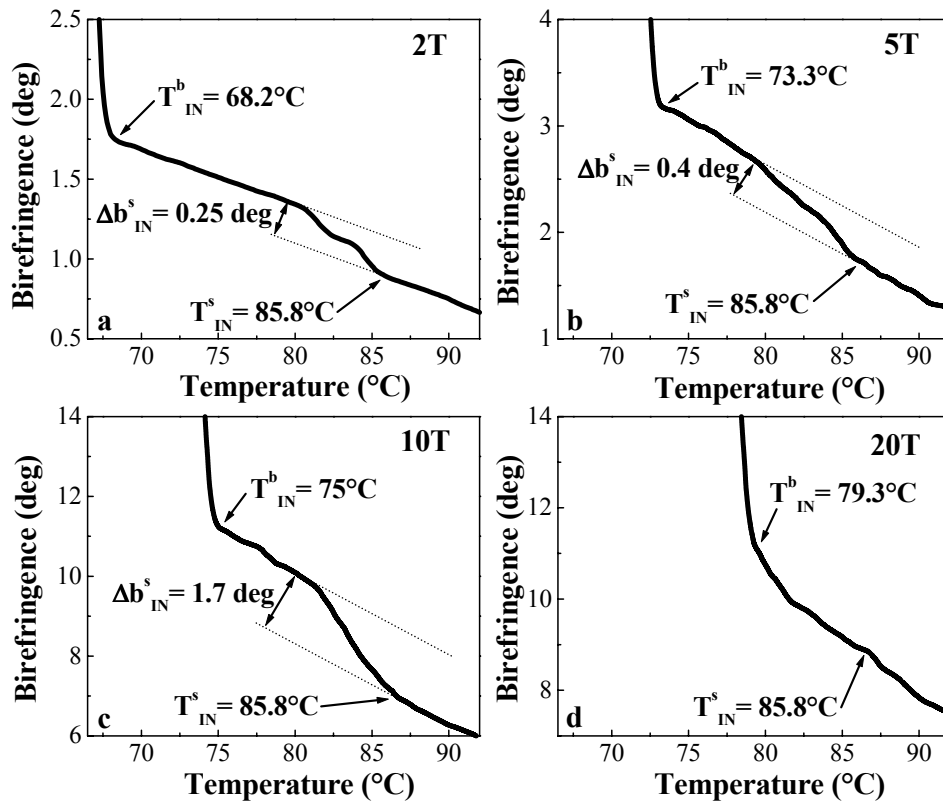

Figure 5.2 *Magnetic field dependence of the surface and bulk transitions. Field induced birefringence evolution of a PVFM coated cell in different magnetic field strengths: 2 T (a), 5 T (b), 10 T (c) and 20 T (d). Detail around the surface and bulk IN transitions.*

Fig.5.3 presents the birefringence and optical transmission of a PVMF coated sample that was cooled in $5T$ and subsequently warmed in $0T$. For the cooling down process the birefringence signal initially show a small increase, corresponding to the pre-transitional order, followed by a small step at T_{IN}^s (for a detail around T_{IN}^s see fig.5.2.b). A few degrees below the surface transition step, the birefringence signal shows a sharp increase, indicative for the bulk IN transition. The curve follows the same initial slope until room temperature is reached. Recorded simultaneously, the optical transmission shows a small, continuous decrease through the surface transition interval.
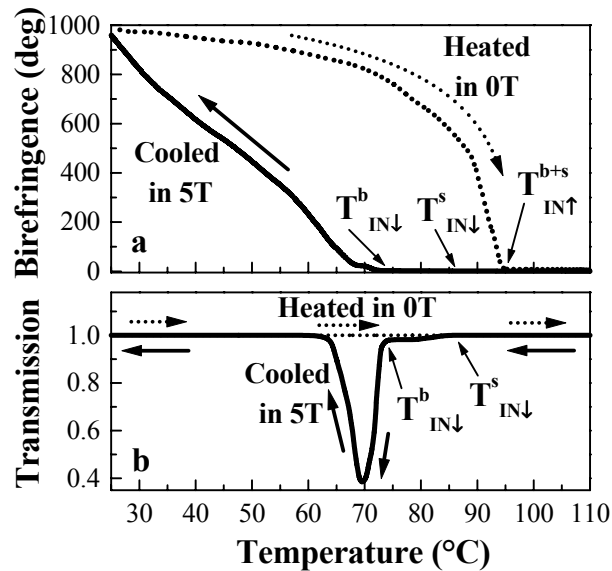
Figure 5.3 *Surface stabilized magnetic field induced alignment. Birefringence (a) and optical transmission (b) of a PVFM coated cell upon cooling down in a 5T field (continuous line) and subsequently warming up in zero applied field (dotted line). The indices $\uparrow$ and $\downarrow$ marks the transition temperatures upon cooling down and respectively warming up.*

This suggests that the surface layer is larger than one molecular layer, being able to produce the amount of light scattering responsible for the observed decrease. Actually the pre-wetting layer connecting the ordered surface layer with the isotropic bulk is responsible for the observed scattering. At T_{IN}^b the transmission strongly decreases, whereas a few degrees below this temperature the sample

completely recovers its transparency and remains transparent until room temperature is reached. Removal of the magnetic field at room temperature leaves both birefringence and transmission signals unchanged. Further optical characterizations show a planar, uniaxial monodomain alignment, with the director along the magnetic field direction. After being aligned in a magnetic field, the sample was heated in the absence of an applied magnetic field and its relaxation was recorded. Upon heating the birefringence follows a different path, and the bulk and the surface IN transition are no longer distinctly observed, fig.5.3.a. Throughout the heating process the sample transmission maintains a constant maximum value, fig.5.3.b. The dip in the optical transmission upon cooling appears always at T_{IN}^b and has the same width of *11.5°C*, independent of the substrate or the applied magnetic field. We associate this behavior to an isotropic/nematic coexistence region, originating from the fact that *E63* is a mixture of various LCs, which causes light scattering.

Some of the samples were cooled only partially in the presence of an applied magnetic field. For the samples that had the field applied below the bulk transition, orientation is observed but when the field is turned off the orientation relaxes. The same results were recorded for the samples that had the magnetic field applied above the bulk transition but below the temperature where the surface transition was complete. On contrary, the cells that had the field on until below the surface transition and removed afterwards showed uniform stable alignment at room temperature, similar to the cells cooled in a field all the way from the isotropic phase down to room temperature. These control experiments prove that Δb_{IN}^s is indeed related to a surface transition and the orientation of the surface layer is locked at the temperature corresponding to the bulk transition. Thus the ordered surface layer imposes its orientation to the bulk, being responsible for the alignment stability after the field is off.

5.4 Theoretical interpretation and discussions

To analyse these observations we start from the free energy density expression [19,20], F, of a single component nematic LC cell in a magnetic field B:

$$F = f(Q,T) + L \cdot \left(\frac{dQ}{dr}\right)^2 + G \cdot \delta(z) \cdot Q \qquad (5.1)$$

with:

$$f(Q,T) = a(T - T^*) \cdot Q^2 - B_{ct} \cdot Q^3 + C \cdot Q^4 + \Delta\chi \cdot Q \cdot B^2 \qquad (5.2)$$

Here Q, T and T^* are the uniaxial order parameter, temperature and minimum super-cooling temperature respectively. G is the surface field, a, B_{ct}, C are LC specific constants, L is related to the elastic LC constants and $\Delta\chi$ is the anisotropy of the diamagnetic susceptibility of the LC molecules. Typical numbers confirmed by experiments [18,21] show that the direct diamagnetic contribution $\Delta\chi \cdot Q \cdot B^2$ is very small: an applied field of $10\,T$ would only cause a change in the transition temperature of about $10\,mK$.

The elastic term can be rewritten as:

$$L \cdot \left(\frac{dQ}{dr}\right)^2 \approx L \cdot Q^2 \cdot \left[\frac{A_D(B)}{\xi}\right]^2 \qquad (5.3)$$

with $A_D(B)$ the mean amplitude of the director fluctuation and ξ the average correlation length. Using [22]:

$$\xi = \sqrt{\frac{L}{a \cdot (T - T^*)}} \qquad (5.4)$$

the free energy expression becomes:

$$F \approx a \cdot (T - T^*) \cdot Q^2 \cdot \left[1 + A_D^2(B)\right] - B \cdot Q^3 + C \cdot Q^4 + G \cdot \delta(z) \cdot Q \quad (5.5)$$

Eq. (5.5) shows that the nucleation of the nematic phase is more likely to appear on the surface. $A_D^2(B)$ varies between $A_D^2 \approx 0.1$ for no induced order and $A_D^2 = 0$ for perfect order, but the bulk starts to grow from the surface nuclei before the surface layer is complete, rendering the fluctuation effect much weaker. This combined with T^* being only a few tens of a Kelvin below T_{IN} (for single component LC), makes the bulk transition to be completed in a narrow temperature range with little influence from the magnetic field.

However for a multi-component LC mixture, the substrate can induce a small compositional drift near the surface, which subsequently leads to a complete separation of the surface and bulk transition, as evidenced in fig.5.1. For the temperature interval $T_{IN}^b < T < T_{IN}^s$, upon cooling, the ordered wetting layer tries to

impose its orientation on the bulk. The free energy expression of the bulk component becomes:

$$F \approx a \cdot \left(T - T^*\right) \cdot Q^2 \cdot \left[1 + \xi_{bulk}^2 \cdot \left[A_D(B)/\xi\right]_{surface}^2 \right] - B \cdot Q^3 + C \cdot Q^4 \quad (5.6)$$

The elastic energy due to the surface order fluctuation acts as an energetic barrier for the bulk component, causing a temperature gap between bulk and surface transitions, allowed by the fact that for LC mixtures T^* can be much lower than T_{IN}. This is supported by the particular shape of the birefringence curves recorded upon cooling (fig.5.3.a). For similar reasons as described above, T_{IN}^s is not affected by the magnetic field. However the field induces an alignment of the surface wetting layer below T_{IN}^s, which tends to suppress the surface order parameter fluctuations. It is this surface-bulk interaction term that is implicitly responsible for the field dependence of T_{IN}^b, as experimentally observed in the data presented in fig.5.2.

When approaching the IN transition from below, the surface-bulk interaction term does not oppose the relaxation and Q follows the typical temperature relaxation path with the director locked by the surface orientation, as experimentally observed in fig.5.3.a. For all cases we consistently find that the cells undergo an isotropic-nematic transition at 94.7°C regardless of the different substrates and we can not resolve the surface transition as separate.

The presented results are consistent with the prediction of Sheng [3] and Sluckin [4], namely that the surface transition is of first order on surfaces with weak anchoring and continuous in the presence of strong anchoring.

5.5 Conclusions

We have shown that the surface IN transition is of first order, combined first order/continuous or continuous, depending of the LC-surface anchoring energy. We find that the surface order affects the cell free energy in the vicinity of the bulk IN transition. An applied magnetic field minimizes the surface order parameter fluctuations, causing the bulk transition to shift to higher temperatures until it finally overlaps with the surface transition.

In addition, these results may also have practical consequences for applications in liquid crystal devices. As shown in fig.5.3, cells obtained upon alignment in a magnetic field, preserve their orientation even after the field removal and are stable, unless the sample is reheated above the IN transition, due to the highly-

oriented/surface-anchored LC wetting layer. The nematic cells we have prepared making use of the present method showed a contrast ratio of 200:1 and a response time of *2.3 ms* (*215 Hz* driving). We attribute these promising results [23] to the uniformity of the surface alignment and of the pre-tilt angle, (the pre-tilt angle was achieved by exposing the cell to a magnetic field slightly out of the cell plane). These results strongly indicate the exciting possibility of magnetically aligned LC cell fabrication, which could eliminate rubbing based alignment with all its subsequent inconveniences [15]. This method would have the inherent advantages of a clean–non contact technique and allows accurate control over parameters of interest such as the pre-tilt angle and the surface-bulk interaction.

References

[1]   W.J. Cahn, *Chem Phys*. **66,** 3667, 1977.
[2]   H. Nakanishi and M.E. Fisher, *Phys. Rev. Lett*. **49**, 1565, 1982.
[3]   P. Sheng, *Phys. Rev. Lett*. **37**, 1059, 1976.
[4]   T.J. Sluckin and A. Poniewierski, *Phys. Rev. Lett*. **55**, 2907, 1985.
[5]   H. Yokohama et al., *Mol. Cryst. Liq. Cryst.* **99**, 39, 1983.
[6]   N.A. Clark, *Phys. Rev. Lett*. **55,** 292, 1985.
[7]   W. Chen et al., *Phys. Rev. Lett*. **62**, 1860, 1989.
[8]   K. Miyano, *Phys. Rev. Lett*. **43**, 51-54, (1979).
[9]   H. Hsiung et al., *Phys. Rev. Lett*. **57**, 3065, 1986.
[10]   P. De Schrijver et al., *Liq. Cryst.*, **21**, 745, 1996.
[11]   G. P. Crawford et al. *Phys. Rev. Lett*. **66**, 723, 1991.
[12]   H. Akiyama et al., *Jpn. J. Appl. Phys*. **36,** L1204, 1997.
[13]   B. Jerome, *Rep. on Prog. in Phys.* **54,** 391, 1991.
[14]   D. Bonn, D. Ross, *Rep. of Prog. in Phys* .**64,** 1085, 2001.
[15]   J. van Haaren, *Nature* **411**, 29, 2001.
[16]   P. Chaudhari, J. Lacey, J. Doyle, et al., *Nature* **411**, 56, 2001.
[17]   Jakli, A. et al., *Mol. Cryst. Liq. Cryst.* **198**, 331, 1991.
[18]   G. Maret, K. Dransfeld, *Topics in Applied Physics*, Vol **57**, 143, ed. F. Herlach, Springer, Berlin, 1985.
[19]   P. G. de Gennes, and J. Prost, *The physics of Liquid crystals,* 2nd ed.*,* Clarendon Press, Oxford, 1993.
[20]   P. Sheng, L. Bo-Zang, Z. Minyao, *Phys. Rev. A* **15**, 946, 1992.
[21]   C. Rosenblatt, *Phys. Rev. A*, **24**: 2236, 1981.
[22]   S. Singh, *Phys. Rep.* **34**, 107, 2000.

[23]   Nematic cells based on a rubbed polymer alignment layer have a response time in the order of 30-50 ms. and a contrast ratio of about 100:1 - 200:1.
Via a direct comparison between rubbed cells and magnetic field aligned cells, we find that the later method produces cells that in average have a 10 times faster response times than the former. (Apart of the alignment method the cells were identical, the same thickness, the same polymer coating, the same LC mixture and the same driving scheme.)

Chapter 6

Magnetic field as investigation technique and manipulation tool for Phthalocyanine molecular aggregates

Using Polarized Absorption Spectroscopy (PAS) of molecular aggregates of Phthalocyanines in high magnetic fields, up to $20T$, we show that magnetic fields can induce macroscopic ordering of molecular aggregates (MA), in a clean, no-contact method, which is well suited for MA manipulation. We also demonstrate that magnetic field induced alignment in combination with PAS can be used to determine the MA size and the precise position of the absorption lines in concentrate solutions as well as to probe inter-aggregate interactions.

6.1 Introduction

Molecular aggregates, MA, are formed by self-assembling of molecules in solution at high concentration and are intermediate structures between single molecules and pure crystals [1]. Their properties make them an interesting system for technological applications such as nonlinear optical materials [2-4] and the photographic industry [4], as well as for fundamental research, due to their presence in most photo-biological processes [1,4]. Individual MA are ordered objects but an ensemble of MA in solution forms a macroscopically isotropic medium, in which the MA are randomly oriented. For several applications as well as for X-ray, neutron scattering or polarized spectroscopy investigations, an ordered MA solution is advantageous. A large number of techniques such as electric fields [5], surface fields [6] and vertical spin coating [7], are currently used to induce order in MA solutions with varying success, but the field is still in its infancy and in search of substantial improvements.

Compared to other methods used to orient MA, a magnetic field has a unique combination of advantages: it is a clean, contact free method that does not dissipate kinetic energy into the system and does not create electrodynamic instabilities or induce charge currents. The technique delivers a uniform effect in the whole sample volume and there is only one mechanism responsible for magnetic field induced alignment.

6.2 Sample preparation and experimental description

We have studied Crown ether substituted Phthalocyanine molecules, PCS, which are disk like and have a *6 nm* diameter and a thickness of *0.4 nm*, fig.6.1 [8]. The delocalization of their molecular orbitals over the entire core, combined with their large size, results in a high dielectric polarizability. When the molecules are dissolved in chloroform, this gives rise to large intermolecular Van der Waals forces, which induce self-assembly of the molecules in long one-dimensional aggregates. Depending on the concentration (typically in the range *0.1 − 10 mg/ml*), aggregates are formed containing up to *10^4* individual molecules, which can be of the order of one micrometer long, fig.6.1. The PCS stacks are formed from molecules assembled in a non-staggered geometry, allowing the ether rings to form hollow tubes throughout the aggregate, which may constitute ideal ionic channels. It is predicted that the overlapping orbitals of the central ions permit electronic transfer along the PCS column, which would form a real 1D quantum wire – ideal object for

the field of molecular electronics [1], fig.6.1. The decoxy chains, which act as an isolating mantle, ensure mechanical and electrical protection of the stacks [8].
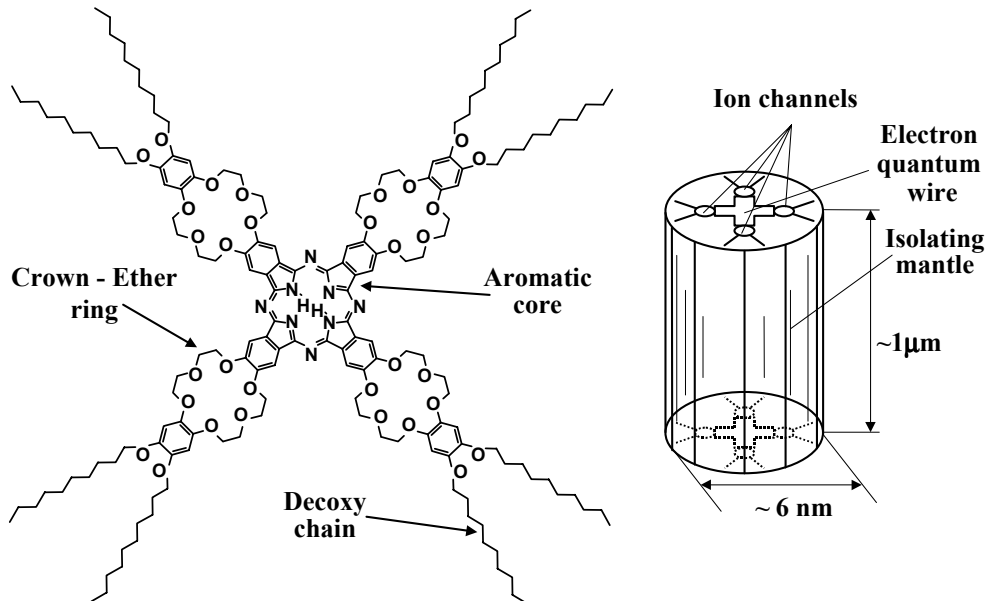

Figure 6.1 *Chemical structure of the PCS molecule (left); Sketch of a PSC molecular aggregate (right).*

The MA solution is prepared by ultrasonic mixing of PCS polycrystalline powder dissolved in chloroform. Placed in an optical cuvette ($0.5-10$ *mm* optical path), the sample is mounted in a temperature-controlled chamber ($5-95°C$ range with $\pm 0.02°C$ stability), in the bore of a $20T$ resistive Bitter magnet. For samples with concentrations in the range $0.1-10$ *mg/ml* , we measured polarized optical spectra in the $400-850$ *nm* range, using a single grating spectrometer-diode array, with the probing light beam perpendicular to the applied magnetic field, see sect.2.9. A sensitive polarization modulation set-up for field induced absorption measurements, see sect.2.8, was used as well for the samples with $0.1-1.5$ *mg/ml* concentrations.

6.3 Experiments and discussions

In magnetic field a molecule acquires an extra energy $E = -\chi \cdot B^2$, where B is the magnetic field induction and χ is the molecular diamagnetic susceptibility. Because of the χ anisotropy this energy is orientation dependent, causing a given molecule to align such that its magnetic energy is minimized, see sect.2.1.

For large molecular aggregates this energy gain can overcome de-alignment due to thermal fluctuations, allowing a significant degree of orientation to be achieved. Because the individual aggregates are ordered structures, the MA alignment is accompanied by changes of the optical properties of the solution, (see sect. 2.6).

Fig.6.2 shows the magnetic field induced dichroic ratio for PCS solutions with different concentrations in the $0.1 - 1.5 \, mg/ml$ range. It can be seen that the magnetic field induced effect becomes larger as the solution concentration increases

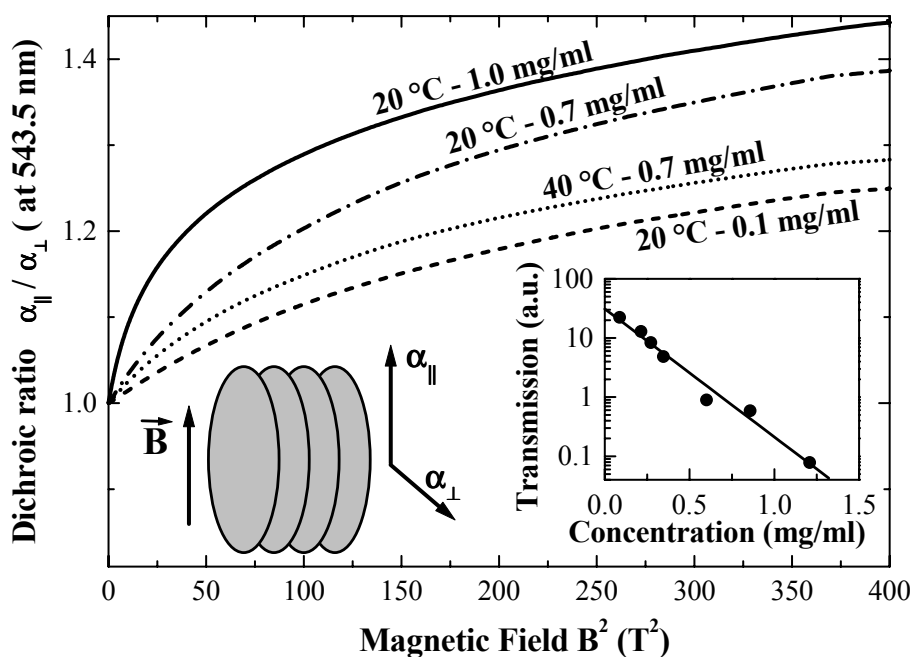***Figure 6.2*** *Magnetic field induced dichroic ratio at low concentration. The induced orientation increases with concentration and decreases with temperature. **Inset:** Zero field dependence of the transmission on the solution concentration. The exponential decay confirms that at low concentrations scattering is not important, see sect.2.6. (Data measured with the set-up described in sect. 2.8).*

and for a given concentration the effect is lower for higher temperatures. The different concentration curves from fig. 6.2 do not overlap showing that the degree of field induced order differs with concentration. This indicates that the size of the aggregates is concentration dependent. The size of the MA increases as the concentration increases or the temperature decreases. The inset of fig.6.2 shows the transmitted light as a function of the sample concentration.
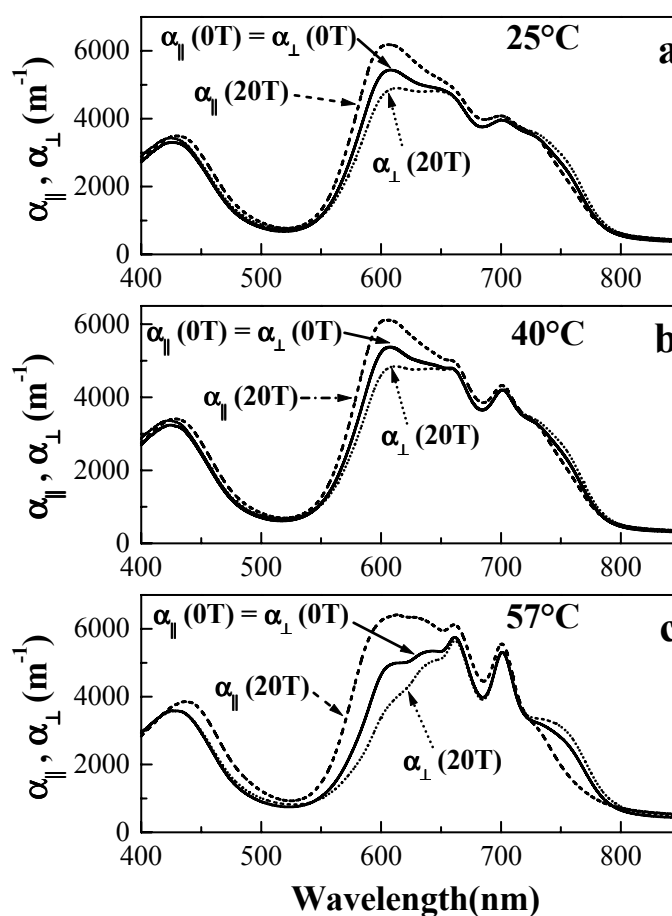
Figure 6.3 *Magnetic field dependence of polarized absorption spectra of a 7 mg / ml PCS solution at 25°C **(a)**, 40°C **(b)**, 57°C **(c)**: Continuous line, the isotropic absorption coefficient in the absence of an applied magnetic field; Dashed line, the parallel to field component of the absorption coefficient, $\alpha_{\parallel}$ in 20T ; Dotted line, the perpendicular to field component of the absorption coefficient, $\alpha_{\perp}$ in 20T .*

The exponential decay found implies that absorption is the only contribution to the observed signal and that in the limit of these concentrations the scattering contribution is negligible, see sect.2.6.

Fig.6.3.a shows the absorption spectra of a *7 mg/ml* PCS solution at *25°C*. In a zero magnetic field the two polarization spectra are identical, indicating that the solution is intrinsically isotropic. In a *20T* applied magnetic field, the polarization ∥ to the field of the probing beam is more absorbed in the *550−650 nm* spectral range and less absorbed in the *730−850 nm* region. Conversely, the polarization ⊥ to the field shows the opposite behavior, less absorbed in the *550−650 nm* part and more absorbed in the interval *730÷850 nm*. The *660−710 nm* region of the spectra shows little magnetic field induced changes.

The *660−710 nm* region is the split Q band of the PCS monomers [8], consistent with the small magnetic dependent changes observed, fig.6.3 and fig.6.4. The *550−650 nm* band originates from MA electronic absorption lines with the transition moment in the molecular plane [8]. From its magnetic field dependence we attribute the *730−850 nm* band to absorption lines with the transition moment perpendicular to the molecular plane. This is a possible indication of electron de-localization along the molecular stacks, see fig .6.1

Fig.6.3.b shows that at *40°C* the situation is similar to the *25°C* case, only that the monomer signature, *660−710 nm*, is more pronounced.
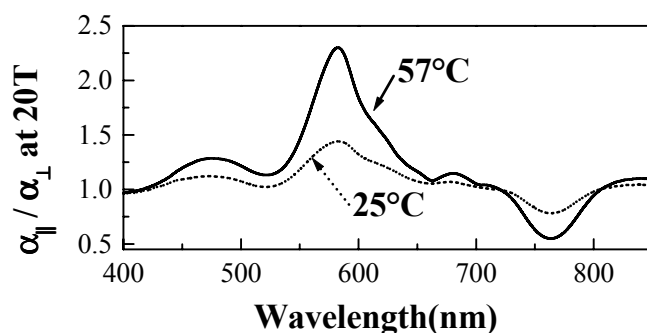
Figure 6.4 *The induced dichroic ratio* $\alpha_{||}/\alpha_{\perp}$ *of a 7 mg / ml PCS solution at 20T ;* $\alpha(\lambda)$ *is the (wavelength dependent) absorption coefficient.*

At *57°C*, fig.6.3.c, the split Q band is clearly visible and the magnetic induced effect becomes significantly larger. This behavior is the opposite of the one observed at low concentrations, *0.1−1.5 mg/ml*. We associate this to the fact that at these

large concentrations, $2-10\ mg/ml$, MA are relatively large in size and they interact with each other. At higher temperature the aggregates are smaller in size and therefore they hinder each other less, resulting in a larger degree of alignment, while because of the high concentration, the MA are still sufficiently large to be magnetically aligned.

Fig.6.4 shows the *20T* magnetic field induced dichroic ratio at *25°C* and *57°C*, indicating that white light propagating through this oriented solution becomes polarized perpendicular to the magnetic field direction in the green-yellow part of the spectrum and parallel polarized to the applied magnetic field in the near-infrared.
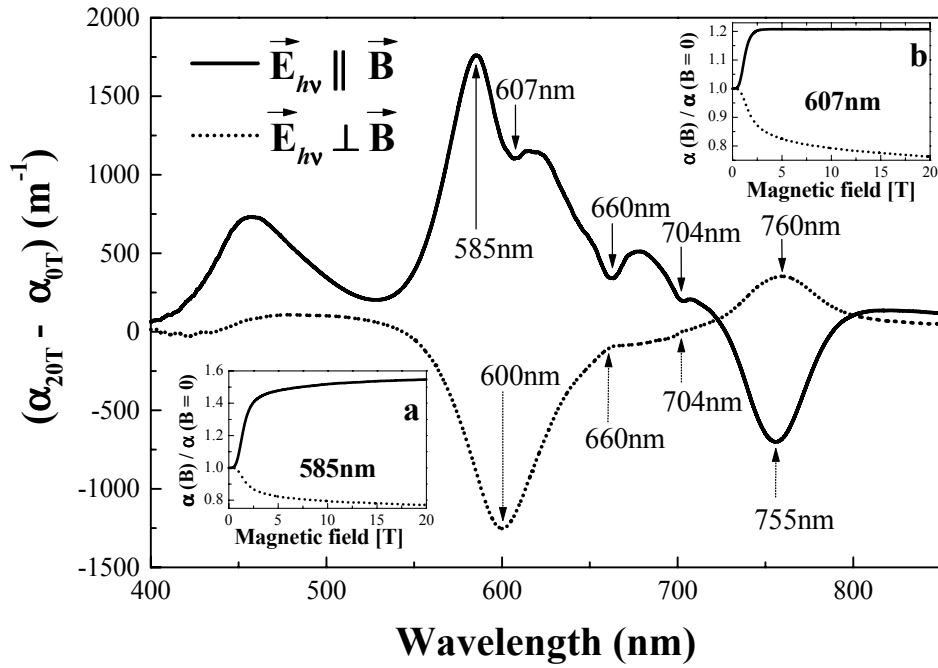
Figure 6.5 *Relative change of the polarized absorption coefficient spectra as a method for absorption peaks identification. (α_{20T} - α_{0T}) of a 7mg/ml PCS solution at 57°C;* ***Inset a:*** *Normalized change of the absorption coefficient $\alpha(B)/\alpha(B=0)$, for 607nm;* ***Inset b:*** *Normalized change of the absorption coefficient $\alpha(B)/\alpha(B=0)$ for 585nm.*
For the whole figure: solid line, parallel to magnetic field component; dotted line, perpendicular to field component.

The magnetic field induced variation of the absorption coefficient, fig.6.2, fig6.3 and fig.6.4, indicates that the PCS aggregates are oriented such that the molecular planes are aligned with the magnetic field lines while the stack has the rotational freedom in the plane perpendicular to the magnetic field.

The studied solution of PCS is a mixture of MA and molecular monomers. The MA, due to their size, give rise to light scattering, which blurs the absorption profile and hides the exact position of the absorption lines. The measured spectra are therefore a combination between absorption and scattering, see sect.2.6. However, at resonant absorption energy, the scattering contribution is minimal [9].

The correct identification of the absorption lines is of fundamental importance for molecule and aggregate characterizations. Even a small uncertainty in the line position, when used as input information could leads to large errors of the properties determined.

Based on the different magnetic field dependencies of the absorption and the scattering components, see sect. 2.6, we propose that the subtraction of the high field and zero field spectra is a simple method to identify the position of the spectral lines, fig.6.5. The method can be affected by errors due to the scattering dependency of the MA shape and due to the MA aggregates size variation around an average size. For reliable results both polarizations have to be analyzed together and the results compared, fig.6.5.

Fig.6.5 shows the relative change of the absorption coefficient $(\alpha_{20T} - \alpha_{0T})$ of the spectrum shown in Fig.6.2. The behavior for the two polarizations is qualitatively different and is not complementary. The dips in the spectra when the polarization is ‖ to the field corresponds to the absorption lines, *607 nm* for MA, *660 nm* and *704 nm* for monomer. At these energies the absorption dominates, as opposed to the neighboring spectral regions where scattering is also present. At *20T* the large MA are completely aligned along the magnetic field therefore the spectra with the ⊥ polarization shows no feature around *607 nm* . The monomer lines appear in the ⊥ polarization at the same positions, *660 nm* and *704 nm* respectively. These values are to be compared with the direct measurement (fig.6.2.c), which indicates the absorption peaks as being at *613 nm* for MA, *662 nm* and *701 nm* respectively for monomers, but their positions are affected by the convolution of scattering and absorption.

The insets a and b from fig.6.5 show the importance of wavelength and polarization. For *607 nm* , fig.6.5-inset a, shows the polarization ‖ to the field saturating at *3T* , while the ⊥ polarization is still increasing at *20T* . For *585 nm* , (fig.6.5-inset b), both components show a sharp change at low fields, but are still changing at *20T* . Only the parallel to field polarization at *607 nm* correctly

describes the induced orientation of the MA, and shows that already at *3T* complete alignment is achieved.

The normalized change of the absorption coefficient at a given wavelength, $\alpha(B)/\alpha(B=0)$, or the dichroic ratio, $\alpha_{||}(B)/\alpha_{\perp}(B)$, are directly related with the degree of magnetic field induced orientation of the particular species that absorbs in that range. This allows accurate determination of the average number of molecules contained within a MA, irrespective of information about the transition moment of the absorption line. In the limit of low concentrations, the relative small size of the MA makes the data less susceptible to scattering and inter-aggregates interactions. In this case the full size distribution of the MA ensemble can be extracted from the data [10].
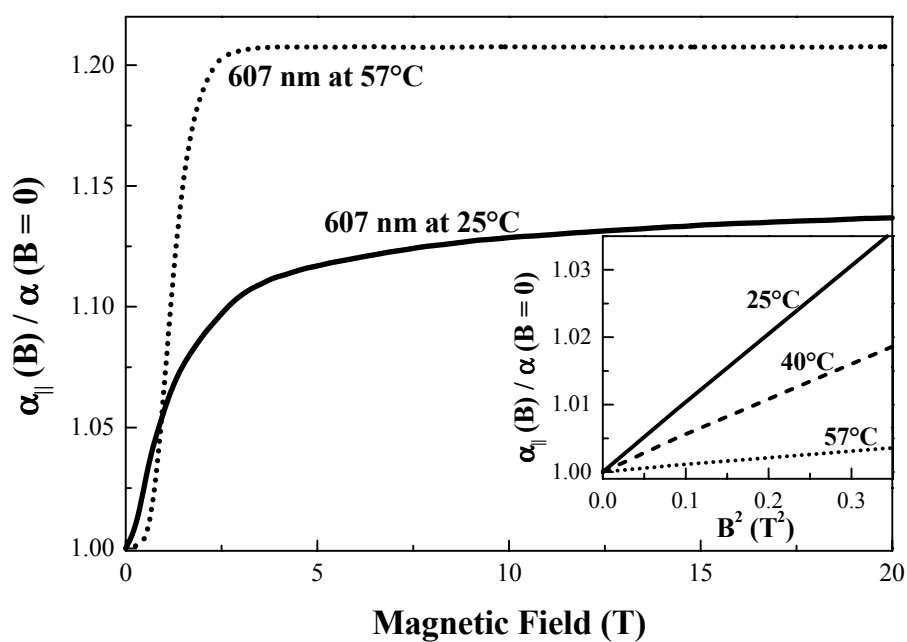

Figure 6.6 *Normalized change of the absorption coefficient for a* $7\,mg/ml$ *PCS solution, at 25°C (solid line) and 57°C (dotted line), recorded for the polarization || to the field at 607 nm.* **Inset:** *The low field part of the large panel, plotted versus magnetic field squared. Higher slope means larger aggregate size.*

For the *7 mg/ml* sample we estimate the size of the MA to be about *50.000* molecules at *20°C* and respectively *4000* molecules at *57°C* . Transmission electron microscopy confirms this large size and shows that the aggregates consist of stacks of about *10⁴* molecules each, bundled together in a larger 1D superstructure [8]. The signal at *704 nm* is constant and magnetic field independent. This indicates that monomers are too small to be oriented by a magnetic field of *20 T* . At low concentrations we found the MA to consist of about *2000* molecules at *1 mg/ml* , *1200* molecules at *0.7 mg/ml* and *500* molecules at *0.1 mg/ml* , all estimation made from the results at *20°C* , fig.6.2. For these determinations we used the low field part of the fig.6.2 and fig.6.6 curves and the diamagnetic anisotropy per molecule: $\Delta\chi = 500 \cdot 10^{-12}$ *m³ / mol [SI]*.

A comparison of the $\alpha(B)/\alpha(0)$ curves with numerical models provides us with information about the inter-aggregate interactions.

Fig.6.6 shows the $\alpha(B)/\alpha(0)$ changes of the MA absorption line (*607 nm*) for the polarization ∥ to the field. Based of the analysis shown in sect.2.6 the experimental curves are expected to fit with the formula:

$$\frac{\alpha_{\|}(B)}{\alpha(0)} = 1 - Q(B) + Q(B) \cdot \frac{\kappa_{\|}}{\kappa_o} \qquad (6.1)$$

with Q the magnetic field induced order parameter of the MA solution and κ the imaginary part of the refractive index, see sect.2.6. Single-parameter fits, $N \cdot \Delta\chi$, fail to describe both low and high field parts and the deviations become larger as the concentration increases. Attempts to fit the curves with a size distribution of MA instead of an average N also failed. The experimental curves always saturate at lower values than expected from the low field part analysis, indicating that the MA orientation effect is hindered, the effect increases as the degree of order increases. The available experimental data allow us to estimate only the strength of this interaction, while its origin can not be fully determined.

The curves from fig.6.6 were well described by the formula (6.1) when the order parameter Q was calculated accounting for the constraint:

$$N \cdot \Delta\chi \cdot B^2 \cdot \left\langle cos^2(\theta) \right\rangle - E_{int}(Q) \geq 0 \qquad (6.2)$$

The expression (6.2) introduces an energy, $E_{int}(Q)$, which represents the mean energy per MA needed to bring the whole statistical assemble in an ordered state characterized by a given order parameter Q . Within the algorithm, (6.2) set the

integration limits of (2.14) as $\theta_{max} - 90°$ instead of $0° - 90°$, with θ_{max} the solution of (6.2).

The natural limit $E_{int}(Q) = 0$ for $Q = 0$ restores the physical nature of the constraint and avoids the *ad hoc* introduction of a threshold field needed for the alignment to occur.
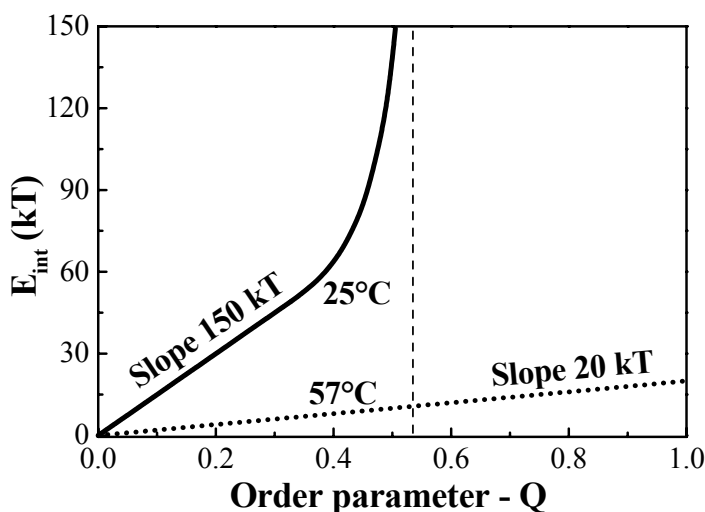

Figure 6.7 Inter-molecular interaction energy versus the magnetic field induced order. Numerical estimation from the experimental data presented in fig.6.7, a $7\,mg/ml$ PCS solution, at 25°C (solid line) and 57°C (dotted line). The 25°C curve divergence was probed up to $E_{int} \approx 4000\,kT$, reached for $B = 20\,T$.

Applying the above procedure to the experimental curves we found that at high temperature the energy is of the form: $E_{int}(Q) = Q \cdot E_{const}$, with $E_{const} \approx 0 - 100\,kT$. On contrary at low temperature $E_{int}(Q)$ diverges rapidly with Q, $E_{int}(0.5) \approx 3000 - 5000\,kT$, see fig.6.7.

We interpret these results in terms of the free volume per MA, with the assumption that E_{int} originates from the mechanical hindrance of the MA with each other. At higher temperatures the effective MA radius allows full rotation and E_{int} represents the energy needed to rearrange the system in the new configuration. At lower temperatures, however, the aggregates tend to be longer and when starting from a completely random distribution, the volume restriction does not permit a full rotation, prohibiting perfect alignment. The fig.6.6 consistently shows that MA are

largest at *25°C* , see inset, but the highest degree of order is achieved at *57°C* , main panel.
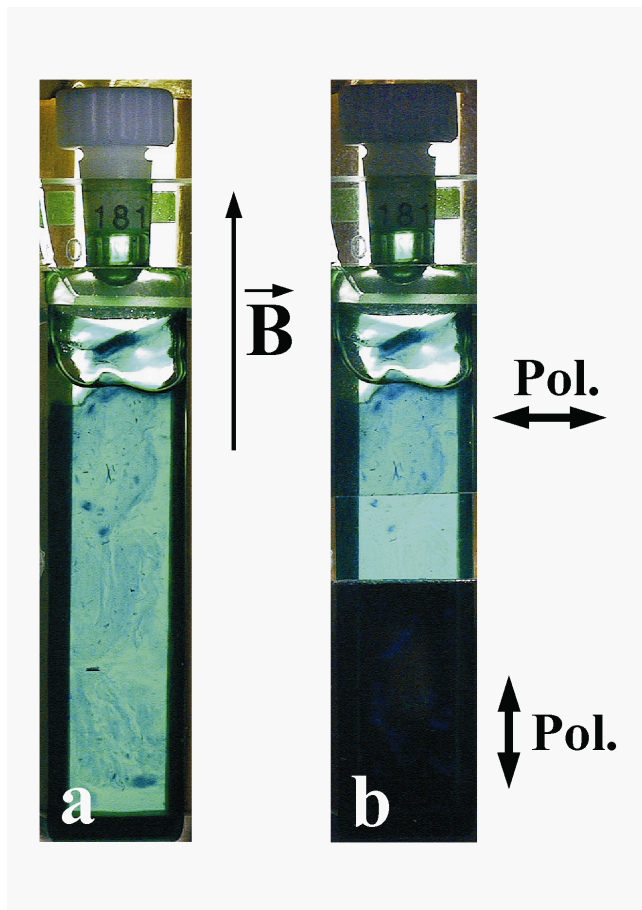
Figure 6.8 *Aligned sample of* $10\,mg/ml$ *PCS gel solution, formed by uniform cooling in* $14T$ *magnetic field: **(a)** Normal photo; **(b)** Same as (a), with two dichroic polarizer films added to show the high degree of induced order. The direction of the applied magnetic field was along the cuvette.*

Making use of these observations we have prepared an aligned sample, mechanically stable at room temperature, fig.6.7. A high concentration sample, $10\,mg/ml$, was first warmed up to *60°C* , a limit imposed by the chloroform boiling point, to ensure a high mobility and minimum inter-aggregate interaction. At *60°C*

we applied a $14T$ magnetic field, which aligned the existing MA, and subsequently started to cool down at $1°C/min$ rate, with the field on. Upon cooling the alignment is preserved and due to the solution's large concentration the MA grow in size and interweave, giving rise to an aligned gel at room temperature. The sample could be de-aligned only by heating above $45°C$. At this temperature the sample crosses-over from the low temperature/long MA regime to high temperature/shorter MA regime.

6.4 Conclusions

We have shown that a magnetic field is able to induce macroscopic order in MA solutions, offering a useful method to control MA orientation at a molecular level. PAS combined with high magnetic fields is a powerful tool, which allows easy access to the MA size and insight into inter-aggregate interactions. These types of studies are a welcome complement to other characterization techniques.

References

[1]   G.M. Whitesides, J.P. Mathias and C.T. Seto, *Science* **254** (5036), 1312-1319, Nov 1991

[2]   F.C. Spano and S. Mukamel, *Phys. Rev. Lett.*, **66** (9), 1197-1200 Mar 1991.

[3]   V.M. Axt and S. Mukamel, *Rev. of Mod. Phys.*, **70** (1), 145-174 Jan 1998.

[4]   T. Kobayashi, *J-Aggregates*, World Scientific, Singapore, 1996.

[5]   S.R. Yeh, M. Seul and B.I. Shraiman, *Nature* **386** (6620), 57-59 Mar 1997

[6]   T. Yokoyama, S.Yokoyama, T. Kamikado, Y. Okuno and S. Mashiko, *Nature* **413** (6856), 619-621 Oct 2001.

[7]   K. Misawa, H. Ono, K. Minoshima and T. Kobayashi, *Appl. Phys. Rew. Lett.*, **63** (5): 577-579 Aug 1993.

[8]   C.F. van Nostrum, *Ph.D. Thesis*, University of Nijmegen, 1996.

[9]   M. Kerker, *The Scattering of Light and Other Electromagnetic Radiation*, Academic Press, New York and London, 1969.

[10]   I.O. Shklyarevskiy, K.Takazawa M.I. Boamfa et al, *Molecular Aggregates Size Distribution by Magnetic Field Induced Orientation*, to be submitted to the Journal of Chemical Physics.

Summary

This thesis describes optical measurements of magnetic field induced alignment and subsequently related phenomena in Polymer Liquid Crystals (PLC), Liquid Crystals (LC) and Molecular Aggregates (MA).

Chapter 2 introduces the general aspects of molecular alignment in magnetic fields, shows how the induced order is connected to optical anisotropy and presents a detailed description for the particular cases of PLC, LC and MA. The analysis of some methods for refractive index anisotropy measurements and their implementation into sensitive set-ups are also described. For the special purpose of this work, we have designed, developed and implemented a novel method based on a polarization-intensity double modulation technique. The method allows sensitive simultaneous measurements of birefringence, related to the induced order, and light scattering, related to the sample morphology.

Chapter 3 presents an analysis of the magnetic field induced order in Side Chain Polymer Liquid Crystals, (SCPLCs). Here we show that the induced order effect in SCPLCs takes place in a narrow temperature window, in the Isotropic-Nematic (IN), biphasic region, when cooling from the isotropic phase in the presence of a field larger than a threshold value, B_{th}. The aligned samples are macroscopically ordered, transparent, strongly birefringent and are stable in the absence of the field and can be de-aligned only by heating them to the isotropic phase. B_{th} is found to depend strongly on the molecular structure of the SCPLCs, namely stiffer polymeric backbones or larger polymerization degrees tend to increase B_{th}, while longer spacers favor a smaller B_{th}. We interpret B_{th} as a marker of the mesogen-polymer backbone coupling. We have estimated its strength and we show that this interaction

is responsible for the stability of the induced alignment after the magnetic field is turned off.

Chapter 4 concentrates on the IN phase transition of SCPLCs in magnetic fields. Intrinsically a weak first order transition with a wide biphasic region, we find the IN transition of SCPLCs to become a strong first order in the presence of high magnetic fields. The temperature window of the IN biphasic region shrinks as stronger magnetic fields are applied, until it completely disappears, giving rise to a sharp first order transition. Within the frame of the Landau-De Gennes theory of LC phase transitions, we explain this behavior in terms of magnetic field induced orientation of the nematic mesophase at the IN transition crossing. This process suppresses the order fluctuation and affects the free energy balance of the system such that allows the transition to occur completely at a fixed temperature. This finding is one of only a few existing experimental evidences that indicate that magnetic field can influence a phase transition at room temperature.

In Chapter 5 the magnetic field induced alignment effect is used to study the surface IN phase transition of LCs. Using a nematic LC mixture, the varied mixture ratio near the surface completely separates the surface transition from the bulk one, allowing us to study them independently, with the help of magnetic fields. This is the first observation of a pure IN surface phase transition of a nematic LC on a substrate, clearly separated from the bulk IN transition. We find the surface IN transition to be of first order on surfaces with a weak anchoring energy and continuous on surfaces with a strong anchoring. We find that the presence of high magnetic fields does not change the surface IN transition temperature, whereas the bulk IN transition temperature increases with magnetic field strength. We attribute this result to the bulk/surface interaction energy, tuned by the magnetic field induced order of the surface-wetting layer, which causes the bulk transition to shift towards higher temperatures. Of major importance for the LC cell manufacturing, we find that a magnetically oriented surface layer, stabilized by surface forces, assures stable cell alignment until heated above the IN temperature.

In Chapter 6 we report a Polarized Absorption Spectroscopy (PAS) study of Phthalocyanine MA in a high magnetic field. We show that magnetic fields can induce macroscopic ordering of MA in a clean, no-contact method, being well suited for MA manipulation. We use magnetic field induced alignment in combination with PAS to determine the MA size and precise position of the absorption lines in concentrated solutions as well as a probe for the inter-molecular interactions.

Samenvatting

Dit proefschrift beschrijft optische metingen aan vloeibare kristallen (LC) polymere vloeibare kristallen (PLC) en moleculaire aggregaten (MA) die door middel van een magneetveld zijn uitgelijnd.

In hoofdstuk 2 worden de algemene aspecten van het uitlijnen van moleculen door middel van een magnetisch veld belicht. Ook wordt in dit hoofdstuk gedemonstreerd hoe de geïnduceerde orde kan worden gerelateerd aan optische anisotropie en wordt een gedetailleerde beschrijving gegeven van PLC, LC en MA. Enkele methoden voor de analyse van metingen aan de anisotropie van de brekingsindex en hun implementatie in gevoelige opstellingen worden hier ook beschreven. Om dit te kunnen doen moest een nieuwe methode ontworpen worden die gebaseerd is op een dubbele modulatie van de polarisatie-intensiteit. Deze methode maakt het mogelijk om met een zeer hoge gevoeligheid tegelijkertijd dubbelbreking en lichtverstrooing te meten. Eigenschappen die respectievelijk gerelateerd zijn aan de geinduceerde orde en aan de vorm van het sample.

In hoofdstuk 3 wordt de door een magneetveld geinduceerde orde van zijketenvertakte polymeer vloeibare kristallen (SCPLCs) geanalyseerd. We tonen aan dat de geinduceerde orde alleen plaatsvindt in een zeer klein temperatuurgebied, namelijk in het Isotroop-Nematische (IN) tweefasen gebied. Dit fenomeen treedt op wanneer er afgekoeld wordt vanuit de isotrope fase in aanwezigheid van een veld groter dan de drempelwaarde B_{th}. De uitgelijnde preparaten zijn macroscopisch geordend, transparant, sterk dubbelbrekend, stabiel in de afwezigheid van een magnetisch veld en kunnen alleen weer uit de uitgelijnde situatie gehaald worden door ze te verwarmen tot ze zich weer in de isotrope fase bevinden. Het blijkt dat B_{th} sterk van de moleculaire details van de SCPLCs afhangt. Bij polymeren met een stijvere ruggengraat of een hogere polymerisatie graad stijgt B_{th}, terwijl polymeren met langere tussenmoleculen een lagere waarde van B_{th} opleveren. We interpreteren daarom B_{th} als een aanwijzing voor tussenmolecuul-ruggegraat koppelingen. We hebben de sterkte van deze interactie geschat en we laten zien dat hij verantwoordelijk is voor de stabiliteit van de geinduceerde uitlijning na uitschakeling van het magneetveld.

In hoofdstuk 4 ligt de nadruk op de IN faseovergang van SCPLCs in magneetvelden. Terwijl deze overgang normaal gesproken een zwakke eerste orde overgang is met een groot tweefasen gebied blijkt dat in een magneetveld deze overgang een sterke eerste orde overgang is. De grootte van het temperatuurgebied van de faseovergang neemt af bij het toepassen van grotere veldsterktes totdat het het temperatuurgebied volledig verdwijnt, waarbij een scherpe eerste orde overgang

optreedt. Gebruik makend van de Landau-De Gennes theorie voor LC fase overgangen, verklaren we dit gedrag in termen van een door het magneetveld geinduceerde orientatie van de nematische mesofase bij het IN overgangsgebied. Dit proces onderdrukt de fluctuaties in de orde en beinvloedt de vrije energie balans van het systeem op een zodanige wijze dat de overgang volledig wordt toegestaan bij een vastliggende temperatuur. Dit resultaat is er één van slechts een paar bestaande experimentele bewijzen die een indicatie geven dat een magnetisch veld een fase overgang bij kamertemperatuur kan beinvloeden.

In hoofdstuk 5 wordt de door een magneetveld geinduceerde uitlijning van vloeibare kristallen gebruikt voor het bestuderen van oppervlakte IN fase overgangen. Als een mengsel van nematische vloeibare kristallen wordt gebruikt scheidt de wisselende mengverhouding in de buurt van het oppervlak de oppervlakte-overgang volledig van de bulk overgang, wat ons in staat stelt deze twee processen onafhankelijk van elkaar te bestuderen met gebruikmaking van het magnetisch veld. Dit is de eerste meting van een zuivere IN oppervlakte fase overgang van een nematisch vloeibaar kristal op een substraat die duidelijk onderscheiden kan worden van een bulk fase overgang. Onze bevindingen zijn dat de fase overgang een zwakke eerste orde fase overgang is in het geval van een zwakke verankerings-energie en de fase overgang is continu in het geval van een sterke verankerings-energie. De aanwezigheid van een magneetveld verandert de faseovergangs-temperatuur van de oppervlakte IN niet, terwijl de temperatuur van de bulk IN faseovergang stijgt met een sterker magneetveld. Dit wijten wij aan een bulk/oppervlakte interactie-energie die wordt bepaald door de door het magneetveld geinduceerde orde van de natmakende oppervlaktelaag die ervoor zorgt dat de bulk faseovergang naar hogere temperaturen verschuift. Het feit dat een door een magneetveld georienteerde oppervlakte laag, die wordt gestabiliseerd door oppervlakte krachten, een stabiele uitlijning van bulk vloeibare kristallen induceert, in ieder geval totdat ze worden verhit tot boven de IN temperatuur, is van groot belang voor het fabriceren van LCDs.

In hoofdstuk 6 wordt het werk aan Phtalocyanine moleculaire aggregaten in een magneetveld beschreven. De aggregaten worden bestudeerd door middel van absorptie spectroscopie met gepolariseerd licht (PAS). We laten zien dat magneetvelden een macroscopische uitlijning van de moleculaire aggregaten induceren in een schone, contactvrije methode, die zeer geschit is voor het werken met MA. Om de aggregaten te karakteriseren wordt PAS gebruikt op de door het magneetveld uitgelijnde aggregaten. Daarmee kan de grootte van de aggregaten bepaald worden en de precieze posities van de absorptie-maxima in geconcentreerde oplossingen. Bovendien kan PAS ook dienen als een meetmethode voor intermoleculaire interacties.

114

List of Publications

M.R. Swift, M.I. Boamfa, S.J. Cornell, A. Maritan, *Scale invariant correlations in a driven dissipative gas,* Physical Review Letters **80**, 4410, 1998.

A.K. Geim, M.D. Simon, M.I. Boamfa and L.O. Heflinger, *Magnet levitation at your fingertips,* Nature **400**, 323, 1999.

M.D. Aguas, L. Affleck, I.P. Parkin, M.V. Kuznetsov, W.A. Steer, Q.A. Pankurst, L.F. Barqúin, M.A. Roberts, M.I. Boamfa and J.A.A.J. Perenboom, *The effect of large magnetic fields on solid state combustion reactions: novel microstructure, lattice contraction and reduced coercivity in barium hexaferrite,* Journal of Materials Chemistry **10**, 235, 2000.

M.I. Boamfa, P.C.M. Christianen, J.C. Maan, H. Engelkamp and R.J.M. Nolte, *Alignment of Phthalocyanine molecular aggregates by magnetic fields,* Physica B **294-295**, 343, 2001.

M.I. Boamfa, K. Viertler, A. Wewerka, F. Stelzer, P.C.M. Christianen, J.C Maan, *Side Chain Polymer Liquid Crystals in High Magnetic Fields,* Molecular Crystal and Liquid Crystals **375**, 143, 2002.

I.O. Shklyarevskiy, M.I. Boamfa, P.C.M. Christianen, F. Touhari, H. van Kempen, G. Deroover, P. Callant, J.C. Maan, *Magnetic field induced alignment of cyanine dye J-aggregates,* Journal of Chemical Physics **116**, 8407, 2002.

M.I. Boamfa, M.W. Kim, J.C. Maan, Th. Rasing, *Observation of surface and bulk phase transitions in nematic liquid crystals*, Nature **421**, 149, 2003.

M.I. Boamfa, K. Viertler, A. Wewerka, F. Stelzer, P.C.M. Christianen, J.C Maan, *Mesogene-polymer backbone coupling in Side Chain Polymer Liquid Crystals, studied by high magnetic field induced alignment*, Physical Review Letters **90 (2)**, 2003.

M.I. Boamfa, K. Viertler, A. Wewerka, F. Stelzer, P.C.M. Christianen, J.C Maan, *Magnetic field induced changes of the Isotropic-Nematic phase transition in Side Chain Polymer Liquid Crystals*, submitted to Physical Review E.

M.I. Boamfa, P.C.M. Christianen, J.C Maan, *Magnetic field as investigation technique and manipulation tool for Phthalocianine molecular aggregates*, prepared, to be submitted.

Curriculum Vitae

Boamfă Marius Iosif
Born on 9th of June, 1972, Făgăraş, Romania

1986 – 1990   High School studies at "Liceul de Chimie Industrială", Făgăraş, Romania.

1990 – 1995   B.Sc. studies in Physics at the Faculty of Physics, University of Bucharest, Romania. B.Sc. thesis under the supervision of Dr. P. Cristea.

1995 – 1996   M.Sc. studies in Electronics at the Faculty of Physics, University of Bucharest, Romania. M.Sc. thesis under the supervision of Dr. P. Cristea.

1996 – 1997   Diploma studies in Condensed Matter Physics at the International Centre for Theoretical Physics, Trieste, Italy. Diploma thesis under the supervision of Prof. A. Maritan.

1998 – 2002   Ph.D. studies in experimental Soft Condensed Matter at the High Field Magnet Laboratory, University of Nijmegen, The Netherlands. Ph.D. thesis under the supervision of Prof. J.C. Maan.

2002 – 2004   Postdoctoral researcher at the Department of Experimental Solid State Physics 2, University of Nijmegen, The Netherlands.